UNIONE EUROPEA

FONDO SOCIALE EUROPEO PROGRAMMA OPERATIVO NAZIONALE 2000/2006
"Ricerca Scientifica, Sviluppo Tecnologico, Alta Formazione"
Regioni dell'Obiettivo 1 – Misura III.4 - "Formazione superiore ed universitaria"

DOTTORATO DI RICERCA IN INGEGNERIA
CIVILE PER L'AMBIENTE ED IL TERRITORIO

Università degli Studi di Salerno

VIII Ciclo Nuova Serie (2006-2009)

SATELLITE REMOTE SENSING FOR SURFACE SOIL WATER CONTENT ESTIMATION

Candidate
GIOVANNA DE CHIARA

Doctoral Coordinator
prof. ing. R.M.A. NAPOLI

Tutor:
prof. ing. VITTORIO BOVOLIN

prof. ing. PAOLO VILLANI

Co-Tutor:
ing. RAFFAELE CRAPOLICCHIO

SATELLITE REMOTE SENSING FOR SURFACE SOIL
WATER CONTENT ESTIMATION

Finito di stampare il 27/03/2010

Ai miei genitori….

"Bear in mind that the wonderful things that you learn in your schools are the work of many generations, produced by enthusiastic effort and infinite labour in every country of the world. All this is put into your hands as your inheritance in order that you may receive it, honour it, and add to it, and one day faithfully hand it on to your children. Thus do we mortals achieve immortality in the permanent things which we create in common. If you always keep that in mind you will find meaning in life and work and acquire the right attitude towards other nations and ages" (Albert Einstein talking to a group of school children. 1934)

"Pensate bene a questo: le cose ammirevoli che imparate a conoscere nelle vostre scuole sono l'opera di numerose generazioni, create in tutti i paesi della terra, a prezzo di grandi pene e sforzi appassionati. Tutto ciò è deposto nelle vostre mani, come un retaggio, in modo che lo accogliate, lo veneriate, lo sviluppiate e lo trasmettiate un giorno, fedelmente, ai vostri figli. E' così che noi, esseri mortali, diveniamo immortali in questa cosa che noi creiamo in comune, contribuendo ad opere imperiture. Se voi pensate sempre a questo, troverete un senso alla vita e allo sforzo e nutrirete una giusta opinione nei confronti degli altri popoli e degli altri tempi" (A. Einstein).

TABLE OF CONTENTS

INDEX OF FIGURES

INDEX OF TABLES

SOMMARIO

Il telerilevamento satellitare è un'utile fonte di osservazione delle variabili e dei processi idrologici superficiali e può essere una pratica alternativa ai convenzionali sistemi di monitoraggio in-situ. La maggior parte dei processi relativi alle dinamiche idrologiche variano non solo su scala annuale ma anche su scale temporali più brevi che richiedono osservazioni più frequenti. Il principale vantaggio del telerilevamento è la capacità di offrire osservazioni sinottiche delle dinamiche e della distribuzione spaziale di fenomeni e parametri spesso difficili da monitorare con una elevata frequenza temporale mediante l'utilizzo delle tradizionali misure in-situ. Molte delle variabili che partecipano al bilancio dell'acqua superficiale possono essere ora osservate con sensori satellitari grazie ad un forte sviluppo di questa tecnologia negli ultimi decenni. Spesso il problema principale connesso all'uso delle acquisizioni satellitari è rappresentato dall'accuratezza delle misure che può variare da moderata ad eccellente in base al sensore utilizzato.
In questa tesi si è valutato l'utilizzo di sensori satellitari per il monitoraggio di due variabili utili per applicazioni idrologiche: l'estensione di corpi idrici e l'umidità del suolo.
La capacità di misurare l'estensione di corpi idrici è importante in molte applicazioni idrologiche; in particolare risulta un elemento rilevante per il monitoraggio delle alluvioni e per la gestione delle risorse idriche. Spesso queste informazioni sono difficili da ottenere mediante tradizionali rilevamenti in caso di aree inaccessibili o di masse d'acqua in movimento. Per questa attività di ricerca, come caso studio è stato selezionato un bacino artificiale per cui sono note le informazioni relative all'estensione della superficie di acqua. Le misure reali registrate giornalmente dal Consorzio di gestione del bacino sono state confrontate con le rilevazioni ottenute mediante utilizzo di immagini satellitari acquisite dai sensori SAR e TM/ETM+ ed hanno evidenziato buoni risultati. L'analisi ha inoltre messo in risalto anche i fattori da tenere in considerazione per i diversi tipi di sensori.
L'umidità del suolo è una variabile chiave in molti processi idrologici ed ecologici in quanto influenza lo scambio di acqua e calore latente tra la superficie del suolo e l'atmosfera. Nonostante l'alta variabilità spaziale di

questo parametro, è stato dimostrato che molti sensori satellitari sono capaci di derivare informazioni sull'umidità superficiale del suolo a livello di bacino idrografico. Tra i vari sensori lo Scatterometro risulta utile per studi climatici e di modellistica grazie ad una buona frequenza temporale, copertura globale ed una serie storica consistente. Sebbene questo sensore sia stato progettato per ricavare informazioni di vento superficiale sul mare, negli ultimi anni è stato evidenziato che le misure di backscattering hanno una elevata potenzialità per applicazioni su superfici terrestri.

La seconda parte di questo progetto di ricerca, relativo all'utilizzo di dati satellitari per il monitoraggio dell'umidità del suolo, è stata sviluppata presso la Serco S.p.A. nell'ambito del progetto Advanced Scatterometer Processing System (ASPS) sviluppato dall'Agenzia Spaziale Europea (ESA-Esrin) al fine di riprocessare l'intera missione ERS-Scatterometer.

Sin dall'inizio della missione ERS-1 nel 1991 quasi 20 anni di misure di backscattering acquisite in banda C sono disponibili per studi e ricerche. Questo dataset molto consistente è importante soprattutto per analisi climatologiche. In questo tipo di studi è importante anche avere dati di alta qualità e soprattutto una serie storica omogenea come anche riconosciuto dal Global Climate Observing System (GCOS) dell'Organizzazione Meteorologica Mondiale.

L'obiettivo principale di questa parte di ricerca è stata la generazione dei nuovi prodotti ASPS caratterizzati da una migliore qualità radiometrica e risoluzione spaziale. Questo lavoro ha richiesto una lunga preparazione ma rappresenta un importante contributo nell'ambito delle serie storiche di dati acquisiti dallo Scatterometro disponibili per la comunità scientifica. Al fine di valutare l'utilizzo dei nuovi dati riprocessati, le misure di backscattering ottenutene con il nuovo processore ASPS sono state confrontate con misure in-situ di umidità del suolo. La relazione tra le due variabili è stata analizzata considerando diversi fattori: l'angolo di incidenza, l'angolo di azimuth, la risoluzione dei prodotti e la copertura vegetativa.

I risultati mostrano che una relazione tra backscattering e umidità del suolo esiste ed è condizionata dai fattori sopraelencati.

ABSTRACT

Satellite remote sensing is a useful source of observations of land surface hydrologic variables and processes and could be a practical substitution of conventional in-situ monitoring. Most of hydrological dynamic processes change not only throughout the years but also within weeks or months and their monitoring requires frequent observations. The most prominent advantage of the remote sensing technologies is that they offer a synoptic view of the dynamics and spatial distribution of phenomena and parameters, often difficult to monitor with traditional ground survey, with a frequent temporal coverage. Many of the variables in the land surface water balance can now be observed with satellite techniques thanks to an extensive development over the last decades. Often the problem connected to the use of remotely sensed data is their accuracy that, according to the sensor used and to the application considered, can ranges from moderate to excellent.

The objective of this thesis has been to evaluate the use of satellite remote sensing techniques for the monitoring of two variables useful for hydrology applications: water body extension and soil moisture monitoring.

The capability to map water surface is important in many hydrological applications, in particular accurate information on the extent of water boundary is essential for flood monitoring and water reservoir management. Often, this information is difficult to retrieve using traditional survey techniques because water boundaries can be fast moving as in floods or may be inaccessible. In this PhD thesis, an artificial basin for which in-situ information about the water extension are available is used as case study. The area extension recorded daily by the dam owner is compared to the one retrieved by using satellite images acquired from SAR and TM/ETM+ sensors. The outcomes of the analysis show that satellite images are able to map water body surfaces with a good accuracy. The analysis also highlighted the factor to be taken into account while using types of sensors.

Soil moisture is recognized as a key variable in different hydrological and ecological processes as it controls the exchange of water and heat energy

between land surface and the atmosphere. Despite the high spatial variability of this parameter it has been demonstrated that many satellite sensors are able to retrieve soil moisture information of the surface layer at catchment scale. Among other sensors, the Scatterometer is very useful for climatic studies and modelling analysis thanks, respectively, to the temporal frequency, global coverage and to the long time series availability. Even though the ERS Scatterometer has been designed to measure the wind over the ocean surface, in recent years it has been pointed out that backscattering measurements have high potentiality for soil moisture retrieval.

The second task of this PhD thesis, concerning the use of satellite data for soil moisture monitoring, has been developed at Serco S.p.A. in the framework of the Advanced Scatterometer Processing System (ASPS) project developed by ESA (European Space Agency) to reprocess the entire ERS Scatterometer mission. Since the beginning of the ERS-1 Scatterometer mission in 1991 a long dataset of C-band backscattering signal from the Earth surface is available for studies and researches. This is a very consistent dataset, but in particular for climatology studies it is important to have high quality and homogeneous long term observation as also stated in the key guidelines included in the Global Climate Observing System (GCOS) from the World Meteorological Organization (WMO).

The main goal of this task has been the generation of the new Scatterometer ASPS products with improved data quality and spatial resolution. This achievement required a long preparation activity but represents an important contribution to the C-band Scatterometer dataset available to the scientific community. In order to evaluate the usage of the re-processed Scatterometer data for soil moisture estimation, the backscattering measurements derived in the new ASPS products have been then compared to in-situ volumetric soil moisture data and the relationship between radar backscattering and soil moisture measurements has been investigated under different conditions: angle of incidence, angle of azimuth, data measurements resolution, season of the year.

Analysis results show that a relationship between the C-band backscattering coefficient and the in-situ volumetric soil moisture exists and takes into account the incidence and azimuth angles and the vegetation cover.

ACKNOWLEDGEMENTS

This PhD research has been mostly carried out at Serco S.p.A. in collaboration with ESA in the framework of the ASPS project. SAR and Landsat images have been provided by ESA within a Category 1 project. Occhito Basin ground measurements have been supplied by the "Consorzio per la Bonifica della Capitanata". In-situ soil moisture measurements have been downloaded from the "Global Soil Moisture Data Bank" (Robock et al., 2000) and the "Soil Climate Analysis Network" web sites.

At the end of this PhD program I need to say 'grazie' to many person involved directly and indirectly in this period of my life.
In first place, I would like to thank Prof. Paolo Villani and Prof. Vittorio Bovolin who gave me the chance to start this project and supported and followed my work since the beginning despite the distance.

I am especially grateful to Raffaele Crapolicchio that followed my Scatt work. His constant support, attempts to teach me all about the Scatt world, the scientific advices on the methodology and on the interpretation of the results at different stages as well as his very big patience, the encouragement and the choice to supervise me for the second time are highly appreciated.
I would also to thank Pascal Lecomte, with which talking of Scatterometer is a big pleasure. And Angelika Dehn to have always encouraged me to go on and shared with me many nights at office.

A special thanks has to be addressed to Marina, my 'guardian angel' during this PhD program, whose help, smiles, bureaucratic support, the emails with the subject 'do not forget…' gave me the chance to arrive at the end of this journey. Thanks Marina!
Thanks also to the other friends at CUGRI and 'al Cubo' for the few but intense moments spent together and the moral support provided: Giusy, Dario, Giovanni, Ersilio, Ferdinando, Agostino, Giuseppe, Serena, Claudia. And to Antonia…for her advice and the "proper words at the right time".

Many thanks to my colleagues in Serco that during these years, despite suffering my stress, showed me their friendship and gave a very big support in terms of cars (Sabrina, Gabriele, Lidia), interesting discussions about UTC times & julian dates (Sabrina), IDL helps (Lidia…mi faro en la niebla!), interesting questions ('ancora il dottorato?') or simply smiling (above all Lauretta). To Aidan for the "English correction service". To Gareth for the "Oceanosophy" discussions and English "wordspots".
A very special mention goes to Michela and Teddy boy: their invaluable support in every moment of the day...and the night…their friendship and total availability have been essential over these years…dico vero!!!

Thanks to my friends and flatmates, a big support network, to have suffered my obsession (PhD): Lucilla & Lucia… are u ready for dancing now on? The Fox Family (Zio Bambo included) for the love they demonstrated me in all the possible ways and the moral and material support they gave me even in the hardest moments; Aleffff…just to be Alefff! Alo for the shared feelings; Valeria to have shared doubts, feelings and experiences (but "no polpette" this time), Lemon for the last minute questions. Lucia which is always present in my life. To the Florentin group: Todz (which has always a thought for me), Pianino (my perl/grib/grads/meteo lighthouse), Massi (my favourite researcher) & my fellow adventure "buddy Louise" (Massi & Ramo...please…start now to write!). To the "Minuetto team" for the never tedious journeys and political discussions: I found friends indeed! And thanks to Chris that is able to send me texts on the right time that always make me smile. Thanks to Pablo, Jeffrey and Mociccione and the others for sure I forget…

And finally a big thanks to my family. Specially to my mother and father that always take care of me, have always encouraged me and taught me to give my best in everything I do. And to my sisters and brothers-in-law above all for my jewels: Simona, Fabiano and the little star Elettra.

ABOUT THE AUTHOR

Giovanna De Chiara ha conseguito la laurea in Scienze Ambientali (indirizzo Marino Oceanografico) presso l'Università degli Studi di Napoli "Parthenope" nel 2002. La parte sperimentale del lavoro di tesi di laurea é stato svolto durante un tirocinio presso l'Agenzia Spaziale Europea (ESA-Esrin) in Frascati lavorando su un progetto dal titolo "Tracking a tropical cyclone with ERS-SCAT: a CMOD4 model review". Dal 2003 al 2005 svolge attività di ricerca presso "l'Osservatorio del Clima" dell'Istituto di Biometeorologia (CNR) di Firenze.
Nel 2006 usufruisce di una borsa di studio al Consorzio Inter-Universitario per la Previsione e Prevenzione dei Grandi Rischi (C.U.G.RI.) lavorando su un progetto relativo all'analisi di pericolosità meteorologica e alluvionale mediante utilizzo di dati satellitari. Nel Novembre 2006 si iscrive al Corso di Dottorato di Ricerca in Ingegneria Civile per l'Ambiente ed il Territorio (VIII ciclo Nuova Serie) con sede presso l'Università degli Studi di Salerno. Durante il corso di Dottorato svolge attività di ricerca sull'utilizzo di dati satellitari per la stima dell'estensione di corpi d'acqua e contenuto di umidità del suolo. Dal 2007 é responsabile presso la Serco S.p.A. dell'attività di controllo e monitoraggio dei dati acquisiti dallo Scatterometro, sensore operativo a bordo del satellite ESA ERS-2.

Giovanna De Chiara received a 5-year Batchelor of Science degree in Marine Environmental Sciences, with a specialization in Oceanography, from the Università degli Studi di Napoli Parthenope in 2002. Her thesis work was developed during an internship period at the European Space Agency (ESA-Esrin) in 2001 where she worked on the project "Tracking a tropical cyclone with ERS-SCAT: a CMOD4 model review".
From 2003 to 2005 she worked at the "Climate observatory" of the Institute of Biometeorology (CNR-National Research Council) in Florence where she collaborated on different projects regarding meteorological hazards and climate changes. In 2006 she was the

recipient of a grant from the National Research Institute C.U.G.R.I. (Consorzio Inter-Universitario per la Previsione e Prevenzione dei Grandi RIschi) which related to remote sensing techniques for meteorological and flood risk analysis.
In November 2006 she took the PhD Course in Civil and Environmental Engineering. As a PhD student she developed research topics related to the use of remote sensing data for water body detection and soil moisture analysis. Since 2007 she has worked for Serco S.p.A. in Frascati where she has been responsible for the quality control of ERS-2 Scatterometer data as part of a support contract with the European Space Agency (ESA-Esrin).

1 INTRODUCTION

1.1 CONTEXT AND AIM OF STUDY

Over the last decade, the importance of the global hydrological cycle has become increasingly clear in understanding global processes. Often information related to the elements of the hydrological cycle are not satisfactorily monitored from in situ sensor networks that do not widely cover extensive areas of the Earth surface. The current observational information available on ground is so often inadequate for the monitoring the hydrological parameters.

It has been recognize that satellite remote sensing systems represents a precious source of observations and is playing an increasing important role in hydrology and water managements (Barrett et al., 1988). The most prominent advantage of this technology is the synopticity of the measurements over a defined spatial zone, with frequent temporal coverage of the observed scenes.
Each sensor has its own spatial resolution, temporal coverage and accuracy. The choice of the instrument to be used depends on the application and analysis considered and often a compromise among the three parameters is needed.
Despite the extensive development of this technique over the last years, one of the questionable point is the accuracy of remote sensing products, which is in general variable in space and times, and often not well known Nevertheless, the integration of remote sensing in hydrological sciences has recently made important progresses (Wagner et al., 2009).

In this research project, the employ of satellite data for hydrology applications has been evaluated. Among the many important areas of remote sensing application in surface hydrology, in this project the following ones have been considered: the water surface monitoring and the soil moisture estimation.

The capability to map inland water surface is important in many practical cases, from the reservoir management, through area planning, hydraulic modeling to flood monitoring. In recent years, the need to properly map water bodies has then gained a growing interest, in a world-wide perspective because of the increasing global water shortage problem.
Often, this information is difficult to obtain using traditional survey techniques due to the lack of ground measurements or because areas could be inaccessible such as in the case of flood events. Moreover accurate information of water bodies areal extension is also important for flood prediction and monitoring (Smith, 1997; Baumann, 1999). In recent years, remotely sensed data collected by radar and optical satellites have been used for flood extent evaluation over regions characterized by different climate, land cover conditions and topography (Brivio et al., 2002). As general approach, a multi-source satellite images technique is used for water body extraction since this allow to overcome the limits connected to both active and passive satellite sensors.
Among different methods developed to extract water bodies, threshold method is the simplest one (Zhang et al., 2006). Despite its simplicity, it has been noticed that the extraction accuracy, related to the use of this method, could be affected by the definition of the threshold.
In this PhD research a straightforward threshold method has been applied to active and passive sensors images, respectively SAR and TM/ETM+ images, acquired over an artificial reservoir selected as case study. The Occhito lake has been chosen because of in-situ data related to the water surface extension is available and also the dynamic of the basin is know. To evaluate the accuracy of the water body extraction, results obtained from the applied method have been compared to in-situ water extension measurements as provided by the dam owner.

The second part of this research project concerns soil moisture estimation. Soil moisture plays a key role in numerous hydrological processes as it drives the water and energy exchanges between soil surface, vegetation and atmosphere. The need for soil moisture observations and the limited availability of field measurements has led to more research in the field of remote sensing. Despite the high spatial variability of this variable, different studies have demonstrated that many satellite sensors are able to retrieve soil moisture information of the surface layer at catchment scale. Long-term availability and continuity of satellite system is also of great concern in Earth Observation (Wagner et

al., 2007) especially when dealing with climatology and modeling applications. Operational hydrology, instead, gives strong requirements in terms of availability, timeliness and reliability of remote sensing products.

Among the various remote sensing techniques, approaches based on the microwave measurements offer the most direct way of retrieving remote sensing as they take advantage of the strong relationship between the soil moisture content and dielectric constant of the soil (Ulaby et al., 1982). In recent years the great interest in microwaves techniques for soil moisture application led to the development of dedicated missions based on microwave sensors such as the case of the Soil Moisture and Ocean Salinity (SMOS) satellite (launched on November 2009) and Soil Moisture Active Passive (SMAP) mission (whose launch is foreseen in 2013). Beforehand, for years satellite hydrology relied on systems designed primarily for other applications such as for oceanography or meteorology (Barrett et al., 1998). This is the case of the C-band radar Scatterometer that has been originally designed for wind retrieval over the ocean. In recent years it has been demonstrated that C-band Scatterometer data may also be useful for soil moisture monitoring over land surface (Wagner et al., 1998). One of the advantage of the Scatterometer data is the long dataset availability, of great interest for climatic and modeling applications.

The first European Scatterometer was launched in 1991 by the European Space Agency (ESA) on board the ERS-1 satellite. It has been followed by ERS-2 Scatterometer launched in 1995 and currently into operation. The ERS Scatterometer mission has being providing so far over than 19 years of backscattering measurements of the Earth surface with a spatial resolution of 50 km. Since 2006 a follow-on of the ERS Scatterometer, the Advanced Scatterometer (ASCAT), is operational on board the METOP satellite. ASCAT technical characteristics are nearly identical to its precursor but it has an enhanced spatial (both 25km and 50 km) and temporal resolution. These satellite will guarantee, in the next future, more than 20 years of observations.

A first multi-year, global soil moisture data set from ERS Scatterometer has been derived by Wagner et al. from the Vienna University of Technology (Wagner et al., 2003). The soil moisture data is retrieved from the radar backscattering using a change detection method: the lowest and the highest backscattering measurements of the time series analyzed over a certain area represent, respectively, the driest and wettest

soil moisture conditions. The soil moisture values can, therefore, range between 0% and 100%. Different studies have been based on this soil moisture dataset (Paris Anguela et al, 2008; Laguardia et al., 2008; Liu et al., 2008) for comparison with in-situ measurements or model outputs finding a quite good agreement. Since 2008 this method is operationally applied to ASCAT data to provide near-real-time soil moisture products.
The soil moisture dataset generated by Wagner et al. (2003) is based on the ERS Scatterometer products operationally distributed to the users since the beginning of the mission in 1991. But since then many events impacted the Scatterometer mission that have affected the quality of the data (Crapolicchio et al., 2004).
The need of high quality and of homogenous long term observations is fundamental not only for soil moisture estimation but for many kinds of applications as also stated in the key guidelines of the Global Climate Observing Systems. These requirements, together with the need of enhanced spatial resolution, leaded ESA to develop the Advanced Scatterometer Processing System (ASPS) with the main aim to reprocess the entire ERS Scatterometer mission and provide the users community with enhanced quality and spatial resolution products (Crapolicchio et al., 2004).
This part of the work has been carried out at Serco S.p.A in the framework of the ASPS project. In this contest different activities has been performed, as described in this thesis, with the main aim to generate the new ASPS products. This activity represents an important contribution to the available Scatterometer datasets as it allowed to provide the scientific community with new enhanced ERS C-band Scatterometer data. This is confirmed by the fact that the generation and distribution of these new enhanced products have been long requested from scientists that work with Scatterometer measurements. To achieve the goal, first of all a calibration analysis is has been completed in order to improve the radiometric quality of the ASPS data. The main objective of this part of research is to compute the best calibration constants and evaluate a new improved antenna pattern profile to be used for the reprocessing project. Other analysis and tests are then necessary to properly define the correct ASPS configuration before the reprocessing campaign start. Within the ASPS reprocessing activity new ERS Scatterometer products with a spatial resolution of 25 km and improved radiometric quality have been generated. To analyze these new products in the perspective of soil moisture applications, the backscattering

measurements derived in the ASPS products are compared to in-situ volumetric soil moisture data and the relationship between radar backscattering and soil moisture measurements is investigated under different conditions.

1.2 OUTLINE OF THE THESIS

Fundamentals of the remote sensing principles and techniques are widely illustrated in Chapter 2. Explanation of the electromagnetic spectrum and the ranges useful for satellite applications are provided together with the description of active and passive systems.
In Chapter 3 the satellite sensors used to carry out this research project are reported in order to understand the acquisition principles and the physical background. SAR sensors on board the ERS-2 and ENVISAT satellites and TM/ETM+ on board Landsat missions have been used to perform the analysis related to the surface water estimation and described in this chapter. The second part of the chapter is dedicated to the description of the ERS Scatterometer with reference also to the backscattering processing and to the geophysical parameter retrieval.
Chapter 4 reports the analysis concerning the water body extraction. The Occhito Lake, selected as the case study, and related water extension ground measurements are illustrated. The threshold method applied to both SAR and TM/ETM+ images is then explained. The water extraction results obtained are further compared to in-situ ground measurements.
The second part of the PhD research, concerning the ASPS project and soil moisture analysis, are then described. In chapter 5 the ASPS project is explained in terms of objectives and facility architectural design. All the investigations performed before the Scatterometer reprocessing project start have been explained. These mainly include the calibration analysis performed to improve the radiometric quality of the Scatterometer data. Furthermore the ASPS facility configuration and the quality control performed on the data are showed.

Once the new ASPS products have been generated, they are analyzed in the perspective of the soil moisture applications. In Chapter 6 some in-situ volumetric soil moisture datasets have been selected and detailed. Then the backscattering coefficient stored in the ASPS products are compared to in-situ soil moisture observation considering different conditions: spatial resolution, azimuth angles and season of the year. Finally Chapter 7 illustrates concluding remarks.

2 REMOTE SENSING PRINCIPLES AND TECHNIQUES

Generally Remote sensing is defined as "the science (and to some extent, art) of acquiring information about the Earth's surface without actually being in contact with it. This is done by sensing and recording reflected or emitted energy and processing, analyzing, and applying that information".

Remote sensing systems, particularly those on board satellite platforms, provide repetitive and consistent views of the Earth and represent an invaluable instrument for monitoring the Earth system and the effect of human activities on our planet.
Some of the important applications of remote sensing techniques are:

- environmental assessment and monitoring
- global changes detection
- retrieval of global parameters for large-scale modeling.

The importance and the interest in remote sensing for Earth monitoring can be explained by the many advantages given by this technique, summarized as follows:

- **Synoptic View**: Remote sensing systems represent a rapid method of acquiring up-to-date information simultaneously over a large geographical area. This facilitates the study of various features of the Earths' surface in their spatial relation to each other and helps to delineate the required features and phenomena. Furthermore often regional phenomena which are invisible from the ground are clearly visible through satellite acquisitions.
- **Repetivity:** Satellite sensors provide frequent and repetitive coverage of the Earth and of the area of interest. These time series are very useful for studying process dynamics, area monitoring or change detection analysis;

- **Accessibility**: The remote sensing technique is a practical way to obtain data from inaccessible regions where it is not possible to do a ground survey (i.e. , e.g. Antarctica, Amazonia).
- **Time Conservation:** Since information over a large area can be gathered quickly, the techniques save time and human effort;
- **Cost Effective:** Remote sensing especially when conducted from space, is an intrinsically expensive activity. Nevertheless, cost-benefit analysis demonstrates its financial effectiveness, and speculative or developmental remote sensing activity can be justified in this way. It is a cost-effective technique as repetitive fieldwork is not required and also a large number of users can share and use the same data.

The use of satellite techniques for the Earth monitoring presents some limitations. Satellite measurements are not direct sensing the geophysical phenomenon. So to use them it is useful to have some knowledge of the theory on how the instrument makes the measurements and the technique used to retrieve the geophysical phenomenon. The use of the satellite data requires also knowing the residual measurements uncertainty, which can be obtained after a proper calibration and validation activity. That uncertainty could be large for specific application and this has to be considered when using satellite products. In this perspective, international board in charge of the calibration and validation of satellite data, named CEOS (Committee of Earth Observation Satellites), has established a Quality Assurance Framework for Earth Observation (QA4EO). QA4EO has the aim to guarantee, for each delivered remote sensing product, the availability of a quality indicator (QI) based on documented quantitative assessment of its traceability to international community agreed reference standards (http://qa4eo.org).

Some remote sensing acquisitions must be corrected geometrically and geo-referenced in order to be useful as maps, not only as pictures.

Distinct phenomena can be confusing if they look the same to the sensor, leading to classification error. Example: artificial & natural grass in green light (but infrared light can easily distinguish them).

Often Phenomena which were not meant to be measured (for the application at hand) can interfere with the image and must be accounted for. Examples for land cover classification: atmospheric water vapor, sun vs. shadow (these may be desirable in other applications).

Resolution of satellite imagery could be too coarse for some applications such as detailed mapping and for distinguishing small contrasting areas.

2.1 ELECTROMAGNETIC RADIATION

All sensors onboard remote sensing platforms use the electromagnetic radiation to acquire information. The sensors contain detectors to record specific wavelengths within the Electromagnetic Spectrum (EMS). The EMS ranges from the shorter wavelengths (including gamma and x-rays), through ultraviolet (UV) at 100nm, visible, infrared (IR) and microwave to the longer wavelengths (including broadcast radio waves) (Figure 2.1).

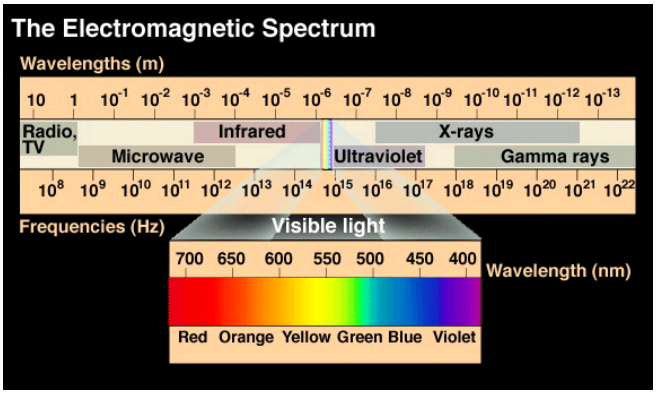

Figure 2.1 Electromagnetic Spectrum

There are several regions of the electromagnetic spectrum often called bands, or spectral bands which are useful for remote sensing. The ultraviolet (UV) portion of the spectrum has the shortest wavelength useful for the remote sensing. The visible spectrum is defined sharply between 0.4 and 0.7 μm (400 to 700 nm) The shortest visible wavelength is violet and the longest one is red. The next portion of the spectrum includes three different categories of infrared (IR) wavelength: near-IR,

mid-IR and thermal IR. At much longer wavelengths (1mm to 1m) is the microwave portion of the spectrum. The differentiation between near-IR and thermal-IR and between the latter and microwave is used rather loosely.
Most common remote sensing systems operate in one or several of the visible, IR or microwave portions of the spectrum. The choice of bands to use is governed firstly by the atmospheric transmission spectrum and secondly by the source of the e.m. energy in relation to the application.

2.1.1 Interaction with the Atmosphere

Before the radiation used for remote sensing reaches the Earth's surface it passes through the Atmosphere where it may be absorbed or scattered by the constituent particles and gases in the atmosphere.

The **scattering** occurs when particles or large gas molecules (atmospheric components) interact with the electromagnetic radiation modifying its original path. The direction of scattering is unpredictable. The amount of scattering depends on the wavelength, the abundance of particles and the distance covered by the radiation. For remote sensing purposes the scattering is important only in the visible and near infrared regions.
Three types of scattering are possible:
Rayleigh Scattering: results from constituents that are much smaller than the radiation wavelengths. It takes place in the upper atmosphere mostly due to molecular gases (N2 O2, CO2 and water vapor). This effect increases with shorter wavelengths and is the cause of the blue skylight and even of red sunsets as seen from the earth.
Mie Scattering: occurs when the particles in the atmosphere are of the same size as the radiation wavelengths. It is mostly due to dust, smoke and water vapor and mainly affects the longer wavelength in the lower portion of the atmosphere.
Non-selective Scattering: when the particles are much larger than the radiation wavelengths a non-selective (wavelength-independent) scattering occurs. This is the case of water droplets and large dust particles.

The **absorption** in the atmosphere is mainly caused by water vapor, carbon dioxide and then ozone and mainly affects the visible and

infrared bands. Each type of molecule absorbs electromagnetic energy in a very specific region of the spectrum. As a result, only the wavelength regions outside the main absorption bands of the atmospheric gases can be used for remote sensing. These regions are known as the Atmospheric Windows.
By comparing the characteristics of the two most common energy/radiation sources (the sun and the earth) with the atmospheric windows available to us, we can define those wavelengths which can be most effectively used for remote sensing (Fig.2.2).

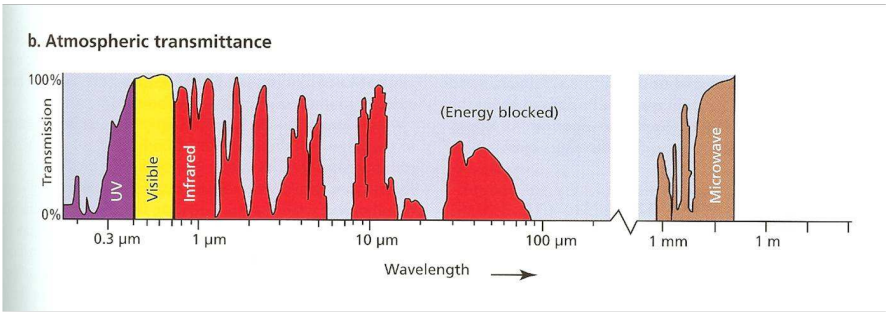

Figure 2.2: Diagram of atmospheric windows—wavelengths at which electromagnetic radiation penetrates the Earth's atmosphere.

The **Faraday Rotation** for polarimetric sensor operated in the microwave range. Ionosphere and Earth Magnetic field play a major role to rotate the polarized signal from the Earth surface. This, for example, has an impact for sensor operated at L-band and used to retrieve Ocean salinity (Le Vine et al., 2002).

2.1.2 Radiation-Matter Interaction

The EMR that is not absorbed or scattered in the atmosphere reaches the Earth's surface and is splitted into 3 modes of energy-interaction response:

- Transmittance (t): a fraction of the radiation penetrates into certain surfaces materials (i.e. water) and if the material is transparent and thin in one dimension it normally passes through with some diminution

- Absorptance (α): a fraction of the radiation is absorbed within the medium; a portion of this energy is *re-emitted* usually at longer wavelengths and some remains to heat the object;
- Reflectance (ρ): a part of the radiation reflects at specific angles depending on the surface roughness and the angle of incidence of the rays. Reflected light is what we know as colour (chlorophyll in plants reflects green).

Because they involve ratios (to irradiance), these three parameters are dimensionless numbers (between 0 and 1), but are commonly expressed as percentages. Following the Law of Conservation of Energy:

$$\alpha + \rho + t = 1$$

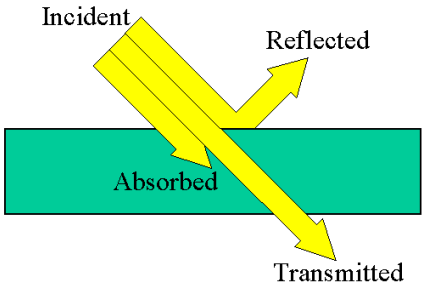

Figure 2.3: Example of Reflected, Absorbed, and Transmitted Radiation

The relative amount of reflection, absorption and transmission depends on the wavelength radiation and the material.

Depending on their application, these interactions may be the source of the signal to acquire or may be the source of the signal, or may confound the desired signal. Below are some examples:
Reflection as the signal: This is probably the most common remote sensing situation. The reflected radiation is what our eyes use to see objects, causes near-infrared film to record vegetation, and allows radar images of the earth to be created.
Absorption as the signal: Atmospheric gases, such as ozone, will absorb at specific wavelengths. By measuring sunlight passing through the

atmosphere to the ground and calculating how much energy was lost by absorption, the concentration of a specific gas can be estimated.
Absorption as a confounding signal: Often absorption of light will introduce uncertainty in the desired measurement. Almost all remote sensing of the earth's surface from space is confounded by atmospheric absorption. For the visible part of the spectrum, absorption is only a serious problem when looking at relatively dark objects, such as the ocean, or if there are clouds. In these cases, the desired signal may be reduced to the noise level of the sensor, making interpretation impossible. For other parts of the spectrum, absorption may be so high that remote sensing at those wavelengths will not work, and only a few "atmospheric windows" through the atmosphere are available.

For any material, the amount of solar radiation that it reflects, absorbs and transmits changes with the wavelengths. By plotting the reflectance (%) against the wavelength the *spectral signature* is obtained for this object. Thus, two features that are indistinguishable in one spectral range may be very different in another portion of the spectrum. For example, water and vegetation may reflect somewhat similarly in the visible wavelengths but are almost always separable in the infrared. This is an important property of the matter that allows identifying different substances or classes by their individual spectral signature.

2.2 REMOTE SENSING SYSTEMS

Remote sensing systems can be organized according to different classifications.
In terms of spectral regions used for the acquisition, sensors can be classified into:

- Visible and reflective infrared
- Thermal infrared
- Microwave

With respect to the type of energy resources they can be divided as:
- **Passive sensors**: that measure the energy reflected (when the illumination source is external) or the radiation emitted by the scene observed;

- **Active sensors**: that illuminate the scene and measure the backscattered signal, as the radars do. These sensors create their own energy and are not dependent on the sun's energy or the thermal properties of the earth. Advantages for active sensors include the ability to obtain measurements anytime, regardless of the time of day or season.

Together with the type of sensor to be used (mainly dependent of the type of the scene to observe), one of the parameters to be considered when selecting the system to use is the resolution. The resolution is defined as the ability of the entire remote sensing system to render a sharply defined image.
For any remote sensing the resolution is specified in terms of spectral resolution, radiometric resolution, spatial resolution and temporal resolution, which are described as follows:

- **Spatial resolution**: refers to the size of the smallest possible feature or object that can be detected as a separate object. Or as the minimum distance the two point features on ground should have in order to be distinguished as separate objects. It is important to highlight that higher resolution systems generally have smaller coverage areas.
- **Radiometric Resolution:** refers to the smallest change in radiation intensity level that can be discriminated by the sensing system. The finer the radiometric resolution of a sensor, the more sensitive it is to detecting small differences in reflected or emitted energy.
- **Spectral resolution**: describes the ability of a sensor to define fine wavelength intervals. The finer the spectral resolution, the narrower the wavelengths range for a particular channel or band. On the basis of the spectral resolution, the system can be classified as panchromatic (single wavelength band with a large bandwidth), multispectral (several narrow bandwidth bands) and hyperspectral (hundreds of very narrow bandwidth bands).
- **Temporal resolution**: is the pass frequency of the satellite above the same point of the Earth surface; It is specified as the number of days in which the satellite re-visits the exact same area with the same viewing angle.

All these characteristics are taken into account when choosing the data for a specific application. Indeed some users may require frequent and repetitive coverage with low spatial resolution (i.e. meteorological applications) while others may need a high resolution with non frequent coverage (i.e. mapping purposes).

2.2.1 Passive sensors

Passive sensors measure radiation naturally reflected or emitted by the Earth and the constituents of its atmosphere.

The fundamental basis of passive remote sensing is that any object above absolute zero (0°K or -273 °C) continuously emits radiation.
A *blackbody* is defined as an idealized, perfectly opaque, material that absorbs all the incident radiation at all frequencies, reflecting none [Ulaby et. al., 1982]. It converts all incident radiant energy into heat energy. Because no light is reflected or transmitted, the object appears black when it is cold. A blackbody is also a perfect emitter, since energy absorbed by a material would increase its temperature if no energy were emitted.
For a given temperature and wavelength, no other body can emit more energy that a black body.
The spectral characteristics of the thermal emission from a black body at temperature T are described by the Planck's law:

$$M(\lambda,T) = \frac{C_1}{\lambda^5[\exp(C_2/\lambda T)-1]} \quad \text{(Eq. 2.1)}$$

With:

M = the spectral radiant exitance (sometimes called emittance) in Wm^{-2} μm^{-1}
λ = wavelength in μ
T = absolute temperature in Kelvin
$C_1 = 3.74 \times 10^{-16}$ W m^2
$C_2 = 1.44 \times 10^{-2}$ m K

Integrating the equation X over all wavelengths (from λ=0 to λ=∞) , the total emittance of a black body can be found:

$$M = \sigma T^4 \quad \text{(Eq. 2.2)}$$

This is called the Stefan-Boltzman law and σ is Stefan-Boltzman Constant and equal to 5.669 x 10^{-8} W m^{-2} K^{-4}.

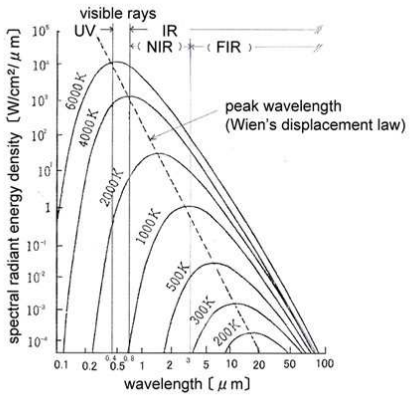

Figure 2.4: Radiant energy of the blackbody in each temperature (Planck's law).

Analyzing the curves in Fig.2.4 it can be noted that the spectral radiant emittance distribution is continuous with a single maximum for each temperature. As the temperature increases, the maximum shifts to the shorter wavelength and all over the spectral range the radiant exitance value is higher than that for lower temperatures.

The relation between the spectral peak for each temperature and the wavelength is given by the Wien's Displacement Law:

$$\lambda_{\max} T = C_3 \quad \text{(Eq. 2.3)}$$

This law gives for each temperature the wavelength at which the emittance is maximum. If λ_{max} is expressed in μm and T in °K, C_3 is constant and equal to 2897μmK^{-1}

Equation 2.1 is valid for a perfect emitter such as the blackbody. Real materials, usually referred as *grey bodies*, emit less than a blackbody does and do not necessarily absorb the entire energy incident upon them.
The emission of a real surface is defined with respect to the blackbody and is described by its *spectral emissivity*, ε(λ):

$$\varepsilon = \frac{M_{\lambda(material,\circ K)}}{M_{\lambda(blackbody,\circ K)}} \quad \text{(Eq. 2.4)}$$

Emissivity is dimensionless with the value ranging from 0 to 1 (0 for an on radiating source a 1 for a blackbody). The spectral emissivity is nearly independent of temperature but it is a function of the type of the material. Significant changes in spectral emissivity can be expected due to change of state (melting, vaporization), oxidation or any other changes that modify the arrangement of atomic and molecular components.

2.2.2 Source of EM radiation for remote sensing

For remote sensing the sun is the most important source of electromagnetic radiation. It emits as a blackbody radiator whose temperature is about 6000K (Fig. 2.5). Its radiation covers ultraviolet, visible, IR and radio frequencies and the maximum (according to the Wien's Displacement) is around 0.55μm within the visible region.

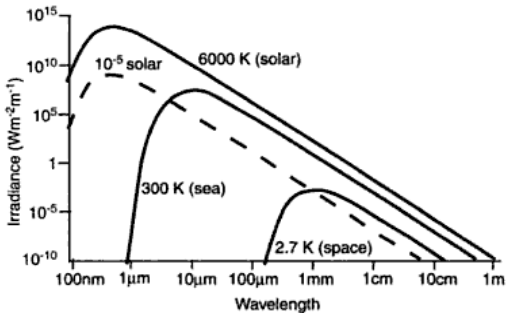

Figure 2.5: Emission spectra at different temperatures.

At the Earth's surface, the sun energy subtends a solid angle of about 7 x 10^{-5} sr, and so the irradiance is reduced by a factor of about 10^{-5} (dashed line in Fig. 2.5). Furthermore the solar radiation reaching the Earth's

surface is modified when passing through the atmosphere due to absorption and scattering phenomena as already mentioned in Par. 2.1.1 (Atmospheric windows).
The Earth's temperature, instead, is about 300K (Fig. 2.5). From the Wien's displacement law, this means the maximum spectral radiance existence from earth features occurs at a wavelength of about 9.7μm. Because this radiation is correlated with the Earth temperature it is called 'thermal infrared' energy.

The visible portion of the spectrum, to which our eyes are most sensitive, corresponds to both an atmospheric window and the peak energy level of the sun. Note also that heat energy emitted by the Earth corresponds to a window around 10 μm in the thermal IR portion of the spectrum, while the large window at wavelengths beyond 1 mm is associated with the microwave region.

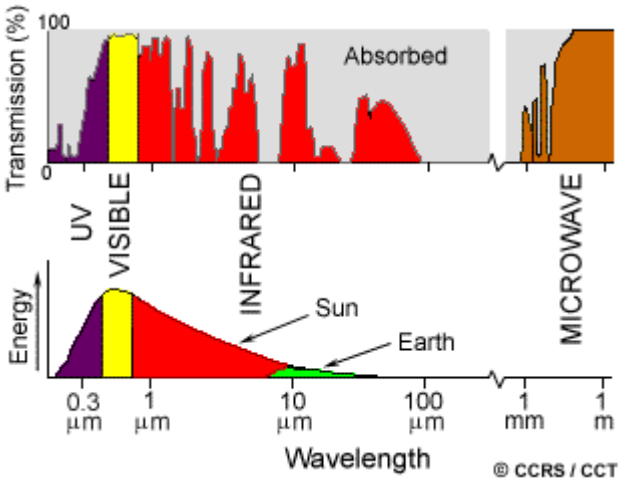

Figure 2.6: Atmospheric windows and Emission spectra at different wavelenght.

Hence, the choice of the portion of the spectrum to be used for remote sensing applications is ruled by the atmospheric transmission spectrum and by the source of the radiation.
When the sun is present we can observe earth features by measuring the reflected solar energy. Indeed most remote sensing systems are designed to collect reflected radiation: if land or sea features are to be observed by the reflection of incident solar radiation then the high frequency of solar

radiations spectrum should be used. Alternatively, if the self-emission of radiation by the sea or land is to be measured, sensors at lower frequency need to be used. The general division between reflected and emitted energy is about 3 μm: below this, reflected solar energy prevails, above it, the emission of the Earth becomes the dominant source for passive remote sensing (Fig, 2.7).

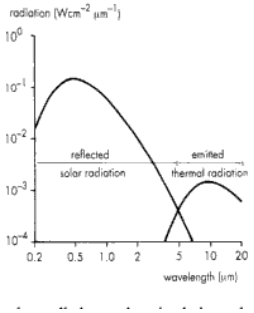

Figure 2.7: Reflected solar radiation and emitted thermal radiation of an average object

The spatial resolution of passive sensors mainly depends on their **Instantaneous Field of View (IFOV)**. The IFOV (Fig.2.8-left panel) is the angular cone of visibility of the sensor (A) and determines the area on the Earth's surface which is "seen" from a given altitude at one particular moment in time (B). The size of the resolution cell is then obtained by multiplying the IFOV by the distance from the ground to the sensor (C). In case of a scanning sensor with constant IFOV (Fig,2.8-right panel) the ground area represented by pixels at the nadir will have a larger scale then those pixels which are off-nadir. This means that spatial resolution will vary from the image centre to the swath edge. IFOV is a combination of geometric, mechanical and electronic properties of the imaging system. Geometric properties include satellite orbital altitude, detector size, and the focal length of the optical system (Simonett 1983).

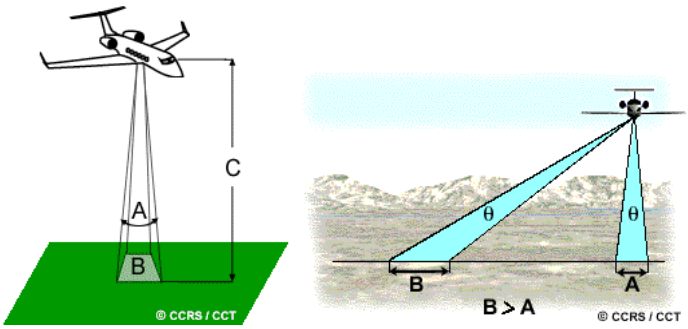

Figure 2.8: Instantaneous field of view

2.2.3 Active Sensors

Some sensors, such as radar systems, supply their own source of energy to illuminate features of interest. These systems are therefore defined as Active systems, in contrast to passive system that sense the energy naturally available.

RADAR stands for RAdio Detection And Ranging. RADAR systems are active sensors which provide their own source of electromagnetic energy. It consists fundamentally of a transmitter, a receiver, an antenna, and an electronic system to process and record the data. The transmitter emits radiation in a series of pulses at regular intervals which are focused by the antenna into a beam. The radar beam illuminates the surface obliquely at a right angle to the motion of the platform. When the energy reaches the target, some of the energy is reflected back towards the sensor.
Radars typically work at microwave frequencies that are able le to penetrate through clouds and most rain and can operate independently from the light of the sun. In Tab. 1 the common Radar Bands used for remote sensing applications are showed.

Band	Frequency	Wavelenght (most common)
X	8 to 12 GHz	2.5 to 4.0 cm (3.0 cm)
C	4 to 8 GHz	4 to 8 cm (6.0)
L	1 to 2 GHz	15 to 30 cm (24.0)
P	0.3 to 1 GHz	30 to 100 cm (65 cm)

Table 2.1: Typical radar working frequencies.

2.2.3.1 Radar Equation

The radar generates a short (microseconds) high power Radio Frequency (RF) pulse of electromagnetic energy. The radar then switches into receiving mode, and waits for the echo to return. The time delay is interpreted in terms of distance to the target.
The fundamental relation between the characteristics of the radar, the target, and the received signal is called the **radar equation**. The geometry of scattering from an isolated radar target (scatterer) is shown in the Fig.2.9, along with the parameters that are involved in the radar equation (Ulaby et al., 1982).

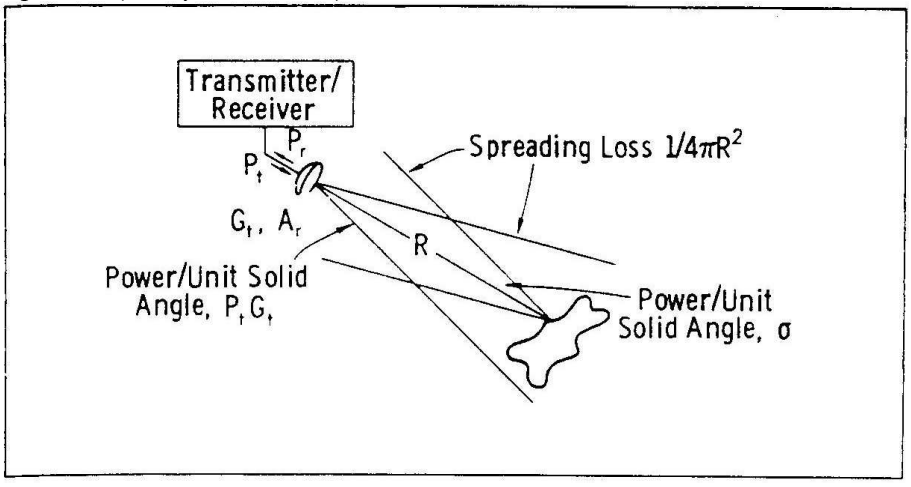

Figure 2.9: **Radar system description**

When P_t is the power transmitted by an antenna, G_t is the gain of the antenna (representing its directional characteristics), R is the distance between the transmitter and the target, the power density of the transmitted beam at the target or scatterer (power/unit area incident on it) is:

$$S_s = \frac{P_t G_t}{4\pi R_t^2} \quad \text{(Eq.2.5)}$$

Where:
P_tG_t = is the power per unit solid angle transmitted by the antenna in the direction of the scatterer
$1/4\pi R_t^2$ = is the reduction in the power density associated with spreading of the power over a sphere of radius R surrounding the antenna.

The power intercepted by the scatterer can be obtained by multiplying the power density S_s for the effective area of the scatterer A_{rs}:

$$P_{rs} = S_s A_{rs} \qquad \text{(Eq. 2.6)}$$

The effective receiving area of the scatterer is a function of its orientation relative to the incoming beam.
Some of the power received by the scatterer is absorbed in losses; it becames an antenna re-radiating with its own antenna pattern the rest of the energy in various directions. The fraction absorbed is f_a, so the fraction reradiated is 1- f_a and the total power reradiated by the scatterer is

$$P_{ts} = P_{rs}(1 - f_a) \qquad \text{(Eq. 2.7)}$$

The power is re-irradiated by the scatterer in all the directions but only a fraction is in the direction of the receiver. The fraction of power at the receiver can be hence described as

$$S_r = P_{ts} G_{ts} \frac{1}{4\pi R_r^2} \qquad \text{(Eq. 2.8)}$$

where
P_{ts} = the total power reradiated by the scatterer,
G_{ts} = is the gain of the scatterer in the direction of the receiver
R_r = distance from the receiving system
$1/4\pi R_r^2$ = is the spreading factor for the reradiation

The power entering the receiver P_r is then:

$$P_r = S_r A_r \qquad \text{(Eq. 2.9)}$$

Where A_r is the effective area of the receiving antenna.
Equation 2.8 and Equation 2.9 can be combined to obtain:

$$P_r = \frac{P_t G_t A_r}{(4\pi R_r R_t)^2} A_{rs}(1 - f_a) G_{ts} \qquad \text{(Eq. 2.10)}$$

The part $A_{rs}(1 - f_a)G_{ts}$ includes the factors associated with the scatterer. These factors are difficult to measure individually and their relative contributions are uninteresting to one wishing to know the size of the received radar signal. Hence one single factor is defined as Radar Cross Section and described as

$$\sigma = A_{rs}(1 - f_a)G_{ts} \quad \text{(Eq.2.11)}$$

The final form of the radar equation is therefore:

$$P_r = \frac{P_t G_t A_t}{(4\pi R_t R_r)^2} \sigma \qquad \text{(Eq. 2.12)}$$

In the most common cases the transmitter and receiver are the same (monostatic radar) therefore $R_t = R_r = R$, $G_t = G_r = G$ and $A_t = A_r = A$.
The effective area of an antenna is related to its Gain by:

$$A = \frac{\lambda^2 G}{4\pi} \quad \text{(Eq. 2.13)}$$

Hence the final equation radar can be written as

$$P_r = \frac{P_t \lambda^2 G^2 \sigma}{(4\pi)^3 R^4} = \frac{P_t A^2 \sigma}{4\pi \lambda^2 R^4} \quad \text{(Eq.2.14)}$$

Equation 2.14 shows that P_t, G and λ are parameters of the radar system, R is determined by the location of the radar with respect to the target. These parameters remain constant and are know during the use of the radar. The factor that governs the average return-power strength is therefore the *radar cross section* σ.

2.2.3.2 Parameter affecting the Radar Cross-Section

The radar cross section (RCS) represents the capability of a target to reflect radar energy toward the receiver and has units in m^2. It specifies the corresponding area of an isotropic scatterer that would return the same power as the observed signal.
The physical area of a target is normally greater than the radar cross section since a portion of the incident energy is scattered and absorbed by the target.

For remote sensing applications it is more useful to consider the radar cross section in a dimensionless form which is independent of the size of the illuminated area. It is therefore defined the **backscatter coefficient** (σ^0) or **normalized radar cross section** (NRCS) that measures the average radar cross section per unit area:

$$\sigma^0 = \frac{\sigma}{A_k} \quad \text{(Eq. 2.15)}$$

Where σ is the radar cross section and A_k is the area of the Earth illuminated by the radar (area of resolution cell).
The backscattering coefficient is typically expressed in logarithmic units (decibel – dB)

$$\sigma^0(dB) = 10\log_{10}(\sigma^0 lin) \quad \text{(Eq.2.16)}$$

The normalized Radar cross section is a function of a radar observation parameter (such as frequency, electromagnetic field polarization, incidence angle) and of the surface parameters (such as roughness, geometric shape and surface moisture).
Hereafter major dependence effects are detailed.

Dependence of the frequency

The frequency of the incident radiation determines the penetration depth of the electromagnetic waves and the roughness of the surface that can be observed. Generally the higher the wavelength used, the greater the backscattering. Furthermore penetration depth tends to be longer with longer wavelengths.
Consider the case of a forest as an observed scene: if X-band wavelengths (λ=3cm) are used the radiation can only penetrate the leaves on the top of the trees; if L-band wavelengths (λ=23cm) are used, the radiation can penetrate leaves and also small branches. This is true for various types of surface or target (Fig. 2.10).
It is important to highlight that the penetration depth is also related to the moisture of the target and the microwaves do not penetrate water more than a few millimeters.

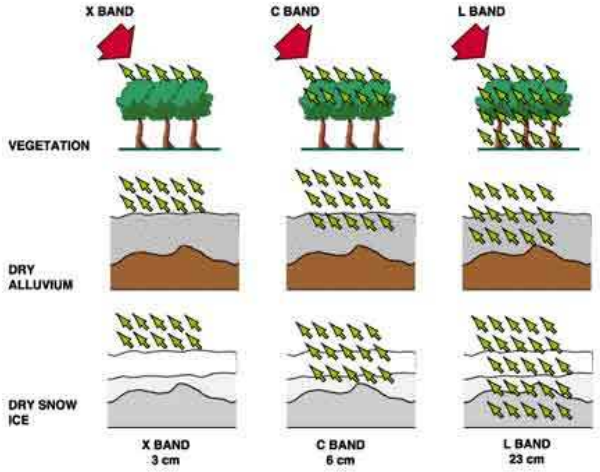

Figure 2.10: NRCS dependence from frequency

Dependence of polarization

Polarization describes the orientation of the electric field components of an electromagnetic wave. Radars can have different polarization configurations.
However, linear polarization configurations HH, VV, HV, VH are more commonly used: The first term corresponds to the polarization of the emitted radiation, the second term to the received radiation, so that X_{HV} refers to X band, H transmit, and V receive for example. For quasi vertical incidence angles, σ^0 is quite similar for the vertical and horizontal polarization. For a greater the incidence angle, σ^0 for VV polarization is higher than that for HH polarization. A crossed polarization signal (HV or VH) is always lower then the co-polarization cases (as in Fig. 2.11 for a case over the sea). The penetration depth of the radar wave varies with the polarization chosen. Polarization may provide information on the form and the orientation of small scattering elements that compose the surface or target: More than one bounce of backscattering tends to depolarize the pulse, so that the cross polarized return in this case would be larger than with a single bounce reflection.

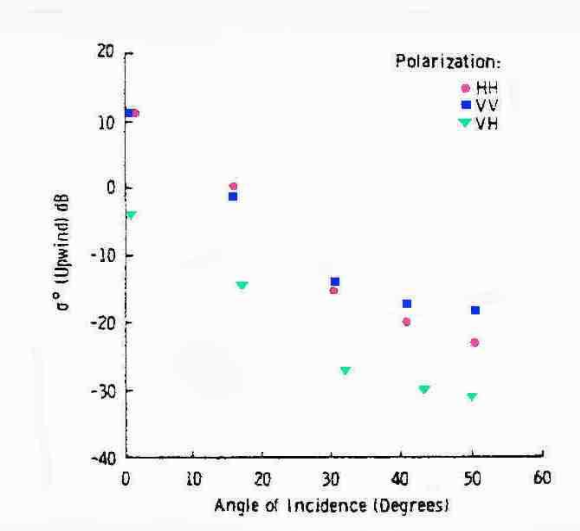

Figure 2.11: Radar cross section (over the sea) dependency from polarization.

Dependence of incidence angle

The incidence angle is defined as the angle between the axis of the incident radar beam and a perpendicular to the surface that the signal beat. The incidence angle changes across the radar image *swath*; it increases from *near range* to *far range*.
In general, reflectivity from distributed scatterers decreases with an increasing incidence angle. Ulaby et al. (1978) performed experimental measurements using five bare soil surfaces to describe the angular patterns of the backscattering coefficients for the slight rough and very rough surfaces but with similar moisture content (Fig.2.12).

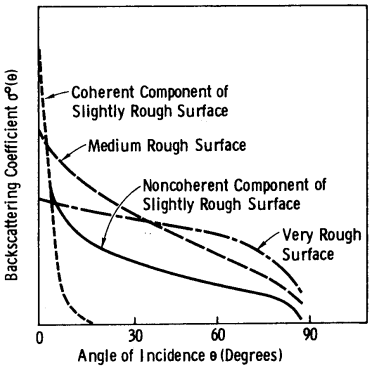

Figure 2.12: angular variation of the backscattering coefficient for different Surface-roughness conditions

It appeared that, when using the L band (1.1 GHz), the backscatter of smooth fields was very sensitive to near nadir incidence angles; on the other hand, in the case of rough fields, the backscatter was almost independent of the incidence angle chosen.

Dependence on Roughness

A wave incident upon a rough-surface boundary is partially reflected in the specular direction and partially scattered in all directions. Monostatic radar receive the backscattered component of the scattered energy. An illustration of rough-surface scattering is shown in Fig. 2.13: the scattering amplitude along the specular direction decreases while backscattering increases as the surface gets rougher (Ulaby at al., 1982).

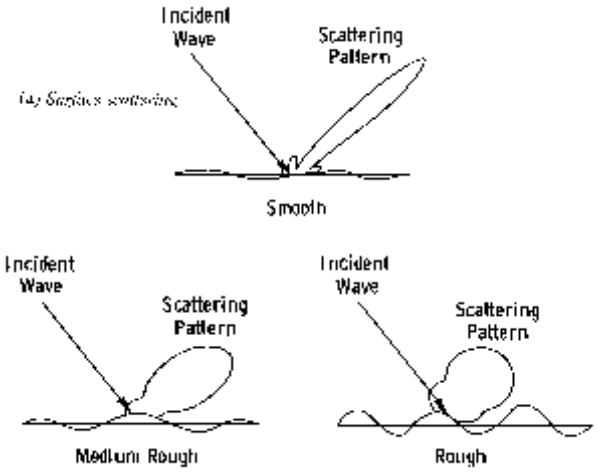

Figure 2.13: Examples of surface-scattering patterns

The definition of roughness depends on the wavelength used and the incidence angle according to the Rayleigh Criterion: a surface is considered "rough" if its surface structure has dimensions that are comparable to the incident wavelength.
According to this criterion, a surface is considered smooth if

$$h < \frac{\lambda}{8\cos\theta} \qquad \text{(Eq.2.17)}$$

and is considered rough if:

$$h > \frac{\lambda}{8\cos\theta} \qquad \text{(Eq.2.18)}$$

Where:
h= mean height of surface variations
λ= wavelength
θ = incidence angle

Water bodies generally have a dark tonality on radar images, except in the case of wind-stress or current that increases the water surface

roughness, which provokes a high backscatter. In the microwave region, this difference between respective properties of land and water can be extremely useful for such applications as flood extent measurement or coastal zones erosion.

Dependence on Moisture

The backscattering coefficient is dependent on the moisture of the observed scene through the dielectric constant of the landscape materials.
The dielectric constant is a measure of the ability of a substance to conduct electrical energy. It consists of two parts (permittivity and conductivity) that are strongly dependent on the soil moisture content. In the microwave region, most natural materials have a dielectric constant between 3 and 8, in dry conditions. Water has a high dielectric constant (80), which is at least 10 times higher than for dry soil. The presence of liquid water strongly increases the dielectric constant in the microwave region, making σ^{o} very sensitive to moisture (Fig. 2.14).

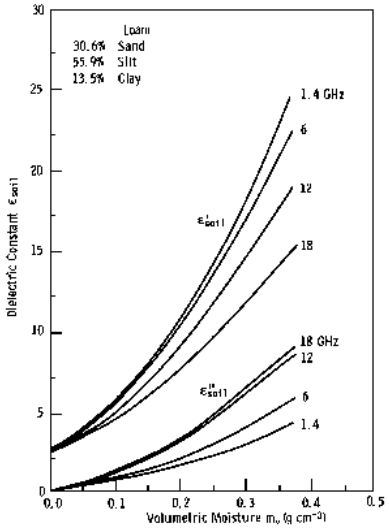

Figure 2.14: variation of dielectric constant as function of volumetric soil moisture

As a result, a change in moisture content generally provokes a significant change in the dielectric properties of natural materials; increasing moisture is associated with an increased radar reflectivity (Fig. 2.15).

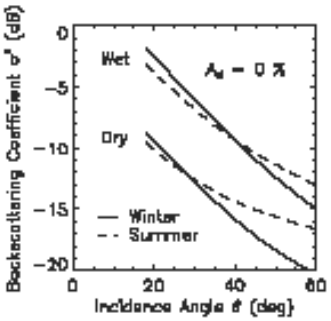

Figure 2.15: Backscattering coefficient as function of the incidence angle for wet and dry conditions.

The moisture also influences the skin depth: the electromagnetic wave penetration in an object is an inverse function of water content.

2.2.3.3 Radar Geometry and Resolution

For active sensors, the platform (in Fig. 2.16) travels forward in the flight direction **(A)** with the nadir **(B)** directly beneath the platform. The microwave beam is transmitted obliquely at right angles to the direction of flight illuminating a swath **(C)** which is offset from nadir. Range **(D)** refers to the across-track dimension perpendicular to the flight direction, while azimuth **(E)** refers to the along-track dimension parallel to the flight direction. The side-looking viewing geometry is typical of imaging radar systems.

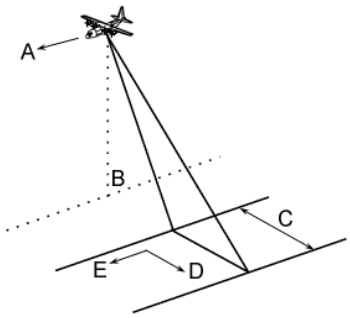

Figure 2.16 Remote sensing systems geometry

A pulse of energy is transmitted from the radar antenna, and the relative intensity of the reflections is used to produce an image of a narrow strip of terrain. Reflections from larger ranges arrive back at the radar after proportionately larger time. When the next pulse is transmitted, the radar will have moved forward a small distance and a slightly different strip of terrain will be imaged. These sequential strips of terrain will then be recorded side by side along the azimuth direction.

The geometry parameters are:

- Near range = portion of the image swath closest to the nadir track
- Far range = portion of the swath farthest from the nadir
- Ground range = the true horizontal distance along the ground corresponding to each point measured in slant range.
- Azimuth = The term azimuth is used to indicate linear distance or image scale in the direction parallel to the radar flight path. Azimuth is also known as along-track direction, since it is the relative along-track position of an object within the antenna's field of view following the radar's line of flight.
- Slant range = radial line of sight distance between the radar and each target on the surface
- Look angle (or elevation angle) = is the angle at which the radar looks at the surface.
- incidence angle = the angle between the radar beam and ground surface which increases, moving across the swath from near to far range.
- Depression angle = generally refers to the line of sight from the radar to an illuminated object as measured from the horizontal plane at the radar.

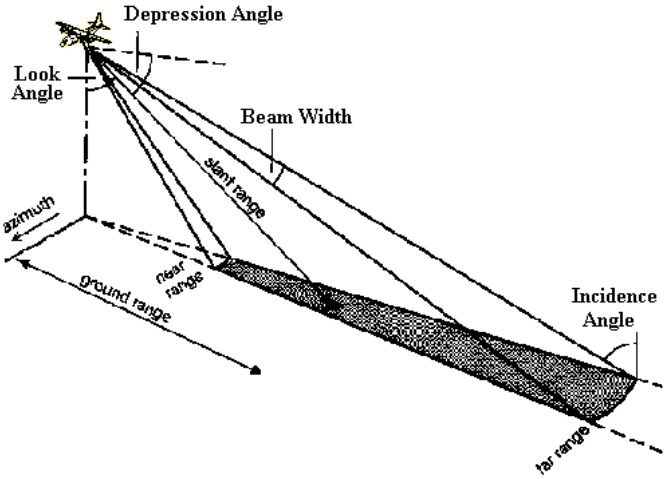

Figure 2.17: Radar geometry

Radars that generates an image in which the digital number of each pixel is determined by the strength of the radar signal reflected from the corresponding scene are named **imaging radar**.
The radar resolution depends on one or more of the following quantities: angle, range and speed.
The angular discrimination depends on the antenna (Antenna pattern): the narrower the beamwidth, the higher the resolution.
The range resolution is obtained by a time-delay measurement of the returned echo as the constant speed of the EM wave is known. The speed measurements depends on the Doppler frequency shift of the received frequency, which is proportional to the relative speed between the area senses and the radar system. The geometry of a radar system is such that different points on the Earth the surface have different relative speeds. Therefore, by using the appropriate frequency filters it is possible to discriminate between signals from different parts of the area observed.

Radars that do not use the speed resolution are called RAR (Real Aperture Radar): the azimuth resolution is proportional to the distance between the radar and the target (slant-range). Finer details on the ground can be resolved by using a narrower beam. The beamwidth is inversely proportional to the size of the antenna, i.e. the longer the antenna, the narrower the beam.

Radars that use the combination of the range and speed discrimination are called SAR (Synthetic Aperture Radar). SAR uses signal processing to synthesize an aperture that is hundreds of times longer than the real antenna by operating on a sequence of signal recorded in system memory. As it passes a given scatterer, many pulses are reflected in sequence. By recording and then combining these individual signals, a 'synthetic aperture' is created during the processing.

3 SATELLITE INSTRUMENTS

In this chapter the active and passive satellite instruments used to carry out this research project are described.
For the activity concerning the surface water mapping the following instruments are described:

- the passive sensors Thematic Mapper (TM) and the Enhanced Thematic Mapper Plus (ETM+) on board respectively the satellites Landsat 5 and Landsat 7.
- SAR and ASAR, radars on board the ESA satellites ERS-2 and ENVISAT.

While for the research activity concerning the soil moisture, the Scatterometer sensor on board the ERS satellite is described in terms of its principles of acquisition, processing and the main events which have occurred since the beginning of the mission.

3.1 TM/ETM+

The **Landsat program** is the longest running enterprise for acquisition of imagery of the Earth from space. The first Landsat satellite was launched in 1972; the most recent, Landsat 7, was launched on April 15, 1999.

Since the first satellite in 1972, this highly successful program has collected a great quantity of data from around the world from several Landsat satellites. Its success is due to several factors, which includes: the combination of sensors with spectral bands tailored to Earth observation; functional spatial resolution; and good areal coverage (swath width and revisit period). The Landsat system provides global coverage between 81 degrees north latitude and 81 degrees south latitude.

Currently only Landsat 5 (launched in 1984) and Landsat 7 (launched in 1999) are still in operation.

Landsat satellites scan the Earth's surface across the satellites' track as the satellites move in their descending orbit (moving from north to south) over the sunlit side of the Earth, so that they cross every point on the Earth about the same time once every few weeks. Landsat satellites cross the equator in the morning, anytime from 8:30 to 10:00 a.m. (local time). Both Landsat 5 and 7 have a repeat Coverage of 16 days and they have been counter-synchronized so that they provide data for any given area on the Earth every 8 days.
The Landsat 5 satellite was launched with the on board **Thematic Mapper (TM),** an advanced, multispectral scanning, Earth resources sensor designed to achieve higher image resolution, sharper spectral separation, improved geometric fidelity and great radiometric accuracy and resolution.
It has been designed to simultaneously collect the reflected energy in six spectral bands (1-5 and 7) and the emitted energy from band 6. This band senses thermal (heat) infrared radiation hence it is the only capable of acquiring night scenes. A TM images a swath that is 185 km wide and provides images with a spatial resolution of 30 square meters in bands 1-5 and 7 while band 6 has a resolution of 120 square meters on the ground (Tab. 3.1).

Band No.	Wavelength Interval (μm)	Spectral Response	Resolution (m)
1	0.45 - 0.52	Blue-Green	30
2	0.52 - 0.60	Green	30
3	0.63 - 0.69	Red	30
4	0.76 - 0.90	Near IR	30
5	1.55 - 1.75	Mid-IR	30
6	10.40 - 12.50	Thermal IR	120
7	2.08 - 2.35	Mid-IR	30

Table 3.1 Landsat 5 TM spectral bands

Radiometrically, the TM sensor has a quantization range of 256 digital numbers (8 bits) which permits observation of small changes in radiometric magnitudes in a given band and a sensitivity to changes in relationships between bands.

Landsat 7 was successfully launched on April 15, 1999 and it is equipped with the Enhanced Thematic Mapper Plus (ETM+) that replicates the capabilities of the highly successful Thematic Mapper instruments on board Landsat 5. Landsat ETM+ imagery however has an extra panchromatic band which is able to produce images at 12.5m resolution. This allows panchromatic-sharpened multispectral images (panchromatic and multispectral merged imagery with 7 band spectral resolution and 12.5m spatial resolution) created without rectifying the imagery to one another. This is because the panchromatic and multispectral imagery will automatically be registered as they have both been scanned by the same sensor. The Landsat ETM+ imagery also has an enhanced thermal IR band with 60m resolution (Table 3.2).

Band No.	Wavelength Interval (μm)	Spectral Response	Resolution (m)
1	0.45 - 0.52	Blue-Green	30
2	0.53 - 0.61	Green	30
3	0.63 - 0.69	Red	30
4	0.78 - 0.90	Near IR	30
5	1.55 - 1.75	Mid-IR	30
6	10.40 - 12.50	Thermal IR	60
7	2.09 - 2.35	Mid-IR	30
8	0.52-0.90	Panchromatic (visible - near infrared)	15

Table 3.2: Landsat 7 ETM+ spectral bands

These characteristics make the ETM+ a more versatile and efficient instrument for global change studies, land cover monitoring and assessment, and large area mapping than its design forebears.

The bands used for both TM and ETM+ were chosen for their value in water penetration, discriminating vegetation types and vigor, plant and soil moisture measurements, differentiation of clouds, snow and ice and identifying rock types. Here are some detailed capabilities for each band:

Band 1 Blue-green: Bathymetric mapping along the coast, useful for soil-vegetation differentiation and forest types;
Band 2 Green: is sensitive to water turbidity differences; As it covers the green reflectance peak from leaf surface it is useful to separate vegetation (forest, cropland with standing crop) from soil.
Band 3 Red: sense in a strong chlorophyll absorption region and strong reflectance region for most soils.
Band 4 Reflected IR: operates in the best spectral region to distinguish vegetation varieties and conditions. Since water is a strong absorber of near IR, this is useful to delineate water bodies.
Band 5 Reflected IR: Discriminates moisture content of soil and vegetation and penetrates thin clouds
Band 6 Thermal IR: Useful for thermal mapping and estimated soil moisture
Band 7 Reflected IR: Useful for mapping hydrothermally altered rocks associated with mineral deposits
Band 8 Panchromatic (only Landsat 7): for "sharpening" of multispectral images
The bands may also be combined in various ways by assigning one band to each of the three visible channels (red, green, blue) to create a false colour image.

3.2 ESA SATELLITE RADARS

The first ESA remote sensing satellite, ERS-1, was launched in 1991 and operational until March 2000. It was followed by ERS-2 in April 1995 which is still into operation. To carry out their mission, ERS satellites orbit so that the instruments can scan along predetermined paths designed to give optimum coverage for a set number of orbits. The elliptical orbit is sun-synchronous, near polar, with a mean altitude of

785 km, an inclination of 98.5deg. and a local solar time at the descending node of 10.30 a.m.
Among different instruments, ERS satellites carry on board an Active Microwave Instrument (AMI) that consists of 2 different C-band non-nadir looking radars (5.3 GHz) which share common electronics: SAR (Synthetic Aperture Radar) and Scatterometer. The AMI is operated in either image (SAR) or Wind (Scatterometer) mode. Another possible working mode is the Wind/Wave mode which consists of nominal Scatterometer operations interrupted every 30 seconds (roughly 200km) by a couple of seconds of a short SAR operation to acquire small SAR 'imagettes'.

To ensure the continuity of the data measurements of the ERS satellite, in March 2002, ESA launched the ENVISAT satellite, with an ambitious and innovative payload. Envisat flies in a sun-synchronous polar orbit of about 800-km altitude. Among all the instruments, the ENVISAT satellite carries on board the ASAR (Advanced Synthetic Aperture Radar), operating at C-band, that ensure continuity with the image mode and wave mode of the ERS satellites. ENVISAT does not carry on board the Scatteromer instrument but Metop satellites series operated by EUMETSAT is ensuring the continuity of Scatterometer acquisition since October 2006.

Before proceeding with the instruments description it could be helpful to define the following terms that could be useful for comprehension in the further sections:
Mission Phase: Part of a satellite mission with a ground track pattern distinctive from the previous and following phases. So for any change of a repeat cycle period we have a new mission phase. For instance ERS-1 has mission phases A through G; ERS-2 only has mission phase A. For ERS-2 the story is relatively simple. The first full cycle (Cycle 1) started on 15 May 1995, 22:29:38 UTC with the equator crossing on an ascending arc closest to the Greenwich Meridian. Since then every 35.000 days a new cycle starts.

Cycle: A cycle is one full completion of the repeat period. A cycle starts by definition on an ascending pass closest to the Greenwich Meridian. In the ESA definition it starts at the equator on that pass, of the ascending pass. Both ERS and ENVISAT satellites have a repeat cycle of 35 days.

Orbit: An orbit is one full revolution of the satellite starting and ending at an ascending node (ascending equator passage - ANX).

Pass: A pass spans half an orbital revolution and is either ascending (South-North) or descending (North-South). This means that a pass always starts at the turnover point, i.e. the crossing of the South or North Pole. Odd pass numbers are ascending, even are descending.

3.2.1 SAR/ASAR

The SAR and ASAR instruments which are respectively on board the ERS-2 and ENVISAT satellites, are non-nadir looking imaging radars. As described in Par. 2.3.3, the radar antenna transmits microwave pulses towards the earth surface and the energy scattered back to the spacecraft is measured. The SAR makes use of the radar principle to form an image by utilizing the time delay of the backscattered signals.

SAR on board **ERS-2** satellites has an antenna 10m long emulating a synthetic antenna of about 4km. It operates at C-band in a single configuration: 23° of incidence angle (the central part of the swath) in VV polarization.

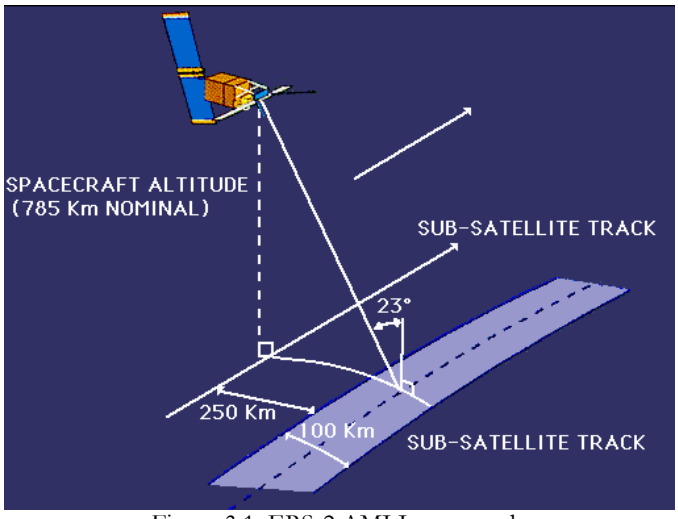

Figure 3.1: ERS-2 AMI Image mode

As described in Par.3.2, the SAR is a part of the AMI instrument which can operate in *image* or *wave* modes. In *image mode* (Fig. 3.1) the ERS-2 SAR illuminates a swath of about 102 km located at 250km to the right of the sub-satellite track. The instrument provides high resolution two-dimensional images with a spatial resolution of 26 m in range (across track) and between 6 and 30 m in azimuth (along track). In the AMI *Wave Mode* (see Fig. 3.2) instead, the SAR generates 5x5 km images (also called 'imagettes') at interval of 200 km along track with a spatial resolution of about 10m. The SAR wave mode provides a global sampling of two-dimensional spectra of ocean surface waves.

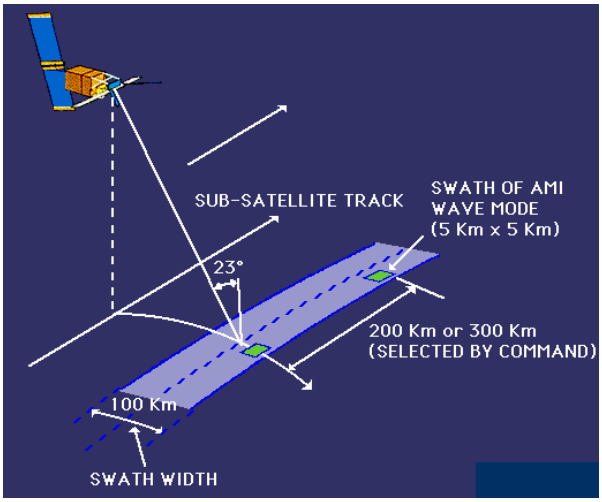

Figure 3.2: ERS-2 AMI Wind/Wave mode.

The **ASAR** (Advanced Synthetic Aperture Radar) on board the ENVISAT satellite ensure continuity of ERS-2 data. As for SAR, ASAR operates at C-band but its features have enhanced capabilities in terms of coverage, range of incident angles, polarization and modes of operation. ASAR indeed works with different acquisition modes that vary for the incidence angles, the polarization and the spatial resolution. Improvements in image and wave mode beam elevation steerage allow the selection of different swaths, providing a swath coverage of over 400-km wide using ScanSAR techniques. Furthermore the transmitted and the received polarization can be selected together allowing for scenes to be imaged simultaneously with alternating polarization.

ASAR can operate as conventional Stripmap SAR (also know as Image mode) or as a ScanSAR.
When operating as a StripMAP the antenna has the flexibility to select an imaging swath by changing the beam incidence angle and the elevation beamwidth. In this mode ASAR has a swath width between approximately 56 km and 100 km across-track and a resolution of about 30m. So even though the image mode allows for a more precise measurement, the swath is small. In the Image Mode (IM), ASAR operates in one of seven predetermined swaths with either vertically or horizontally polarized radiation; the same polarization is used for transmit and receive (i.e., HH or VV). Swath width is between approximately 56 km (swath 7) and 100 km (swath 1) across-track. Spatial resolution is approximately 30 m (for precision product).
To improve the swath width, ASAR uses the ScanSAR principle: the swath width is increased by electronically changing the elevation of the antenna beam. Radar images are then generated by scanning the incidence angle and sequentially synthesizing images for the different beam positions. Each area imaged is named a sub-swath. The principle of the ScanSAR is to share the radar operation time between two or more separate sub-swaths in such a way as to obtain the full image coverage of each. In ScanSAR mode ASAR uses five predetermined overlapping antenna beams which cover the wide swath of about 400 km by 400 km. Spatial resolution is approximately 150 m by 150 m for a nominal product.

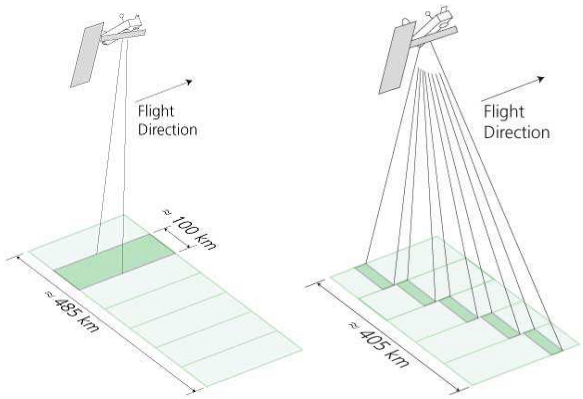

Figure 3.3 ASAR Image Mode (left panel) and ASAR Wide Swath Mode (right panel)

An additional ASAR measurement mode, called Alternating Polarization Mode is also possible. Instead of scanning between different elevation sub-swaths, the Alternating Polarization Mode scans between two polarizations, HH and VV, within a single swath (which is preselected, like the Image Mode).

SAR/ASAR data products can be generated with different levels of SAR signal processing, from Level 0 (raw data) to data completely calibrated, geocoded and corrected. In this study SAR/ASAR Precision Images (PRI) have been used. The Precision Image is a multi-look ground range image. The product is calibrated and corrected for the SAR antenna pattern but the image is not geocoded, and terrain distortion has not been removed.

3.2.2 The ERS Scatterometer

The ERS Wind Scatterometer is a radar remote sensing instrument which is capable of measuring the normalized backscattering σ^0 of the ocean surface with great radiometric accuracy and under multiple observations, i.e. azimuth angles. These measurements are independent of cloud coverage and the sun's illumination and provide a global coverage within 2 to 4 days. The Scatterometer has been originally designed for wind retrieval over the ocean but now it is proved that, despite the coarse resolution, the data may be also useful to other applications over land which requires high spatial resolution products and long term backscatter information such as soil moisture, vegetation and ice cover.
The Scatterometer deployed on board of the ERS satellites mission is composed of three antennas that make almost instantaneous three σ^0 measurements at different azimuth angles. The antennas point to the right of the space-craft in three directions: 45 degrees forward (Fore beam), sideways (Mid beam) and 45 degrees backwards (Aft beam) with respect to the satellite flight direction (Fig. 3.4).

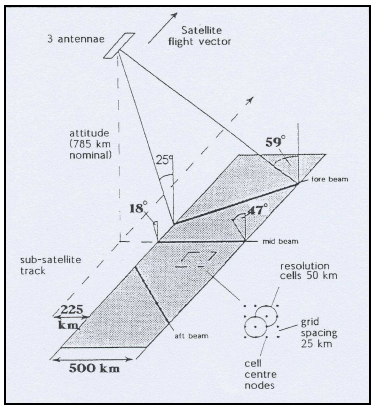

Figure 3.4: ERS-2 Scatterometer

As the satellite moves along its orbits the antennae illuminate a 500km wide swath. Since the beginning of the ERS missions, the backscattering measurements acquired from each antenna have been provided referred to overlapping resolution cells of 50km using a grid spacing of 25km. Meaning that, along the swath there are 19 nodes (Fig. 3.5).

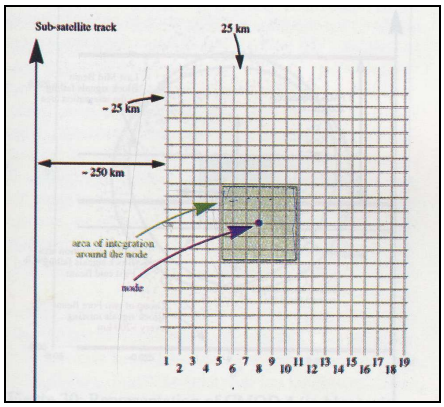

Figure 3.5: Scatterometer Node localization

The incidence angle across the swath varies from a minimum of about 18° at near range to a maximum of about 56° at the far range. Due to the different azimuth angles between Fore/Aft beams and Mid beam, side antennae have the same incidence angle which is greater than the central one. In Tab. 3.4 the incidence angles for each antenna.

Node	Mid Antenna [deg]	Fore/Aft Antenna [deg]
1	18.0	24.8
2	19.8	27.3
3	21.6	29.6
4	23.4	31.9
5	25.2	34.1
6	26.9	36.2
7	28.6	38.2
8	30.2	40.1
9	31.8	42.0
10	33.3	43.8
11	34.9	45.5
12	36.3	47.1
13	37.7	48.7
14	39.1	50.1
15	40.5	51.6
16	41.8	53.0
17	43.0	54.3
18	44.2	55.5
19	45.4	56.7

Table 3.3: Scatterometer beams incidence angles.

Due to the satellite movement, subsequent pulses of each antenna illuminate adjacent areas along the satellite direction (Fig.3.6)

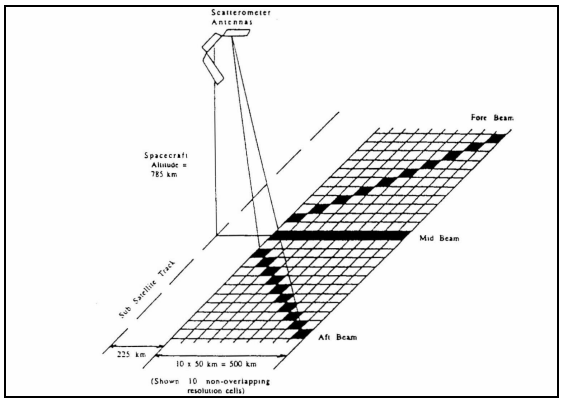

Figure 3.6: Scatterometer geometry acquisition

The result is three independent backscatter measurements for each cell center node on a 25-km grid, obtained fro the three different viewing directions, 2 different incidence angles and separated by only a very short time delay. It should be noted that different incidence angles and look directions provide enhanced geometric sensitivity of the backscatter measurements.

3.2.3 Sigma nought acquisition and processing

The three antennae operates in sequences of 32 Radio Frequency pulse each starting with the Fore Antenna (F, M, A, F, M, A,…).
The Pulse Repetition Interval (PRI) is 10.21 ms for the side antennae and 8.7 ms for the mid antenna, with the total length of a repeat cycle (called a FMA sequence) of 940.84 ms. Four FMA sequences last 3.763 seconds and correspond to 25 km along the sub-satellite track when the satellite is at an altitude of 785 km and is continuously repeated in the Wind mode with any gaps. The fixed duration of this sequence means that it does not always correspond exactly to 25 km along the subsatellite track as the satellite altitude varies over the total ERS orbit. The echoes are sampled at 30 KHz that correspond roughly to 5.2 km on the ground at an 18° incidence angle (Mid) and about 13.3 km at a 68° incidence angle (side beams) (Lecomte, 1998).
Due to the relative motion between the satellite and the Earth the transmitted signal and the echo don't have the same frequency because

of the Doppler shift. This depends on the satellite velocity, the antenna look angle and the earth's rotation. The range of the Doppler shift is low for the Mid Beam and higher for the side beams. By yaw-steering the satellite, the doppler shifts in the mid antenna are minimized but not entirely compensated. Therefore continuous frequency tuning of the Scatterometer receiver is required to keep the echo signals within the nominal range.

The digital radar echoes acquired by the three antennae are converted into backscattering coefficients on the defined grid during the on ground processing. The main processing steps to be performed are listed in sequence below [Lecomte, 1998, Wagner, 1998]:

• *Resampling*: data are resampled to avoid aliasing during later processing steps.

• *Doppler compensation:* an on-ground Doppler correction is performed to improve the on-board compensation of the Doppler shift of the returned signal due to the spacecraft motion and Earth rotation.

• *Low pass filtering:* to improve the signal to noise ratio data are low pass filtered. Until the output of this stage, data are represented in complex format (I and Q).

• *Envelope detection:* during this step the instantaneous signal power is calculated by summing the square of each I and Q samples.

• *Block averaging:* samples with the same echo time are averaged over a block of 32 pulse. This stage is done to reduce both the data throughput for the following steps and the variance of the signal power samples.

• *ADC-non linearity correction*

• *Noise correction:* this step is done to improve the measurement accuracy;

• *Internal calibration correction:* to compensate for the transmitter and the receiver fluctuations;

• *Power to σ^0 conversion*: conversion to relate the measured signal power to the wanted quality σ^0 (radar Backscattering coefficients per unit area).

• *Spatial filtering:* echo signal samples are averaged to increase the radiometric resolution of the final σ^0 values. The spatial filtering process consists of two different steps:

1) Calculation of the node positions on the earth's surface in an adequate coordinate system,
2) Weighted integration of samples belonging to an area around these nodes (integration area).

The calculation of the nodes position is based on the Mid antenna: the central node of the swath (node 10) is firstly located at the intersection of the Mid antenna line of sight with the earth (defined by GEM6) (see Fig. 3.7).

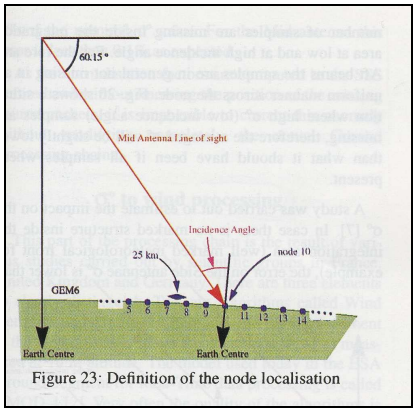

Figure 3.7: Definition of node localization

The other nodes are then localized every 25 km in both directions to generate a regular grid. A total of 19 nodes are localized like that for a given Mid antenna measurement block. This is repeated every four measurement blocks (equivalent to four FMA sequences), which corresponds to 3,763.36 ms or roughly 25 km on ground.

After that to the block signal samples belonging to an area around each node an *averaging process* is applied. This process gives a high weight to the samples near the node and a low weight to those far from the node (weighted averaging). The contributions of the pulses from this area are weighted by a Hamming function which takes the following form:

$$w(n) = \alpha + (1-\alpha)\cos\left(\frac{2\pi}{N}n\right) \qquad (3.1)$$

where $|n| = \frac{N}{2}$ and α=0.54.

The Hamming is a cosine squared function which sites on a pedistal above the zero level (Fig. 3.8).

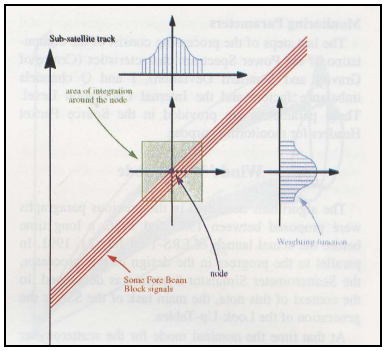

Figure 3.8: Funzione di Hamming

The dimension of the Hamming window influences the spectral and spatial resolutions. For the side beams the Hamming function is 84.5 x 84.5km along and across track while for the Mid Beam is 86x86 km.

3.2.4 Geophysical parameter retrieval

Once the σ^0 for each grid point is computed, applying suitable algorithms is it possible to retrieve geophysical parameters from the backscattering coefficient.
As already mentioned, the main purpose of the Scatterometer is to obtain information on wind speed and direction over the ocean. The backscattering mechanism over water is dominated by the Bragg resonance, which describes the interaction of the radar signal with capillary waves, generated by the near-surface winds that have a wavelength of a few centimeters (Stoffelen, 1998).
The relationship between the near-surface vector winds and the normalized radar cross section of the ocean surface is described by a geophysical model function (GMF). The model used in the near-real time ERS Scatterometer processing is the semi-empirical model CMOD4 that provides wind speed and direction at 10 m above the surface. (Stoffelen, 1997)
Since the beginning of the ERS mission, Scatterometer data is stored in the so called UWI products and delivered to the users. Each product consist of 19x19 nodes corresponding to the 500 x 500 km2 area on the ground. For each nodes the geographical location, the sigma nought for the three antennas and the respective incidence and azimuth angles are

provided together with the wind speed and direction and quality flags (Lecomte, 1998).

Though the Scatterometer was designed for wind retrieval over the ocean, many studies highlighted that Scatterometer data may be also useful for other applications over land (Liu, 2002). This is because radar backscattering from land depends on a combination of surface and volume scattering associated with the radar penetration depth. The surface roughness, vegetation cover, and terrain dielectric properties play an important role in determining the dominant backscatter regime. This allows assessing surface type, vegetation cover, and soil moisture content (www.eumetsat.int).
While it is easy to distinguish land from sea trough the use of land-sea mask more difficult is discriminating between sea-ice and open water. Several methods have been proposed to discriminate between them (Liu, 2002; Neyt, 2004) but none of them is currently used in order to operationally provide sea ice data information.

3.2.5 ERS-2 SCAT Mission Events

The ERS-2 Scatterometer mission started in April 1995 and is still into operation. On 16th November 1995 the first Scatterometer data was received.
Since 15th January 1996 to 19th March 1996 the commissioning phase was carried out. During this period the in-flight antenna pattern and the exact gain constant were computed. The calibration level was set at the same level of ERS-1 Scatterometer to assure continuity and data homogeneity between the two missions. The distribution of calibrated data to the users started on 16 April 1996.
ERS-2 was piloted in yaw-steering mode using three gyroscopes since the beginning of the mission until February 2000, when a new yaw-steering mode using only one gyroscope was implemented. The ERS-2 gyroscopes had experienced several problems during the mission. In January 2001, after the failure of 5 of the 6 gyroscope, a new test piloting mode using no gyroscopes, the Extra-Backup Mode (EBM), was implemented as a first stage of a gyro-less piloting mode. The aim of this challenging mode was to preserve the one remaining gyroscope for the

orbital manoeuvres. With that new configuration the satellite attitude was slightly degraded in particular for the yaw angle (Crapolicchio, 2004).
The impact in the received signal of the satellite mispointing cannot be corrected in the existing ground processor mainly based on pre-computed Look Up Table derived with the assumption of a very high stability of the spacecraft. As consequence the backscattering coefficients derived from the returned echoes were not calibrated anymore and the distribution of the Scatterometer data to the users was discontinued.
A more accurate version of this zero-gyro mode (ZGM) was operationally used since June 2001 and the performance was further improved with the implementation of the yaw control monitoring mode (YCM) at the beginning of 2002. With this configuration a good improvement in the yaw error pointing was achieved (roughly from 10° to 2°).
A complete review of the Scatterometer processor has been carried out to guarantee the continuity of the ERS Scatterometer mission with the nominal high data quality (Neyt, 2002). ESA contractor engineers, research department and industries had been involved to re-design and re-implement the Scatterometer ground processing chain and in about two years a new ground processor called *ESACA* (ERS Scatterometer Attitude Corrected Algorithm) has been put into operation on August 21st 2003. From that day onward Scatterometer data are available for the end users and meteorological centre via the GTS network.
A further event that had a strong impact on the Scatterometer mission occurred at the end of June 2003 when the two on-board tape recorders have been declared unusable. That fact caused the lost of the global Earth coverage because the data cannot be recorded on-board (in Fig. 3.9 the Global Mission Scenario is shown).

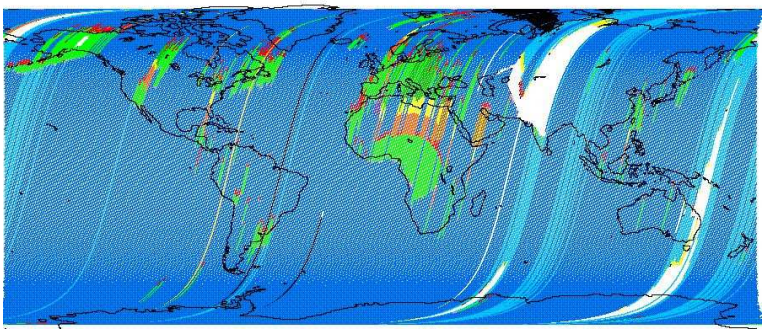

Figure 3.9. ERS-2 Global Mission Scenario

To face out that problem, on one side the ESA engineers reconfigured the Instrument Data Handling and Transmission (IDHT) on board the satellite in such a way to allow the transmission of the data on the ground every time the satellite is within the visibility of an acquisition station and on the other side ESA is continuous improving the data coverage by deploying new ground stations. An example of the data coverage for the "Regional Mission Scenario" currently available is shown in Fig. 3.10 (ascending passes during Cycle 140).

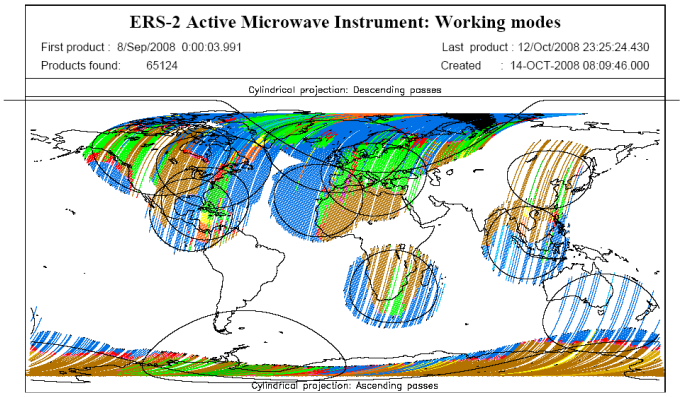

Figure 3.10: ERS-2 Regional Mission 2003 – 2010: ascending passes coverage during Cycle 140.

4 WATER SURFACE ESTIMATION

An accurate mapping of inland water surface is essential for hydrological modeling, flood monitoring and water resources assessment. Since space borne sensors provide the possibility to cover large areas with minimum acquisition time, remotely sensed data soles out to be the only practical source of information for large-scale surface water mapping. Satellite data can also cover remote or inaccessible areas which are impossible to monitor from the ground.
In this chapter results from the analysis performed on radar and optical imagery to evaluate how accurately water surface could be mapped with satellite techniques are presented.
A multi-sensor approach has been undertaken by analyzing images from both active and passive sensors. This choice was led by the necessity to overcome limits due to both kind of sensors.
During extreme events such as flooding, data from optical sensors are limited by cloud cover, which is a typical presence in case of this kind of events. Limitation due to cloud cover could be overcome by using a radar system, such as the SAR which provides information independent of light and weather conditions. SAR however has a low penetration capacity of vegetation and therefore is not completely able to solve ambiguities in the image.

Water bodies hold different radiometric characteristics between radar and optical satellite images due to the different kind of imaging principles (Zhang et al., 2006).
In radar images the identification of a water body (even in the case of floods) is possible as the backscattering is low over the water surface due to specular reflection of the incident signal. Indeed in radar images water body appears as dark areas.
In case the water body is large enough the action of the wind could generate ripples or waves on the water surface with an increase of roughness and a subsequent increase in backscattering.
Generally, the contrast between water and land decreases with a decreasing incidence angle or increasing wind speed. This implies that

high-incidence radar data allows us to more accurately detect water surface.
In optical satellite images water bodies could show different intensity levels in the same band due to different contents. The way the same water body is seen in the image also varies from one band to another (Zhang et al., 2006). Generally water reflects high in the visible spectrum but clearer water has less reflectance than turbid one. In the IR regions water increases absorption of the light and became darker. Furthermore increasing amounts of dissolved inorganic material in the water moves the peak of visible reflectance from green toward red regions of the spectrum.

4.1 CASE STUDY AND DATA SET

The test area used in this research is the Occhito Lake, an artificial lake located in the Southern Apennines between the Regions of Molise, Puglia and Campania. It is an artificial reservoir formed by the damming of the Fortore River.

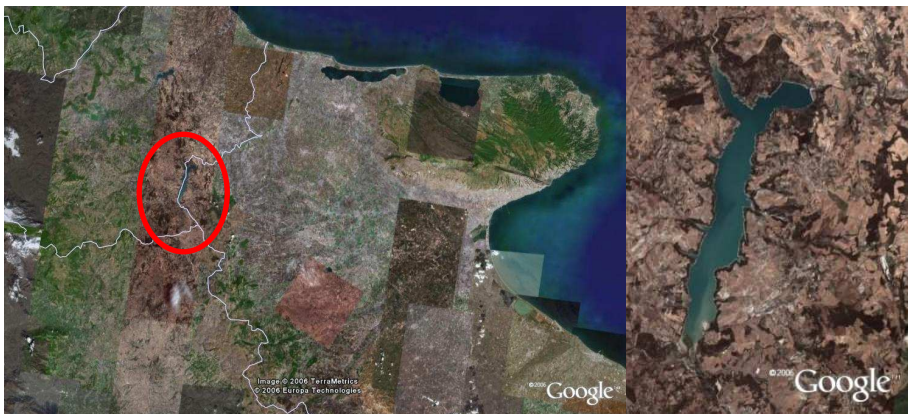

Figure 4.1: Detail of the Occhito lake: dam is located at the end of the north-est branch.

Such a case provides a useful benchmark because precise water elevation and surface area data are available. Moreover the dynamic of the basin is know and this is fundamental for the results analysis. A survey carried out before the dam construction provided a precise topographic basin

description that allowed to relate for each water level the related water volume and surface. Furthermore Italian regulations on dam safety requires dam owners to record the water surface elevation on a daily basis. This information allows a comparison between in-situ data and remotely sensed information. In the Occhito case records at our disposal covered the period from 1972 to 2005.

To best assess the accuracy of remote sensing based measures in detecting water bodies, for this research two datasets of imagery have been selected: radar images acquired from ERS-2 SAR and ENVISAT ASAR sensors and images from Landsat satellites (sensors TM/ETM). These instruments images have been chosen following literature analysis and even taking into account the accessibility of the data sets. SAR/ASAR images and Landsat ones have been provided by ESA in the framework of a Category 1 (Data Policy for ESA EO data procurement) proposal.

Images to use for carrying out this research have been selected in order to cover different levels (and the surfaces extension) of the water basin (Tab.4.1). This choice has been taken in order to verify the accuracy of using satellite images in all the conditions from a low surface level that includes large shallow and turbid water areas to high surface levels.

Images	**Images Selected**	
	Date	***Water level (m)***
SAR	27/02/1999	186.3
SAR	17/07/1999	181.8
SAR	12/01/2002	168.8
SAR	28/12/2002	177.25
ASAR	04/05/2003	194.8
ASAR	27/02/2005	195
TM (Landsat 5)	20/08/1992	184.2
ETM+ (Landsat 7)	16/08/1999	177.8

Table 4.1: images selected and Occhito water levels

The analysis has been carried using with the ENVI software tool.

4.2 SURFACE WATER DETECTION METHOD

Several water body extraction methods have been developed as multi-stage threshold and segmentation, knowledge-based decision-tree classification, geo-morphological measurement, etc. Among these, threshold method is the simplest one (Zhang et al., 2006). It consists to apply a filter to the backscattering values (for SAR images) or to the pixel values (for optical ones) in order to select a given object in the images.

4.2.1 Analysis based on SAR images

Traditionally, SAR based detection of surface water is performed by thresholding the image intensity (Solbo, 2003). In SAR images water bodies correspond to a low backscattering areas, as they are considered as specular reflector. Thus applying a proper filter to the pixels value it is possible to extract the water surface.
In this study, a two-step procedure has been applied. As first step, the thresholds to apply to the backscattering values to identify the water surface has been identified. For each image, backscattering profiles over different sections of the basin have been checked to verify the sigma nought values over the surface water. Therefore a minimum and maximum values have been identified. Using a proper function of the ENVI tool, the thresholds values have been applied to the area of interest in the image and a water mask has been derived.
Some of the images selected presented problems because of the presence of bright areas over the water body. There bright areas could be due to the wind that induces waves or ripples on the water surface which increase the backscattering. To correct for this, as secondary step, a manually correction of the mask has been performed in order to include also the bright areas.
This approach has been applied to all the selected SAR and ASAR images. In each image the water mask has been identified and, as the pixel size is known (about 30m), the water surface estimation can be obtained.
Hereafter the images analyzed: on the left panels the Occhito lake as seen by the SAR images for each date selected is shown; on the right panel the water mask obtained is highlight with different colors.

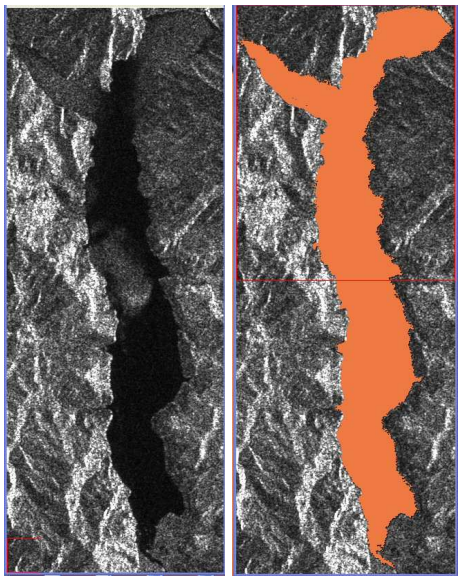

Figure 4.2 ERS-2 SAR image acquired on 27 February 1999. On the right panel water mask is shown.

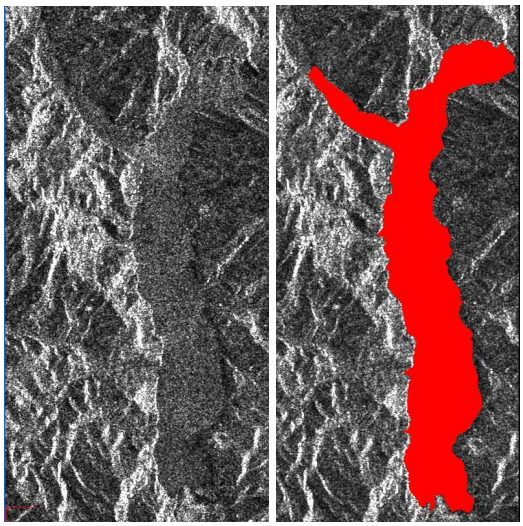

Figure 4.3 ERS-2 SAR image acquired on 17 July 1999: on the right panel the water mask is delineated.

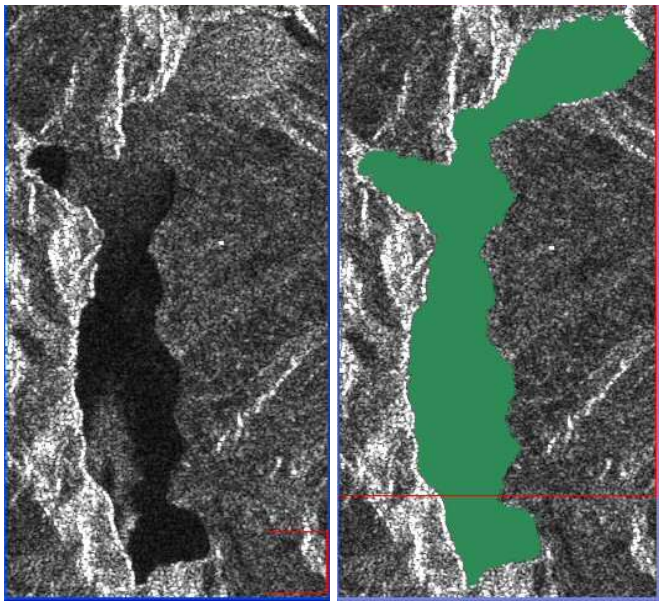

Figure 4.4 ERS-2 SAR image acquired on 12 January 2002: on the right the water mask is delineated.

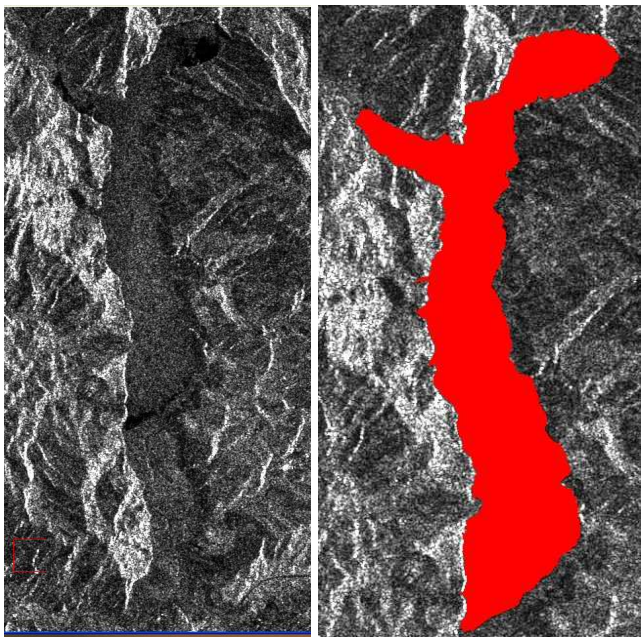

Figure 4.5 ERS-2 SAR image acquired on 28 December 2002: on the right the water mask is delineated.

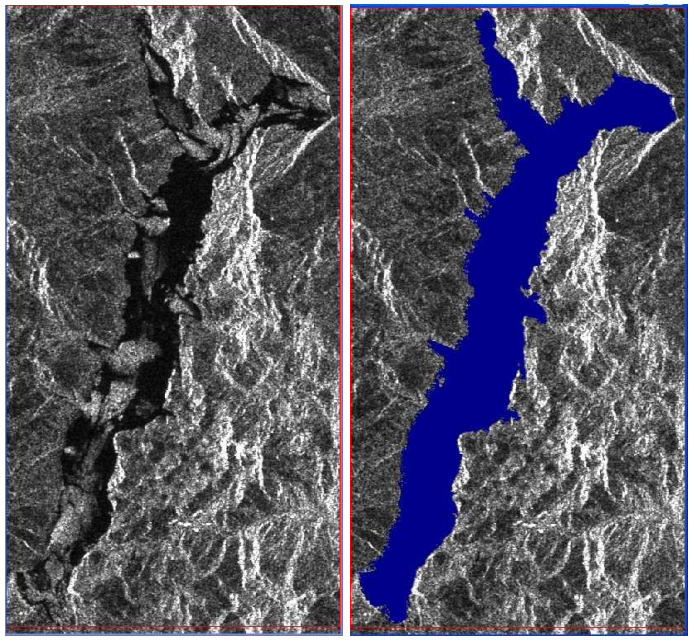

Figure 4.6 ENVISAT ASAR image acquired on 4 May 2003: on the right the water mask is delineated.

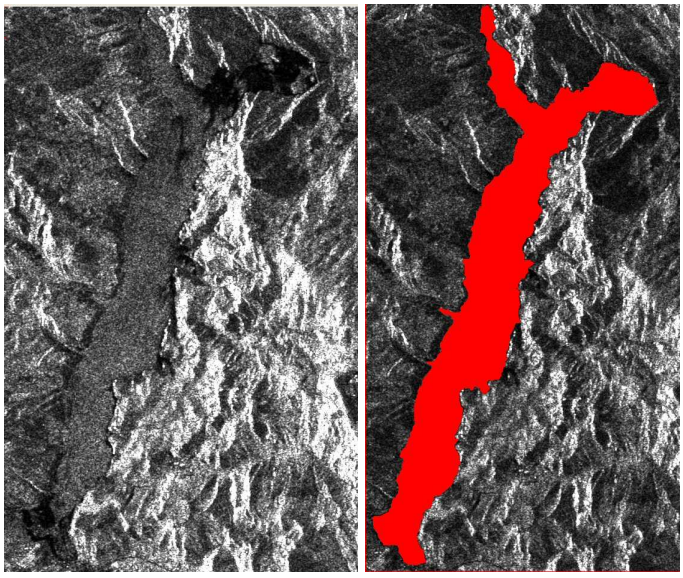

Figure 4.7 ENVISAT ASAR image acquired on 27 February 2005: on the right the water mask is delineated.

In Fig.4.1, 4.3 and 4.5 is it possible to distinguish the lake contour and the water body though bright areas over the water surface are observed. In Fig 4.2, 4.4 and 4.6, a clear separation between land and water is not evident: in fact all the water surface of the Occhito Lake is very bright. So it is difficult to distinguish the lake area if the basin position is not known. notice
In all the images analyzed the lake is located near to the far range with the resulting acquired data having quite high incidence angles. The bright responses from water areas are probably due to the windy weather conditions that have roughened the surface of the lake. This is more evident in Fig. 4.5 where wind seems to be blowing from canyons.

4.2.2 Analysis Based on Landsat images

Landsat Thematic Mapper (TM/ETM+) images have been used to detect the water body. It is well known that water, when compared to the surrounding landscape, has a different spectral response in the various electromagnetic bands. In particular the IR spectral band is recognized as the best suited to distinguish surface water.
The analysis of the two Landsat images selected (acquired on 20/08/1992 and 16/08/1999) has been based on straightforward thresholding of the NIR band (band 4).

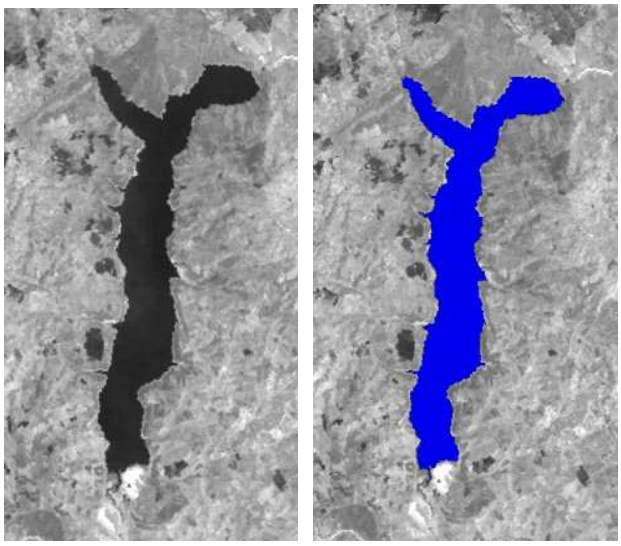

Figure 4.8 LANDSAT 5 TM band 4 image acquired on 20 August 1992: on the right the water mask is delineated

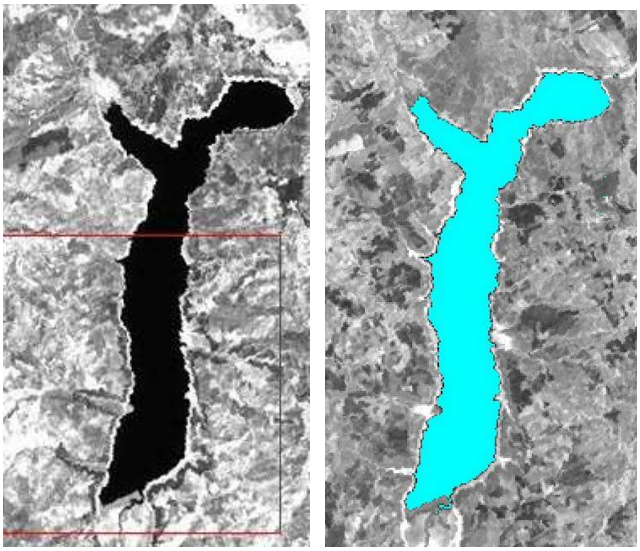

Figure 4.9 LANDSAT 7 ETM+ band 4 acquired on 16 August 1999: on the right the water mask is showed.

First, water areas have been visually detected (images on the left). As for SAR images, the thresholds values have been determined by checking

the minimum and maximum pixels value on different basin sections. Then, applying a filter, the water mask has been created (images on the right) and, as the pixel size is known, the surface extension has been calculated. Since in NIR images the contrast between water and land is evident, in this case no manual corrections have been necessary to completely define the water mask.

4.3 ANALYSIS RESULTS

After the image examinations have been performed, SAR and LANDSAT water surface analysis results have been compared to in-situ lake extent measurements (Tab. 4.2).

Sensor	Images Selected				
	Date	***Water level (m)***	***In situ surface (m2)***	***Elaboration surface (m2)***	***Δ%***
SAR	27/02/1999	186.3	10896800	10712281	1.7
SAR	17/07/1999	181.8	9685600	9618750	0.7
SAR	12/01/2002	168.8	5091200	4970625	2.3
SAR	28/12/2002	177.25	8117000	8193593	0.94
ASAR	04/05/2003	194.8	13701600	13443125	1.8
ASAR	27/02/2005	195	13740000	12065625	4
TM	20/08/1992	184.2	10266400	10017479	2.4
ETM+	16/08/1999	177.8	7834963	7834963	6

Table 4.2 Comparison between remote sensing water surface analysis and in situ surface value.

The last column of Table 4.2 contains the percentage difference between in-situ and satellite-based estimated reservoir extension.
Before discussing quantitative results it must be noted that both surface measurements are affected by errors. At the moment there is no information about in-situ surface measurement errors that could be originated by modification of the basin topography which have occurred since the dam construction and therefore of the relationship between surface level and surface extension. For the sake of simplicity, we

hereafter consider the in-situ measurements as reference, i.e. having no errors.
SAR results show a better agreement with the ground data than optical ones. In particular the error in the SAR detection results range from 0.7 to 4%. Generally, the main factors affecting SAR imaging of water surfaces are geometric problems connected to the incidence angle and the influence of wind on the water surface.
Landsat results shows less agreement with the in-situ data. The error ranges are from 2.4 to 6.0 %. This result may be connected to the characteristics of the water body. In fact deep water bodies have quite a distinct and clear representation in the imagery. However, very shallow water/turbid water can be mistaken for soil while saturated soil can be mistaken for water pixel. And very shallow water could have the same color and brightness as very turbid (high concentration of suspended sediment) water. This problem can explain the greater error in the 16/08/1999 scene. In fact, due to the particular basin conformation, lower water levels are characterized by larger shallow water/transition areas, that are rich in suspended matter, in the section where the rivers flow into the lake.
Despite SAR image analysis shows better results, this approach often requires a manual correction as for the case of wind over the water surface. For the optical data, instead, the thresholds can be defined with a lower uncertainty thanks to the very different response of water and land and no manual corrections are needed.
It is worth to highlight that the knowledge of the basin dynamic it has been important to understand the results. Indeed a simple 'satellite' interpretation of the images can lead to misunderstand the outcomes. In a previous study performed in 2004 (Lo Curzio et al.) a water extension reduction in successive Landsat images led to suppose that a progradation of the sediments occurred where the Fortore river gets into the lake. For the case of Occhito lake, instead, the different observed surfaces are due to the common management of an artificial basin. Therefore, a proper 'hydrology knowledge' of the dynamic of the basin allowed to a more accurate evaluation of the results.

5 THE ADVANCED SCATTEROMETER PROCESSING SYSTEM

The ESA ERS Scatterometer mission has provided so far a dataset of about 19 years of backscattering signal from the Earth surface since the launch of the first satellite in 1991. That data has been largely used by the scientific community in particular for assimilation in the meteorological forecast model and for climatology studies. For emerging applications, such as land ones, the spatial resolution of 50km could be a constraint but in the last years the possibility to improve the resolution of the initially ERS Scatterometer data was long investigated.
The need of high quality, homogeneous and long term satellite observations is fundamental for many kinds of applications, from climatology studies to oceanography or hydrological analysis. This is also one of the key guidelines included in the Global Climate Observing System (GCOS) from the World Meteorological Organization (WMO).

The need to fulfill the requirements of the scientific community leaded ESA to initiate the Advanced Scatterometer Processing System (ASPS) project.
The basic idea for the Advanced Scatterometer Processing System (ASPS) was born from the initial phase of the ESACA (ERS Scatterometer Attitude Corrected Algorithm) project at the end of 2001 (Lecomte, 2002). The re-design of the Scatterometer ground processor was a unique opportunity to have on one side a processor able to operate with the data acquired in Zero Gyro Mode (ZGM) in order to continue the Scatterometer mission and on the other side, to have the core element for a new state-of-the-art facility (Neyt et al., 2002) to re-process up to 20 years of ERS Scatterometer data once in 2011 the ERS-2 mission will be likely discontinued.

The main aim of the ASPS project is the reprocessing of the entire ERS-1/2 Scatterometer mission (Crapolicchio, 2004) in order to provide a homogeneous dataset of the measurements of the Earth surface at C-band through the different phases of the ERS missions. In particular,

ASPS is capable to process data acquired in ZGM from 2001 onwards and provides yaw correction information.
The second aim is the reprocessing of the "Regional Mission". In that scenario data is available only for a small segment in the visibility of each ground station and different ground stations can acquire data over the same area simultaneously. Due to the Scatterometer acquisition geometry a set of sigma nought triplets is only available in the central part of the segment with a loss at the beginning and at the end of the acquisition. ASPS reprocesses all the data segments available from the different ground stations in one segment, by selecting the best row data quality from the different stations in case of overlaps (Crapolicchio, 2004).
Another aim is to provide new products with the enhanced spatial resolution (25km) and Sea Ice detection algorithm.

5.1 ASPS ARCHITECTURAL DESIGN

The ASPS processor is a chain of signal processing modules, the input of the chain is the echo signal power and the output are sigma triplets for each node. A quality control is performed at each stage of the processing chain. Depending on the result of this control, different actions are performed and flags are set to indicate the quality control results (Crapolicchio, 2004).
The ASPS system is composed of different modules each with a specific function (Figure 5.1).

The ingestion modules are responsible for the acquisition of the Instrument raw data packets (echoes, calibration pulse, noise measurements and instrument auxiliary data), the acquisition of the instrument telemetry data (instrument working modes, temperatures, currents and voltages of the transmitter and calibration chain, the antenna temperatures) and the acquisition of the auxiliary data (the state vectors to derive the satellite position and velocity, the correlation time to relate the on-board time with the universal time, the background wind information used to perform the ambiguity removal in the wind retrieval module).

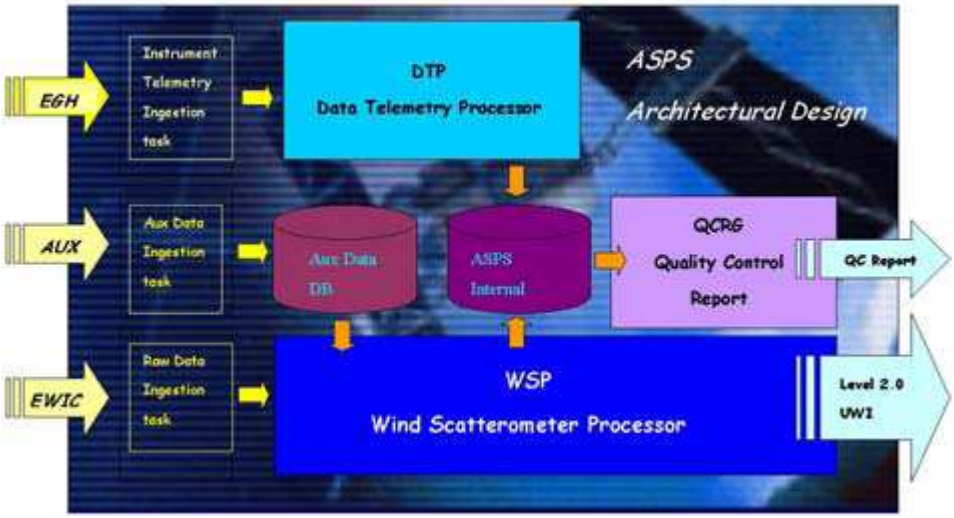

Figure 5.1: ASPS Design overview

The raw data ingestion task is also responsible to perform a quality analysis of the ingested packets. It is able to patch up corrupted packets or reject low quality packets. In case of a duplicated packet is available from different acquisition data streams (that is the nominal case for the "Regional mission scenario") the ingestion task is able to select the one with the best quality.
The auxiliary data ingestion task is responsible to store into an internal database the state vector and the time correlation data. It is also responsible to extract from the meteorological forecasts the background wind values used in the ambiguity removal algorithm.
The Telemetry ingestion task is responsible to collect and prepare the instrument telemetry data for the Data Telemetry Processor.
The ASPS main processing modules are (Crapolicchio, 2004):
• The Wind Scatterometer Processor (WSP)
• The Data Telemetry Processor (DTP)
• The Quality Control Report Generator (QCRG)

The WSP is responsible to process the Scatterometer raw data in order to obtain calibrated sigma nought measurements and, over the Ocean, wind speed and direction estimations. It is basically the ESACA processor put into operation in June 2003 with some upgrades concerning the ingestion of the raw data and the detection of the arcing

event in the transmission tube. The main advantages of this new processor with reference to the old processing chain named LRDPF are (Crapolicchio et al., 2004):

• The LRDPF processor was based on a large number of pre-computed off-line parameters (Look Up Tables) interpolated throughout the processing while the ESACA computes exactly all the data on the fly.
• ESACA contains the yaw estimation module to process data acquired in ZGM.
• The computation of the sigma nought values is performed only if at least 50% of the spatial filter is filled with valid samples.
• The computation of the radiometric resolution (Kp) has been refined with a more accurate algorithm to estimate the real variance present in the echo samples.
• The wind retrieval is performed with the CMOD-5N geophysical model function developed by ECMWF (Hersbach, 2008).
• The ambiguity removal scheme has been upgraded with the Modified Successive Correction (MSC) algorithm developed by DNMI (Schyberg et al. 1997).
• Generation of an intermediate product for Quality Control (QC) and instrument long loop assessment (ASPS Level 1.5) and a new user product (ASPS Level 2.0).
• Generation of a scientific Level 2.0 product with high-resolution sigma nought (25 Km) and Sea Ice detection flags based on a neural network output.
• Processing of ASCAT data

The QCRG is responsible for the generation of a report containing data quality and long-loop instrument performances information. The report is an output product of the ASPS and its content is mainly based on the parameter monitoring during the ERS mission lifetime. The scope of the report is to provide the user with a good level of confidence on the data quality.

5.2 SPATIAL RESOLUTION ENHANCEMENT

One of the main aims of the ASPS facility, of great interest for the users, is the spatial resolution enhancement. Indeed the improved algorithm works in a way that the return signal is processed to provide backscattering coefficients (and all the geophysical parameters derived) with the nominal spatial resolution of 50km but also with an enhanced resolution of 25km (Neyt et al., 2002).
Therefore in the products the geometrical resolution of the node is about 50x50 Km^2 in nominal resolution and 25x25 Km^2 in high resolution. The distance between two adjacent nodes is constant and equal to about 25 Km in nominal resolution and 12.5 km in High resolution.
Figure 5.2 show the backscattering coefficient (σ0) for the Aft beam over England and Northern France. On the right the nominal resolution data is displayed, on the left the high resolution one.

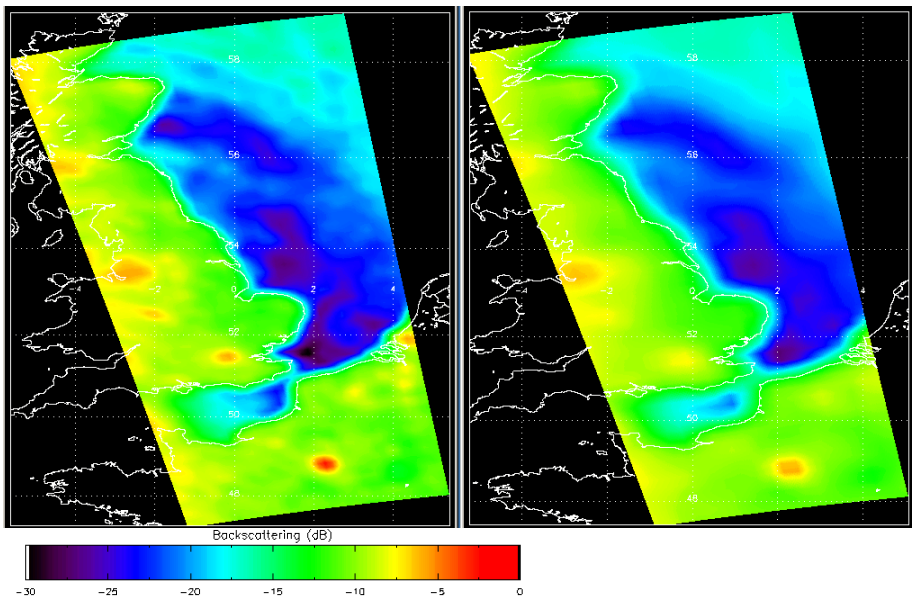

Figure 5.2: Backscattering coefficient for the aft beam: ASPS nominal resolution (on the right) and high resolution (on the left) data.

As it can be noticed, the high resolution data allows better recognizing image details as large cities, coastline and structures on the sea backscattering.

5.3 ASPS SCATTEROMETER PRODUCTS

The standard ASPS product available for the users is the Level 2.0 product. ASPS generates also an intermediate product for Quality control (QC) and instrument assessment called ASPS level 1.5. To maintain the compatibility with the actual ERS ground segment one additional output from ASPS is the UWI product.

The Level 2.0 product is generated for both nominal and high resolution and is structured as follow (Crapolicchio, 2004):

- MPH (Main Product Header)
- SPH (Specific Product Header)
- DSR (Data Set Record)

The MPH contains information regarding the quality of the acquisition chain, the data acquisition time, the processing time, the auxiliary data and the version software used.
The SPH contains information regarding the processing performed (nominal or high resolution), the window type applied for the spatial filtering, the distance to the CMOD used to retrieve the wind, the algorithm used for wind retrieval. The SPH stores also averaged values for QC: statistics on the PCD flags at node level, mean wind speed and direction biases (Scatterometer winds vs Meteorological background winds), mean distance to the CMOD model.
The DSR contains one row of across track node (19 in nominal resolution, 41 in high resolution). Each data set record has a small header with the record number (starting with 1 at the equator ascending crossing node), acquisition time of the Mid beam relative to the mid swath, the sub-satellite track heading relative to the North for the node 10 or 21 (high resolution). At node level, the main parameters of the node are the following:

- 3 beam sigma nought
- The incidence angle for each beam
- Rank 1-4 Wind Vector
- Ambiguity removed Wind Vector
- Sea/Land Flag
- Ice flag and Ice probability (Neyt et al., 2004)
- Yaw angle flag.

5.4 ERS-2 SCATTEROMETER DATA CALIBRATION

In order to improve the radiometric quality of ASPS Scatterometer data, a calibration analysis of the ERS-2 data has been performed. The aim of this study was to compute the best calibration constants and evaluate a new improved antenna pattern profile to be used for the reprocessing project.

For the calibration activity the tropical rain forest in South America has been used as a reference distributed target. In fact, at the working frequency (C band) of ERS-2 Scatterometer rain forest acts as a very rough surface, and the transmitted signal is equally scattered in all directions. Consequently, for the incidence angles used by the ERS-2 Scatterometer, the normalized backscattering coefficient (sigma nought) depends solely on the surface effectively seen by the instrument (Crapolicchio et al., 2003). This surface S' is depending on the incidence angle by the relation

$$S' = S \bullet \cos\theta \qquad (5.1)$$

With this hypothesis it is possible to define the gamma nought as a backscattering coefficient totally independent from the incidence angle (flat over the incidence angle) with the following formula:

$$\gamma^0 = \frac{\sigma^0}{\cos\theta} \qquad (5.2)$$

The gamma noughts over the rain forest is independent of the incident angle, allowing the measurements from each of the three beams to be compared. Furthermore, if the hypothesis of this relationship are correct,

the gamma noughts over a distributed target such as the rain forest should be flat across the entire swath and equal for all beams.
Thanks to these characteristics, to the extension of the Amazonas region and to its stability, it is possible to compare measurements over this area to monitor the calibration performances of the instrument.
The reference area used is located between 2.5 degrees North and 5.0 degrees south in latitude and 60.5 degrees West and 70.0 degrees West in longitude. That area is actually only partially covered by the Regional mission scenario.

5.4.1 Antenna pattern

The radiation or antenna pattern describes how the antenna gain varies across the spectrum of angles (various directions from the antenna) at a fixed or constant distance.
At the beginning of the ERS-1 and ERS-2 Scatterometer missions proper antenna patterns were computed for each instrument and used in the data processing.
One of the goals of the ASPS project is to improve the radiometric quality of Scatterometer data. This could be reached by computing an improved antenna pattern to be used in the reprocessing activity.
In 2003 a first exercise was carried out and the Tool for Scatterometer Calibration (TOSCA) developed by the Royal Military Academy (RMA – Belgium) was used to compute a new antenna pattern for the ERS-2 Scatterometer. The new antenna pattern has been defined using data acquired over the rain forest during cycle 41 (15-Mar-99/19-Apr-99).
The antenna patterns have been computed with a bin size for incidence angle of 1.5 deg. in order to have roughly 19 values across track. The new processor ESACA takes into account the "real" acquisition geometry (in particular the yaw angle) and this causes a variation of the "mean" incidence angle on the same node across track. For that reason the Fore and Aft incidence angles for one node are not exactly the same because the two signals are acquired at different times with a small change in the satellite attitude. This explains why for the Fore and Aft profiles do not range exactly on the same angles.

In the framework of the ASPS project, the nominal antenna pattern (used since the beginning of the mission) and the new one have been compared in order to verify the expected improvement.
The comparison analysis has been executed by processing data cycles 31 (30-Mar-98/03-May-98) and 51 (28-Feb-00/03-Apr-00) with both the nominal and the new antenna patterns. These 2 data cycles have been chosen as they cover quite the same time of the year of cycle 41 and therefore the rain forest is observed in the same conditions.
The assessment included the following calibration quality parameters:

- the antenna profiles
- the gamma nought's histogram

5.4.1.1 Antenna pattern: Gamma-nought as a function of incidence angle

As explained in 5.1, gamma nought should be flat and equal for the three beams over distributed target, as in the case of rain forest. Therefore an improved antenna pattern should mean a flatter gamma nought profile.
As first analysis, the gamma nought profiles over the rain forest based on cycle 31 data processed with both antenna patterns have been computed (Fig.5.2).

CYCLE 31
ERS-2 OLD ANTENNA PATTERN (Amazonas Area)

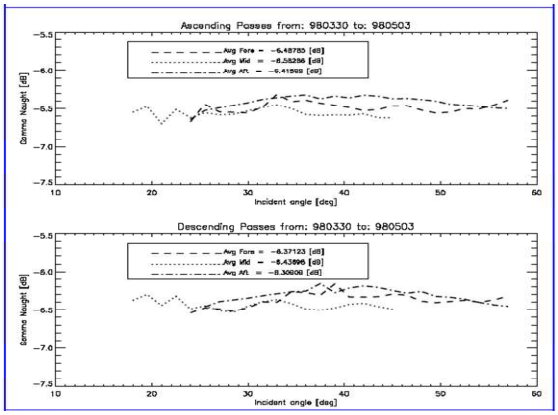

ERS-2 NEW ANTENNA PATTERN (Amazonas Area)

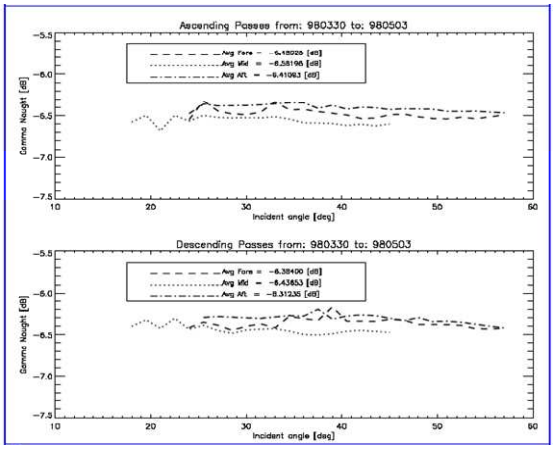

Figure 5.3 Gamma nought across the swath over the rain forest for cycle 31 data: In the upper panel the nominal antenna pattern; in the lower one the new antenna pattern.

Figure 5.3 shows the same analysis based on cycle 51 data.

CYCLE 51
ERS-2 OLD ANTENNA PATTERN (Amazonas Area)

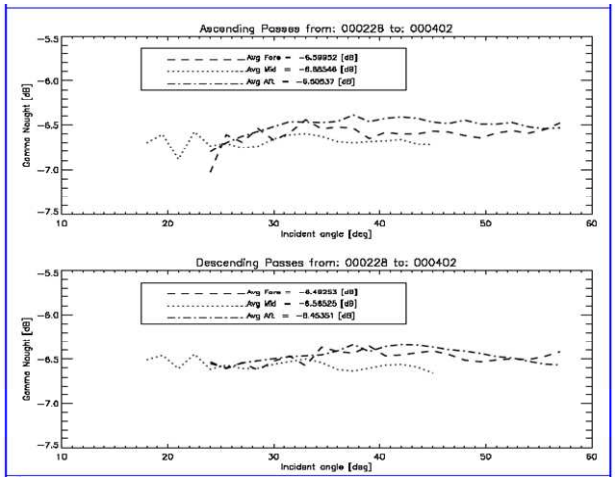

ERS-2 NEW ANENNA PATTERN (Amazonas Area)

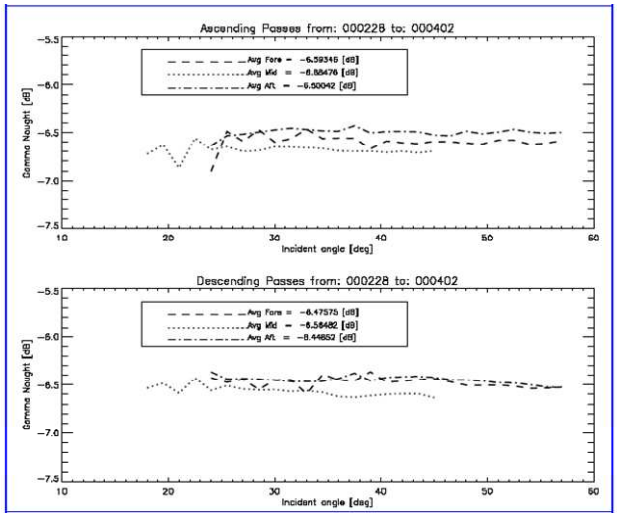

Figure 5.4: Gamma nought across the swath over the rain forest for cycle 51 data: In the upper panel the nominal antenna pattern; in the lower one the new antenna pattern.

The results for both cycle 31 (Fig. 5.2) and 51 (Fig. 5.3) show that the new antenna pattern is flatter than the nominal one.

For cycle 31 the mid beam profile is flatter within a range of around 0.25dB (both for ascending and descending passes) for the new antenna pattern against the 0.4 dB of the nominal pattern. Also the Fore and Aft beam show a shorter range for the new antenna pattern (about 0.2dB against 0.4 dB of the nominal one).
The same behavior is shown for cycle 51. The mid beam profile varies in a range of 0.3dB with the new antenna pattern against 0.25 for the nominal one. Fore beam fluctuates in a range of around 0.55/0.25 db (respectively Ascending/Descending passes) against 0.45/0.2 of the nominal one. Aft beam varies in a range of 0.2/0.15dB (respectively Ascending/Descending passes) in the new antenna pattern against 0.4/0.23 in the nominal one.

5.4.2 Gamma nought histograms and peak position evolution

As the gamma nought is independent from the incidence angle, the histogram of gamma nought over the rain forest is characterized by a sharp peak. The time-series of the peak position gives some information on the stability of the calibration.

Figures 5.4 and 5.5 show the gamma nought histograms over the rain forest for cycle 31 data processed with respectively the old and the new antenna pattern.

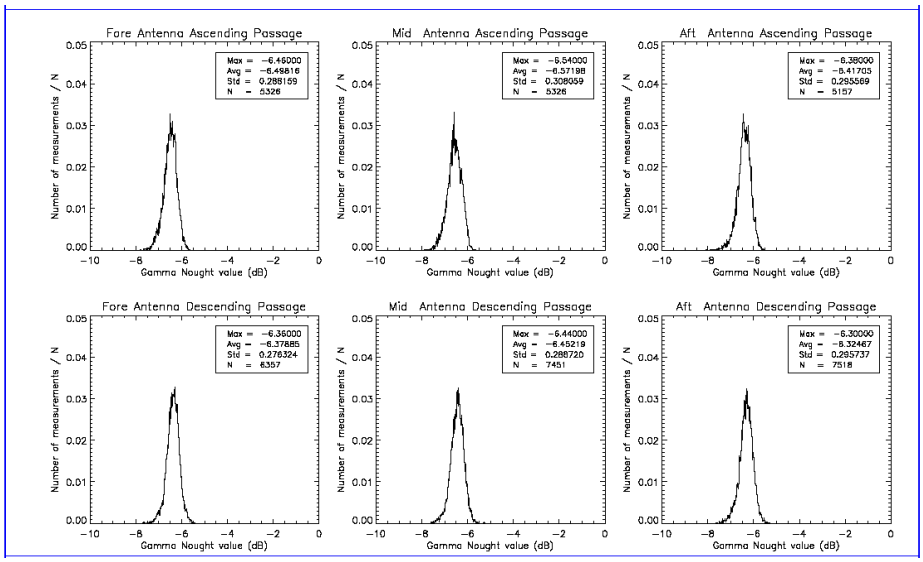

Figure 5.5 ERS-2 Gamma Nought histograms (Amazonas Area) for Cycle 31– Nominal Antenna Pattern

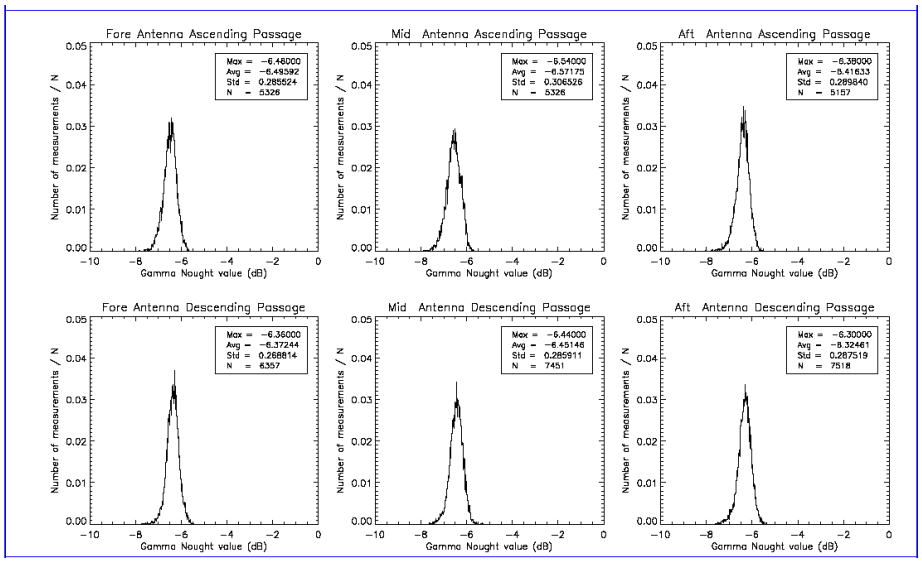

Figure 5.6 ERS-2 Gamma Nought histograms (Amazonas Area) for Cycle 31 – new antenna pattern

Figures 5.6 and 5.7 show the same for cycle 51 data.

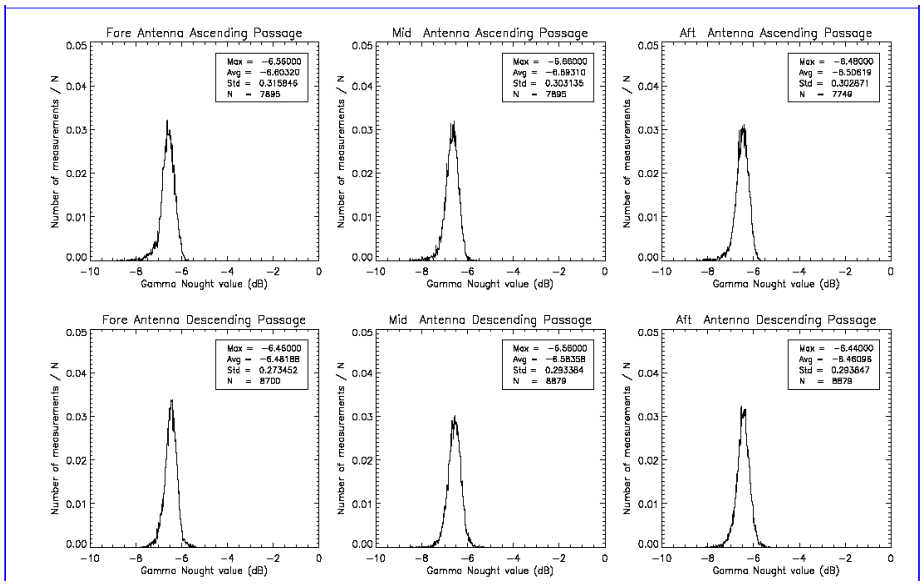

Figure 5.7 ERS-2 Gamma Nought histograms (Amazonas Area) for Cycle 51– Nominal Antenna Pattern

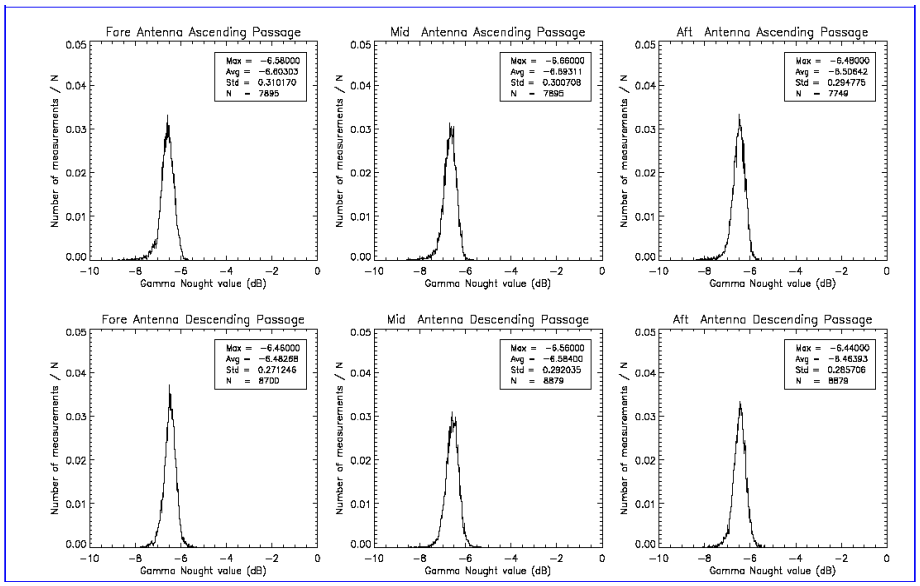

Figure 5.8 ERS-2 Gamma Nought histograms (Amazonas Area) for Cycle 51– New Antenna Pattern

Starting from the data of the gamma nought histogram, a detailed analysis has been made on the gamma nought standard deviation and the gamma nought peak positions (Figure 5.9 and 5.10).
The gamma nought standard deviation (Fig. 5.9) is smaller for the new antenna pattern than the nominal one.

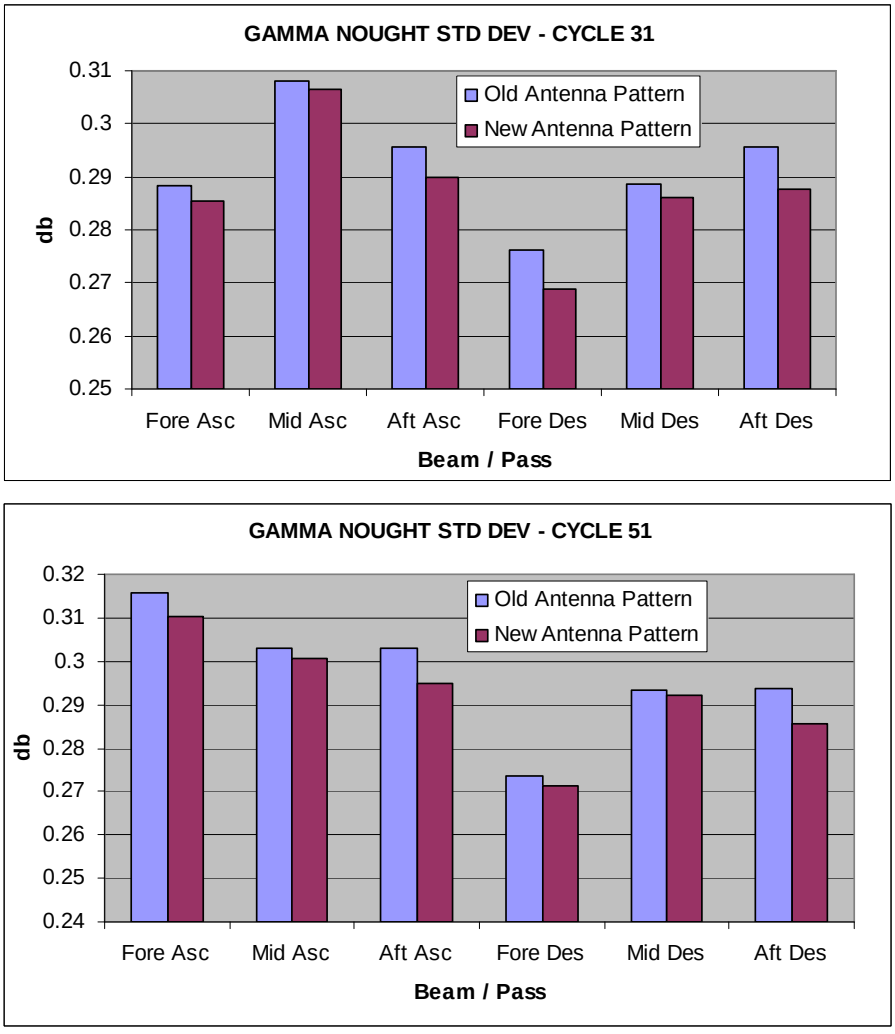

Figure 5.9 Gamma Nought Standard Deviation for Cycle 31 (upper plot) and Cycle 51 (lower plot). In each histogram data processed with new and nominal antenna pattern are compared.

Analysis of the gamma nought peak position (Figure 5.10) shows that for both the antenna patterns used the descending passes are more stable

than the ascending as they show smaller differences between the beams (interbeam calibration). The mid beam is biased both for ascending and descending passes. In fact mid beam gamma nought values are lower than fore and aft beam ones. And Fore beam values are fewer than Aft beam ones. The mean Mid beam bias has also been estimated.

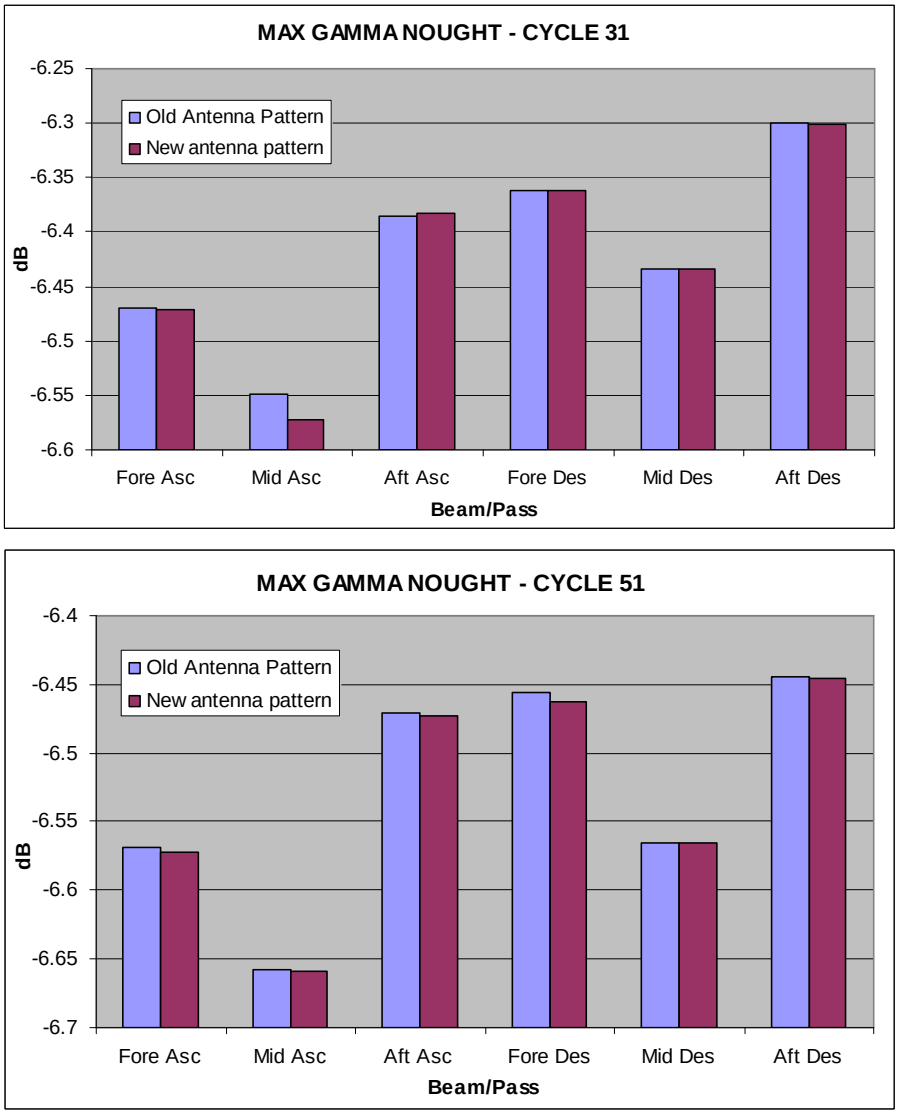

Figure 5.10: Maximum value of Gamma Nought for Cycle 31 (upper plot) and Cycle 51 (lower plot). Each histogram compare data processed with new and nominal antenna pattern.

5.4.3 Calibration analysis results

The whole calibration analysis performed has shown that the new antenna pattern profile is flatter than the old one and its gamma nought standard deviation is lower. These results confirm the need to use the new improved antenna pattern instead of the nominal one in the ASPS project in order to enhance the radiometric quality. The interbeam calibration for the descending passes is lower than the ascending one and the three beams are biased. From the gamma nought peak position analysis (Fig. 5.10), the mean bias values between the Mid and the side antennas have been estimated. One of the ASPS configuration files contains a parameter, named 'External Rescale Factor' that gathers different constants and is used to convert the 'counts' to power unit for each beam (Manise, 2004).
Starting from the estimated value of the mean Mid beam bias (§5.4.2), the External Rescale Factor for the Mid beam has been modified in order to reduce the difference between the side antennas and the Mid one. In Table 5.1 the new ERF applied in the ASPS reprocessing project.

	Fore	**Mid**	**Aft**
Old	0.00159783	0.00142407	0.00159783
New	0.00159783	0.00142686	0.00159783

Table 5.1: External Rescale Factor values for the three beams

5.5 ASPS FACILITY CONFIGURATION

To put the ASPS facility into operation and starting the reprocessing project different steps have been required and involved mainly analysis for the configuration of the system parameters.
After a complete analysis of the whole ASPS facility, aimed to better understand the different processing phases, the ASPS system has been installed on the operational machines located in ESA-ESRIN and devoted to the Scatterometer reprocessing project.
Several tests have been carried out, by processing some reference orbits, in order to verify the correct processing: proper ingestion of the auxiliary files has been verified as well as the correspondence between the expected outputs and the obtained ones. Also the right products

generation in terms of fields included and their definition have been checked.
During the test and validation phases some bugs have been highlighted and for some of them a software correction has been required.

The set up of the ASPS needed to define the proper configuration of the system. Indeed from the right configuration depends also the quality of the data generated.
The ASPS configuration involved many parameters and system variables. Some of them are not strictly linked to the topics of this thesis but are compulsory to meet the ASPS project requirements. Therefore for sake of completeness short descriptions of the main parameters analyzed and of the final configuration selected are here specified.
The configuration of the ASPS system has primarily concerned the following parameters:

1) Antenna characteristics
2) Land-sea configuration
3) Wind Retrieval configuration
4) Sea Ice detection configuration
5) Threshold configuration

Antenna characteristics: as described in 5.5.1 for the reprocessing activity a new antenna pattern has been selected. In this configuration step therefore the antenna gain expressed in azimuth and elevation is defined according to the antenna pattern selected. Furthermore in order to reduce the bias between the three antennae, as described in 5.4.3, the relevant 'Rescaling factor' parameter has been tuned.

Land-sea configuration: The sea-land mask has to be defined to assign the land/sea flag at each processed node. This implies to select the areas over which to apply wind retrieval and sea ice probability algorithm. The mask is the same since the beginning of the ERS Scatterometer mission and is based on the USGS (U.S. Geological Survey) coastline database. A cross check to validate the mask has been performed with ECMWF: this validation highlighted a difference between the mask used for ERS-2 Scatterometer processing and the ECMWF one. Indeed USGS mask considers ice shelves (i.e. Ross Sea and Weddell Sea ice shelves) as sea areas while ECMWF consider them as land area due to their stability.

Despite the differences highlighted, it has been decided to maintain the mask used since the beginning of the mission.

Wind extraction configuration: Another validation phase involved the geophysical model function to be used for the wind extraction.
The Scatterometer products (UWI) generate in NRT and distributed to the users are based on the CMOD4 model. Although the CMOD4-based wind product meets ESA's original instrument requirements, it could be improved in several ways (Hersbach, 2003). Most of the model limitations were resolved by the development of CMOD5 (Hersbach et al. 2007). CMOD5 gives rise to a more uniform performance across the AMI swath. Improvements are especially obtained for extreme cases. The CMOD5 model function had been derived on the basis of a collocation study between ERS-2 AMI triplets and ECMWF short-range forecast winds. In 2007, at the OSI SAF workshop (Ocean and Sea Ice Satellite Application Facility) several users requested to produce neutral winds rather than 10m winds (Verhoef et al., 2008). Following this request, in 2008 ECMWF developed the new CMOD5N model.
Therefore, in order to keep the ASPS products aligned with the state of the art, the facility has been configured with the CMOD5N model coefficients.

Sea-ice detection configuration: ECMWF output has also been used to configure the sea ice probability retrieval. After some test and validation against ECMWF data, the sea-ice probability processing has been configured to be applied to data located at a latitude over 50°N and 50°S. Furthermore the system has been configured so that nodes are flagged as sea ice in case the probability resulting from the neural network processing is higher than 10.05%.

Threshold configuration: threshold values need to be applied for determining the PCD flags of the Scatterometer products. Main threshold are related to Doppler compensation values, Yaw angles, Internal Calibration levels and Kp values. The choice of the threshold values has been performed according to the history of the instrument status and indeed they have to be changed according to the period (cycles of data) processed.

5.6 ASPS REPROCESSING ACTIVITY AND DATA QUALITY CONTROL

Reprocessing activity started in October 2008 and is still on-going. About 4 cycles a month are generated since one cycle of data requires about 10 days to be reprocessed in both nominal and high resolution. The reprocessing plan has foreseen to first process data in ZGM in order to compensate for the low quality of the data generated before that the ESACA processor has been put into operation. Therefore processing started with data from May 2003 (cycle 81) backwards.

Each ASPS data cycle (35 days of data) generated has been subject to a quality control procedure aimed to verify:

1) the completeness of the time series processed according to the instrument unavailability and data archive availability;
2) that the processing has been performed in a proper way and with the proper auxiliary files;
3) the correct instrument parameters and data quality.
4) For each cycle reprocessed a detailed report, to monitor the instrument performances and the data quality, is generated. The main parameters, checked at orbit level, are: yaw angle, Doppler frequency shift, Noise power, Internal Calibration Level, Number of nodes with valid sigma nought values, Antenna Pattern, Radiometric Stability Monitoring. In Fig. 5.11, as example of the QC report, the page of the yaw angle monitoring is showed.

A first geophysical validation of the ASPS products has been performed by ECMWF. Since the beginning of the ERS-1 mission, ECMWF is involved in the global validation and long-term performance monitoring of the Scatterometer UWI Products. The geophysical content of the products, that for the Scatterometer case are wind speed and direction, is compared with corresponding parameters from the ECMWF atmospheric model as well as in-situ observations (when possible). In the framework of that cooperation some ASPS reprocessed cycles (Level 2

products) have been validated with reference to both winds and backscattering values (Fig. 5.12).
The wind validation (top four panels in Fig. 5.12) has been performed by comparing the following three wind data sets to the ECMWF short-forecast (i.e. first-guess) winds:

1) ASPS selected winds (red)
2) ASPSD as the ambiguity solution closest to ECMWF one (black)
3) Winds inverted at ECMWF from backscattering values based on CMOD5.N (blue)

For the backscattering validation sigma nought measurements, as stored in the ASPS products, are compared to one obtained by inverting first guess winds in the CMOD5N model: the backscattering bias for the three antennas (fore, mid, aft) and stratified with respect to the ascending and descending tracks is computed (lower four panels in Fig. 5.12).
Results of the wind speed validation show that the biases are similar between these three datasets. For wind direction validation, instead, ASPS20D values seem agree better than the others. From these results it has been highlighted a possible difference between the algorithm used at Esrin and ECMWF and results from Esrin one compare better to ECMWF winds.
Regarding the backscattering validation, the comparison between ASPS20 measurements and the ECMWF inverted values is fair.
These validation results confirm the good quality of the ASPS products.

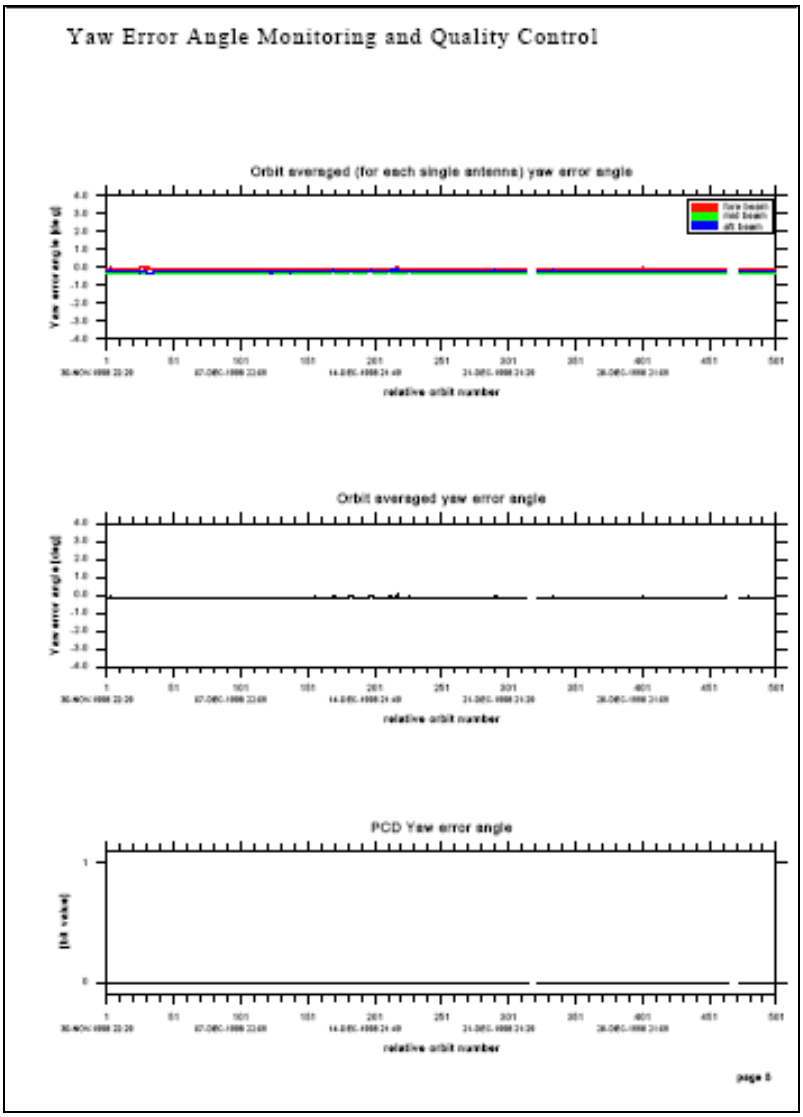

Figure 5.11 ASPS QC report: Yaw angle monitoring page.

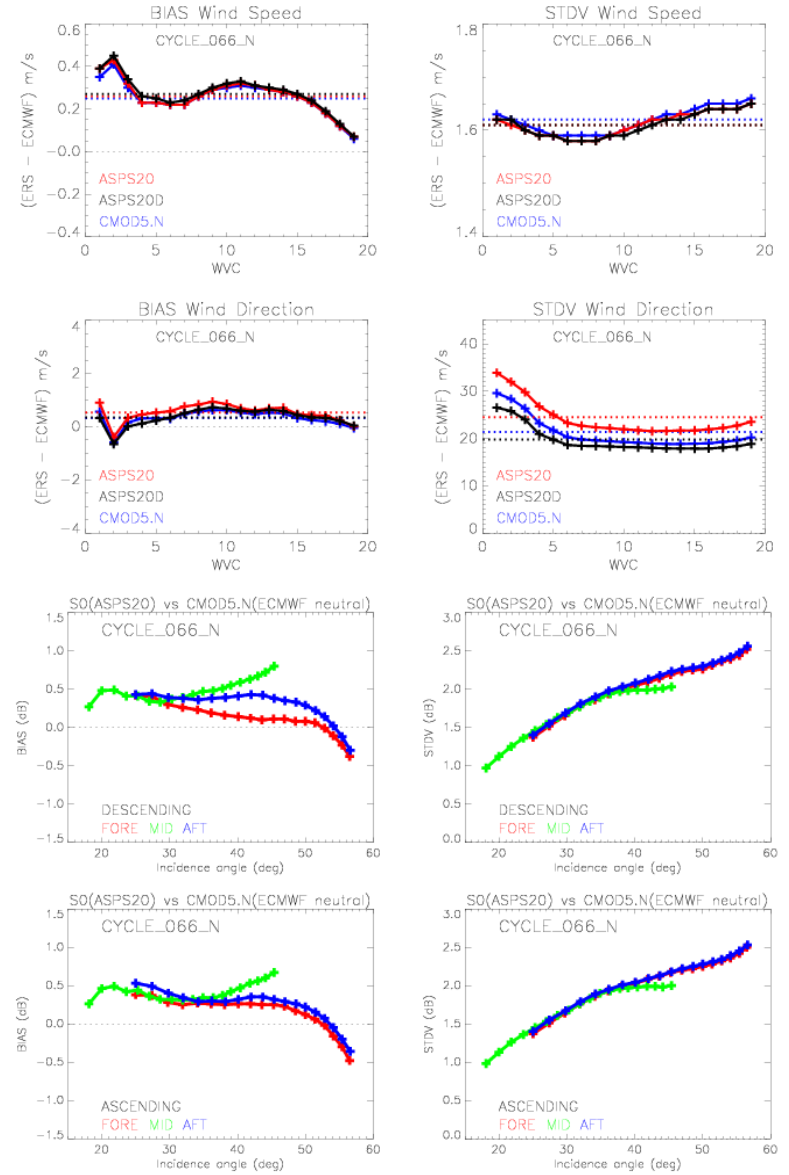

Figure 5.12: comparison between ASPS winds and backscattering and respectively ECMWF first guess winds and backscattering values derived by inverting CMOD5N model[Hans Hersbach-ECMWF].

6 ASPS MEASUREMENTS FOR SOIL MOISTURE ESTIMATION

As explained in Chapter 3, the Scatterometer has been designed to measure the wind field over the ocean. In recent years several studies have been carried out in order to evaluate the use of Scatterometer data for surface land applications. Long and Hardin (1994) were first to show that the Seasat Scatterometer backscattering, normalized for the incidence angle, was highly correlated with the type of Amazonian area. Schmullius (1997) found a good agreement between ERS-1 Scatterometer data and the Siberian forest canopy. Boehnke and Winsmann (1996-2000) developed a method to monitor the state (frozen/thawed) of the upper layer of the soil in artic to temperate climate regions. Wismann (2000) examined the freeze-thaw transition in Siberia between 1992 and 1999. In 1999 Wagner et al. used ERS Scatterometer data to examine the effects of the seasonal changes of soil moisture on vegetation over the Iberian Peninsula. Subsequently they developed a method to retrieve the soil moisture content from the backscattering coefficient.

The use of Scatterometer measurements for soil moisture application is possible since the dielectric properties of the soil strongly depends on the moisture content. However due to the limited penetration depth of C-band microwaves into the soil, Scatterometer measurements can be used only for estimations related to the surface soil layer (0-5 cm). This layer is the interface between the highly dynamic atmosphere and the deeper soil layers therefore its moisture content is subject to short term fluctuations on temporal scales of less than one day, depending on the soil type (Winsmann, 1998).
In addition to the soil moisture content, the vegetation and ice water in the soil are parameters affecting the backscattering coefficient.
In case of sparse or absent vegetation, the backscattering coefficient mainly depends on the soil moisture content, the dielectric constant, the penetration depth and the roughness.

When the water in the soil freezes, the dielectric constant of the soil rapidly decreases. This process is reversed in spring when the soil thaws (Winsmann, 1998).
In case of vegetated areas, the radar cross section is ruled by both volumetric and surface scattering: volumetric scattering depends on the density of the canopy coverage. The presence of vegetation is important not only for the volumetric scattering but because even its water content affects the dielectric constant.
Habermeyer (1998) showed that the vegetation starts to emerge above 30 degrees of incidence angles.

So far, the main study performed about the use of Scatterometer measurements for soil moisture monitoring has been carried out at the IPF TU-Wien. Wagner et al. (1998) developed a method to monitor the soil moisture content with 'moderate' vegetation. The soil moisture retrieval is based on a change detection method: the reference backscattering values σ^0_{dry} and σ^0_{wet} are estimated from the lowest and highest σ^0 values recorded in the time series analyzed. These are considered as, respectively, the dry and wet soil conditions. Each σ^0 value are then compared with the reference values and a relative measure of soil moisture referred to the surface layer is obtained which ranges between 0 and 1 (degree of saturation). To retrieve a profile soil moisture contents down to 100 cm depth from Scatterometer data, a simple two-layer water balance model is used, which only considers the exchange of soil water between the topmost remotely sensed layer and the "reservoir" below. The resulting quantity is called the Soil Water Index (SWI) and ranges between 0 (wilting level) and 1 (field capacity) (Wagner, 2003).
The first global soil moisture dataset from ERS Scatterometer data was implemented in 2003 and an updated dataset is now available including ERS-1 and ERS-2 Scatterometer measurements. The latest algorithm version takes into account new features such as the azimuthal anisotropy correction of the backscattering signal (Bartalis et al., 2006) and a soil moisture noise model (Naeimi et al., 2008a). It is worth highlight that the current soil moisture dataset is based on the operational Scatterometer UWI products provided to the users since the beginning of the ERS Scatterometer missions.
This soil moisture dataset has been used for calibration (Parajka et al., 2009), evaluation (Liu et. al., 2008) and data assimilation in hydrology

modeling showing good results. Few study, instead, compared this global soil moisture dataset with field measurements.
Soil moisture in-situ observations are fairly accurate but they are point measurements. It is in fact challenging to compare Scatterometer soil moisture data, which represents large-scale variability, with field measurements since Scatterometer data is more sensitive to the atmospheric-forcing related component of the soil moisture than the small scale land surface related variability (Parajka et al., 2009). Wagner et al. (1999) validated soil moisture from Scatterometer data against some in-situ measurements in Ukraine founding mean correlations from 0.35 to 0.53 for the upper soil layer (0-20cm). Ceballos et al. (2005) validated Scatterometer data against soil moisture field measurements from 20 REMEDHUS project stations. Paris Anguela et al. (2008) compared the ERS Scatterometer soil moisture data with in-situ and model data, over the Grand Morin watershed showing that ERS Scatterometer data was able to capture the temporal variability dynamics of the soil moisture in the watershed.

From the above detailed analysis we made two observations:

1) Despite the soil moisture dataset seems to work satisfactory, the soil moisture is provided in terms of relative percentage: 0% for dry soil, 100% for wet soil. The limits are tuned on the time series analyzed. This means that to ensure that all the possible soil conditions are covered, a very long time series is needed. Indeed, in case of limited time series, if a soil moisture content greater than the highest one recorded is found, a percentage over 100% would be found.
2) The dataset is based on the operational UWI products processed with the nominal antenna pattern used since the beginning of the ERS missions and with a spatial resolution of 50km.

Starting from these observations, this part of the PhD project was aimed at analyzing with a high detail directly the backscattering coefficient as a function of the soil moisture. To investigate the relationship between the backscattering coefficient and the soil moisture content, the sigma noughts as generated in the ASPS products have been compared to in-situ volumetric soil moisture values. This part of the research is innovative with respect to the existing studies as it benefits of the higher

quality and spatial resolution of the new ASPS products that have been generated since October 2008 (as explained in Chapter 5).

6.1 DATA SETS

The dataset used in this study includes the ASPS reprocessed data and in-situ volumetric soil moisture datasets from selected measurement stations.

a) ASPS data
The ASPS reprocessed data used for this study includes data from ERS-2 mission cycle 38 to cycle 81 covering the period December 1997-January 2003. ASPS Level 2.0 products in both nominal and high resolution have been analyzed. For each Scatterometer node the following parameters have been extracted from the Level 2.0 products in support to the analysis:
- Latitude and longitude;
- Fore, Mid, Aft beams backscattering values;
- Fore, Mid, Aft beams incidence angles;
- Fore, Mid, Aft beams azimuth angles;
- Acquisition time (UTC).

b) Volumetric soil moisture
Volumetric soil moisture measurements have been extracted from the Global Soil Moisture Data Bank collected by the Center for Environmental Prediction at the Department of Environmental Studies of the Rutgers University.

A first dataset referring to the Boissy-le-Châtel station, in France, has been selected. Boissy-le-Châtel is a hydrological station in the Orgeval catchment, located in the Seine Basin at 47.8°N, 3.1°E. The time series selected for this study includes data from December 1997 to January 2003. Soil moisture observations were taken twice daily at 11 different levels (from 5 to 155 cm) using a TDR (time domain reflectometry) probe, which was calibrated with gravimetric data. Each of the top five

levels had observations from two different TDR probes. Data is expressed as total volumetric soil moisture (%). In this study we have used the average of the 2 measurements recorded at 5cm depth. The location of Boissy-le-Châtel is showed in Fig.6.1.

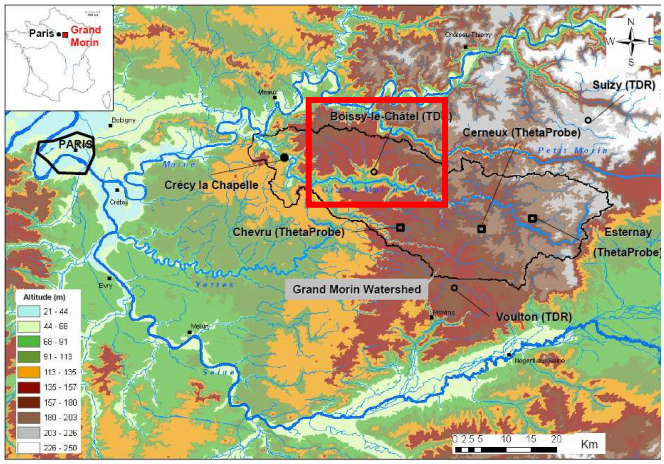

Figure 6.1: Boissy Le Chatel location.

The vegetation at the site is grassland and the soil is white silt through the observed column. In Fig. 6.2 the site observed from Google map is reported: in red an area of about 50x50 km is highlighted corresponding to about one Scatterometer resolution cell.

Figure 6.2: Boissy-Le-chatel site as observed from the satellite.

Other datasets have been extracted from the *Soil Climate Analysis Network* (SCAN) operated by the United States Department of Agriculture-Natural Resource Conservation Service (USDA-NRCS). This network includes more than 150 stations in 39 states (http://www.wcc.nrcs.usda.gov/scan/).

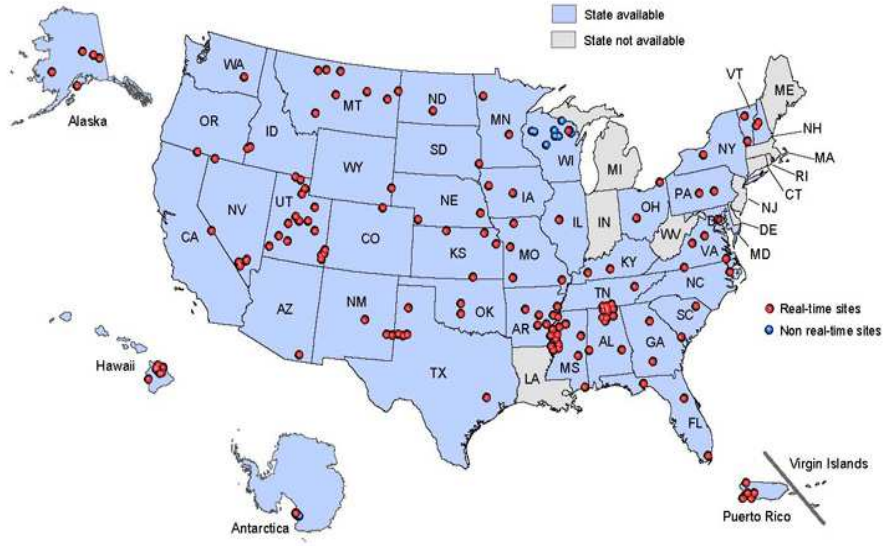

Figure 6.3 SCAN network stations

In each site, among other instruments, a Hydra probe is installed to collect soil measurements at different depth (from 2" to 40" inches where possible). Data received from the stations, are automatically validated to verify that are within acceptable ranges.
The stations to be used for this investigation have been selected according the following criteria:

- Time span availability (the same of the ASPS data reprocessed);
- Location far from the sea, high mountains and great lakes;

For this validation activity, volumetric soil moisture collected at 2" inches (~5.1 cm) from three stations in Alabama has been extracted.
The dataset period that matches the ASPS data availability covers the period from January 2000 to January 2003.
The stations analyzed are shown in Fig. 6.4 and Fig. 6.5

Figure 6.4 Location of Alabama stations from the SCAN project: stations selected are highlighted in the green box.

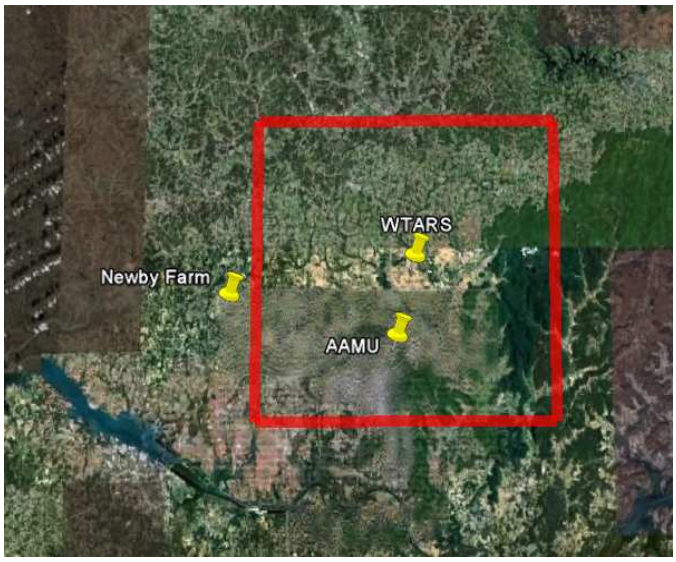

Figure 6.5 SCAN stations analyzed as viewed from Google Map: for comparison with the Scatterometer node dimension a square of about 50km x 50km centered over WTARS station is shown.

6.2 ANALYSIS PERFORMED

To validate the new ASPS products generated in the perspective of soil moisture applications, the ASPS dataset has been compared to in situ volumetric soil moisture observations: the relationship between radar backscattering and soil moisture measurements is derived considering different conditions: incidence angle, azimuth angle, Scatterometer data resolution (25 or 50 Km) and season of the year.
To perform the analysis, ASPS nodes whose area cover the ground stations have been chosen. For each sigma nought triplet available, the relevant soil moisture measurement recorded within 6 hours from satellite acquisition has been selected. The time span of 6 hours have been selected as the soil moisture does not change significantly in this period in case of stable weather conditions.

6.2.1 Backscattering against incidence angles

As first analysis, to verify the theoretical model of the backscattering evolution (§ 2.2.3.2), the sigma noughts have been plotted against the incidence angles.
In Fig. 6.6 and Fig. 6.7, the backscattering as function of the incidence angle is shown for both nominal and high resolution data. The related soil moisture measurements are represented by the colors of the points.

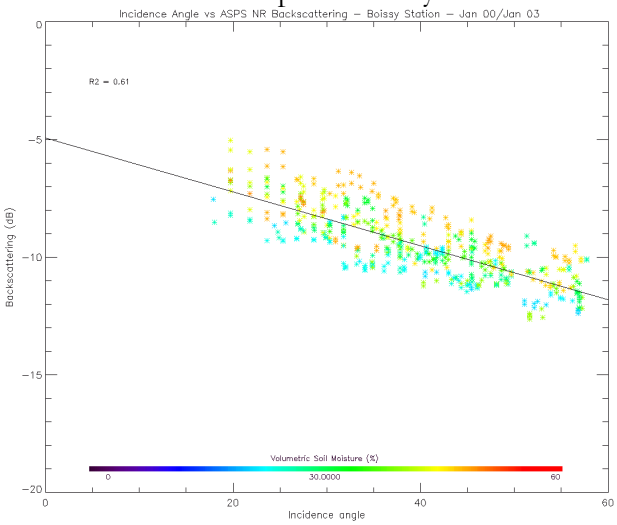

Figure 6.6: Backscattering measurements (fore, mid, aft beams) from NR products as function of the incidence angle

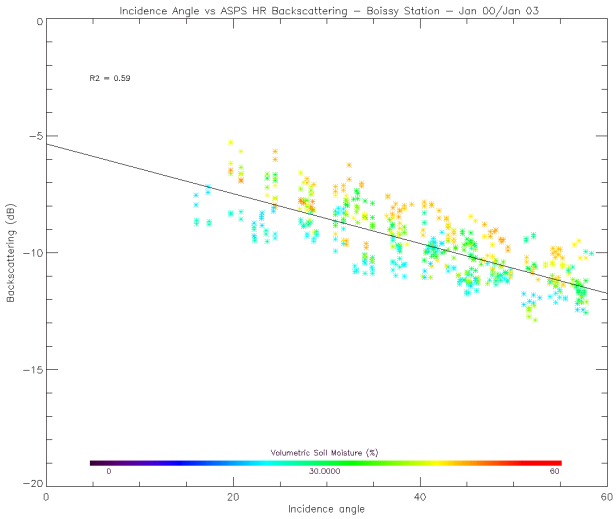

Figure 6.7: Backscattering measurements (fore, mid, aft beams) from HR products as function of the incidence angle

As expected, the incidence angle and the backscattering are inversely proportional. Furthermore, for higher soil moisture values the sigma nought increases.

6.2.2 Backscattering against volumetric soil moisture

For each node of the scatterometer grid three backscattering measurements ($\sigma_F^0, \sigma_M^0, \sigma_A^0$) are available but the corresponding incidence angles are different. As remarked in Par.2.3.2.2 the backscattering coefficient varies with the incidence angle. Based on these considerations, the comparison between the backscattering and the in-situ soil moisture measurements has been performed for ranges of incidence angles not greater than 6 degrees (i.e. 25°-31° or 36°-40°).

a) Boissy Le Chatel station

In Fig. 6.8 the sigma nought against the volumetric soil moisture value for the case of Boissy-le-Châtel station is shown. The analysis is based on measurements from all the available beams (Fore/Mid/Aft) and for the incidence angle range selected for both ASPS Nominal (left side) and High resolution (right side) data.

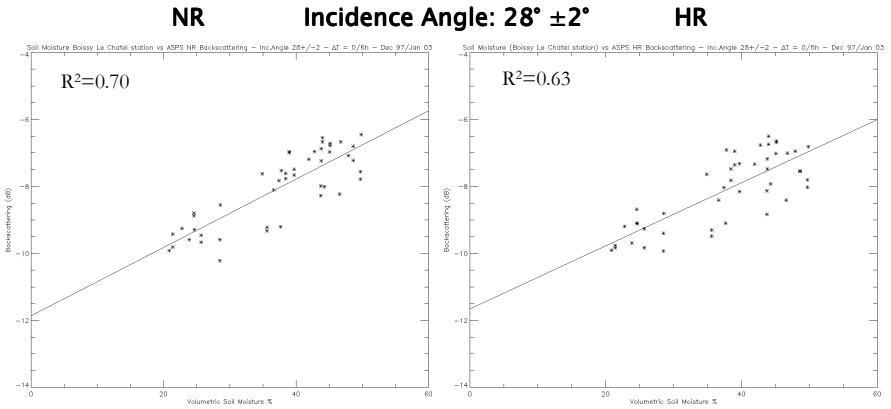

Figure 6.8 Backscattering as function of in-situ soil moisture measurements: incidence angles range [26°-30°].

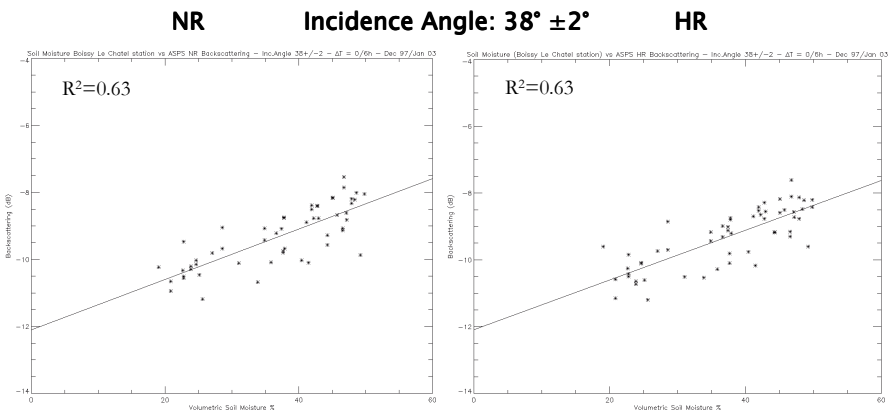

Figure 6.9 Backscattering as function of in-situ soil moisture measurements: incidence angles range [36°-40°].

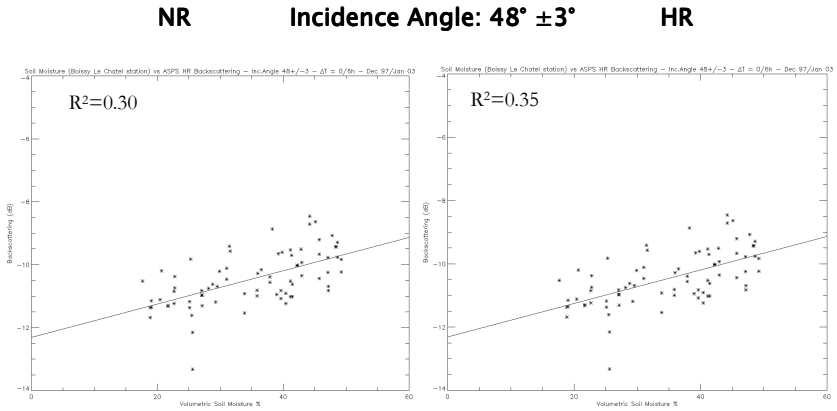

Figure 6.10 Backscattering as function of in-situ soil moisture measurements: incidence angles range [46°-50°].

The correlation coefficient is quite similar for NR and HR and decreases with the increasing incidence angle.

The correlation decrease at higher incidence angle could be explained by the presence of the vegetation: at higher incidence angles the volumetric scattering also affect the backscattering coefficient. The area of Boissy-le-Chatel is characterized by moderate vegetation of grassland so that the correlation is not high but still present.

These results have been also related to a study found in literature. Paris Anguela et al. (2008) compared the soil moisture derived from the TU Wien (based on the operational Scatterometer products with spatial resolution of 50 km and normalized incidence angle of 40°) with the volumetric soil moisture dataset recorded at Boissy-Le-Chatel station. In that study the correlation coefficient was R^2 =0.53.

Azimuthal effects analysis

The Scatterometer antennae observe the same area with three different azimuth angles. This difference affects the result of the observation. In order to account for the azimuthal effects, the analysis has been repeated by separating the single beam measurements.

ASPS sigma noughts from each single beam (Fore, Mid, Aft beams) have been compared to volumetric soil moisture values as show in the following figures for each range of incidence angle.

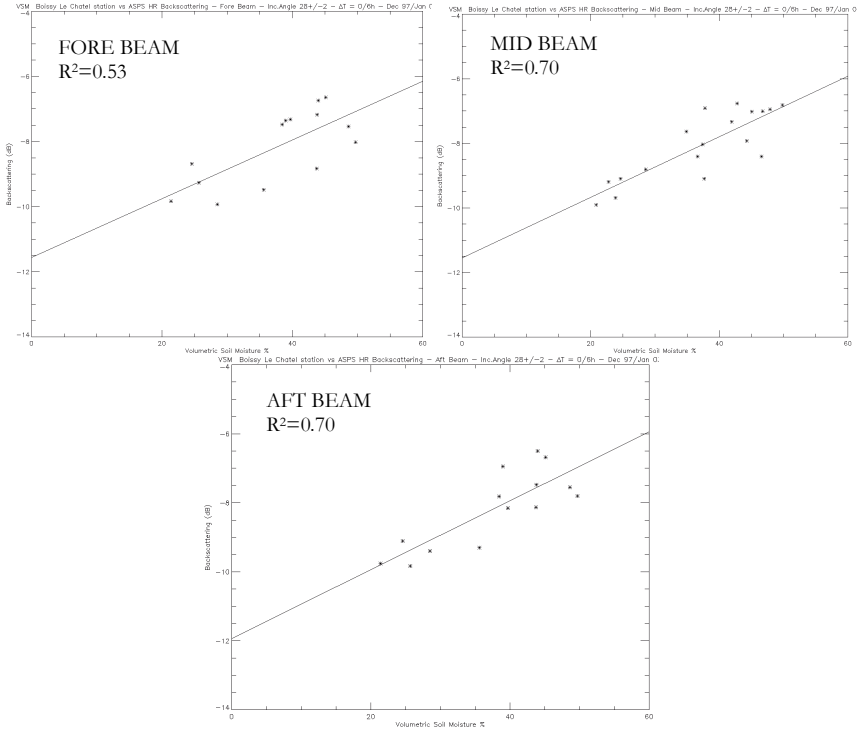

Figure 6.11 Single beam backscattering as function of soil moisture measurements: ASPS HR data, incidence angle range [26°-30°].

As seen in Fig. 6.11, the analysis based on the single beam measurements shows, for at least 2 beams up 3, a higher correlation with respect to the case with all beam sigma noughts values (that was R^2=0.63).

The same results have been found considering a different incidence angles range [36°-40°] for nominal resolutions data (see Fig. 6.12).

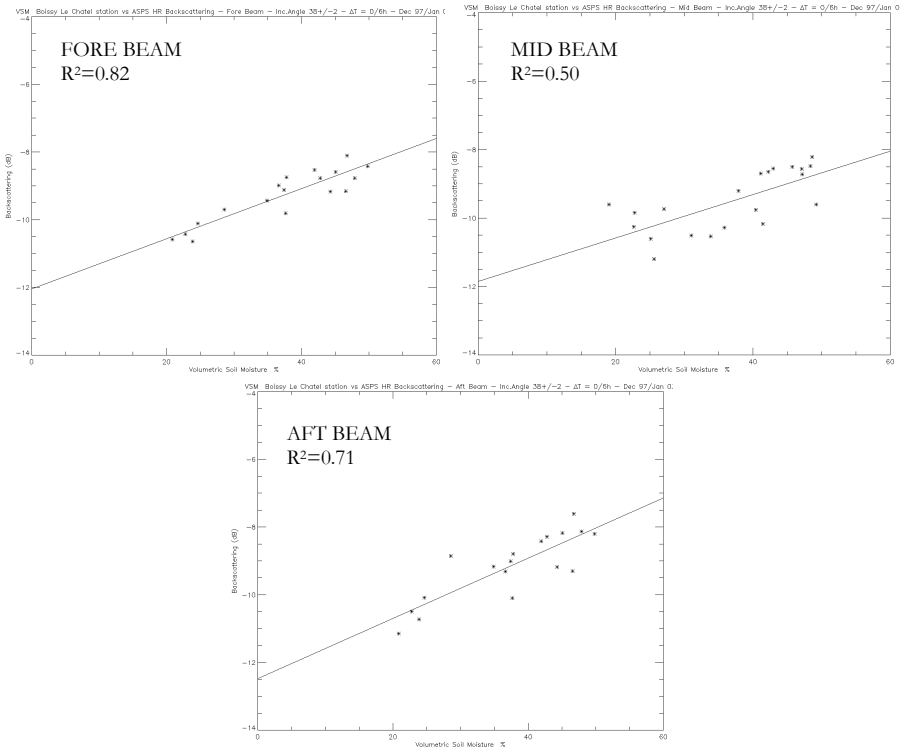

Figure 6.12 Single beam Backscattering as function of in-situ soil moisture measurements: HR products, incidence angles range [36°-40°].

For the Fore and Aft beam datasets, the correlation is higher than for the case of all beams sigma noughts (for which R^2 was 0.63).

In case of higher incidence angles an improvement of the correlation for all the beams has been found as shown in Fig. 6.13.

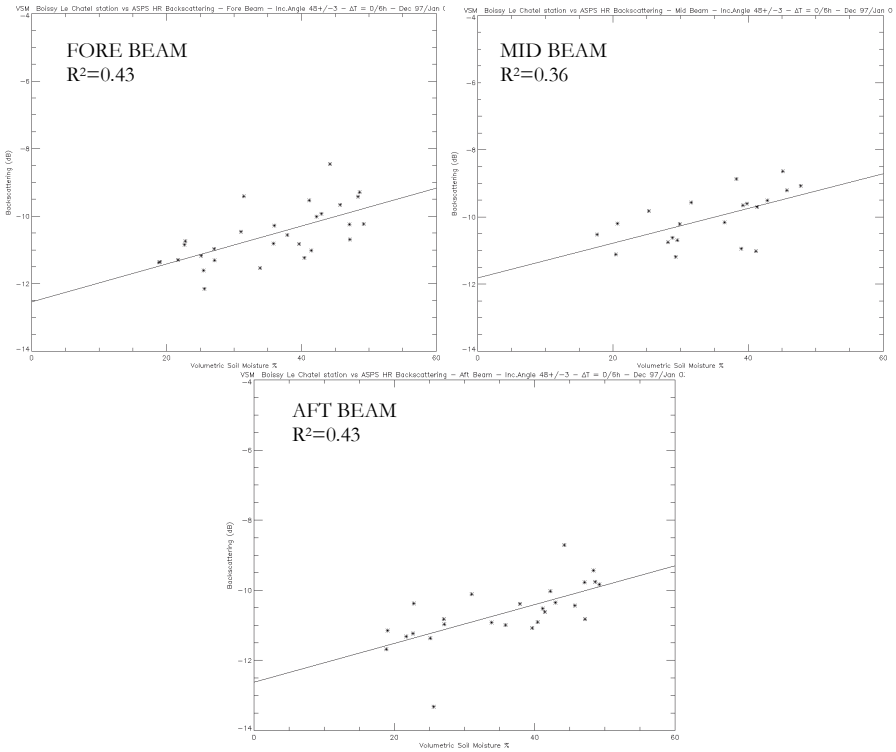

Figure 6.13 Single Beam Backscattering as function of in-situ soil moisture measurements: HR products, incidence angle range [35°-41°].

We then compared the NR products with the HR ones in order to verify the sigma nought behavior in both cases.

NR Incidence Angle: 48° ±3° HR

FORE BEAM

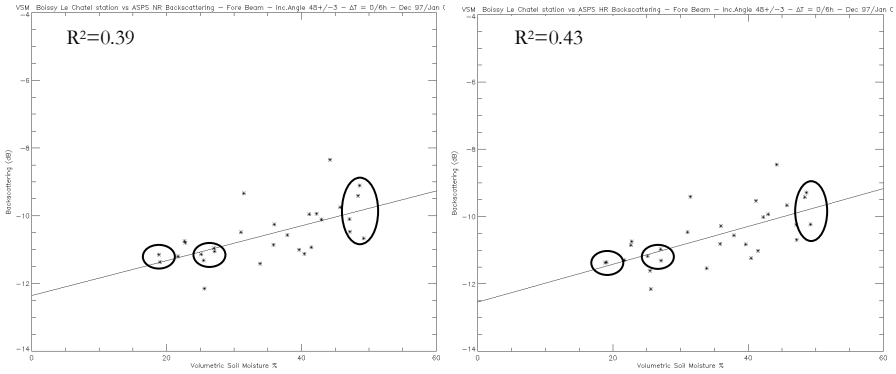

Figure 6.14 Fore Beam Backscattering as function of in-situ soil moisture measurements (incidence angles range [45°-51°]).

Having a detailed look at the plots in Fig. 6.14, it can be seen that for HR sigma nought values have a slightly lower dispersion than NR data, resulting in a higher correlation coefficient. Same results for the Mid beam dataset (Fig. 6.15).

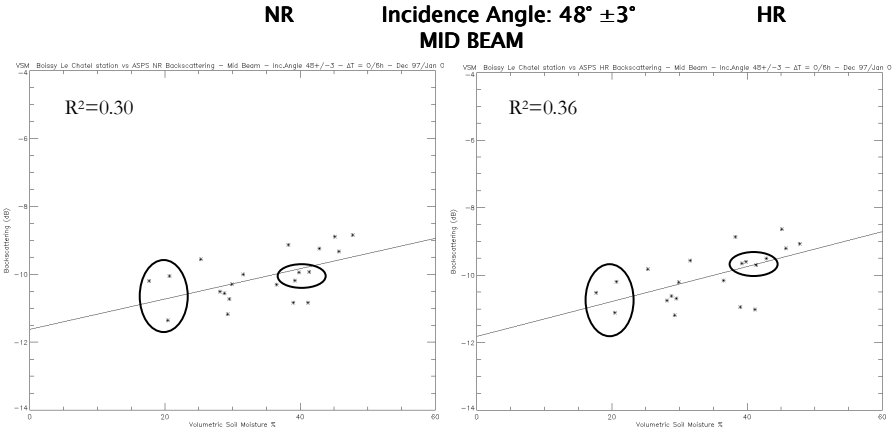

Figure 6.15 Mid Beam Backscattering as function of in-situ soil moisture measurements (incidence angles range [45°-51°].

This investigation based on single beams measurements shows that the correlation is higher if the sigma noughts values are analyzed separately confirming the expected azimuthal effects. Indeed, for at least 2 beams the correlation index is higher than for the case of three beams measurements analyzed together. A more detailed analysis also showed that HR data have in many cases higher correlation than NR data.

Vegetation effects analysis

As already mentioned, the vegetation is one of the factors affecting the dielectric constant and therefore the backscattering measurements. In order to consider the effects of the vegetation cover, that varies throughout the year, the comparison between sigma noughts and in-situ volumetric soil moisture values has been also based on seasonal time spans.

The seasons have been divided as follows:

- Winter (DJF): December, January, February;
- Spring (MAM): March, April, May;
- Summer (JJA): June, July, August;
- Autumn (SON): September, October, November.

In Fig. 6.16, the relationship between sigma nought and in-situ volumetric soil moisture values for the case of HR products and for incidence angles between 26°-30° is shown.

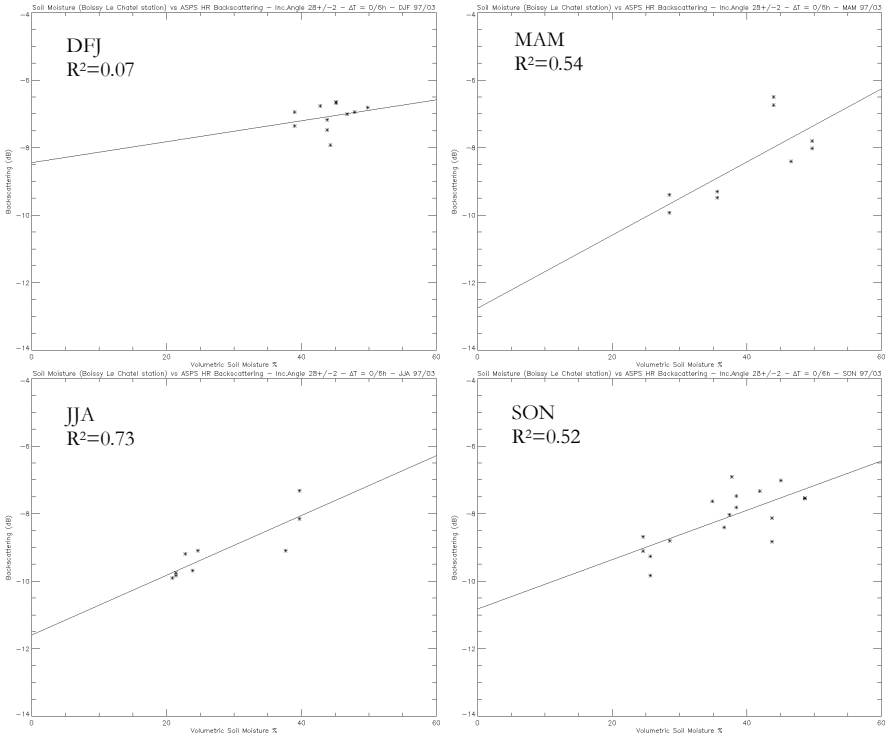

Figure 6.16 Backscattering as function of in-situ soil moisture measurements on seasonal base: HR products, incidence angles range [26°-30°].

In the analyzed cases, i.e. for all beams measurements and incidence angles range [26°-30°], a very low correlation is noticed for the winter season (DJF).

As general rule, at lower incidence angles the backscattering is dominated by the surface roughness more than by the vegetation. For the winter

season it appears that the dynamic between the backscattering and the soil moisture is completely lost. This could be explained by the presence of frozen water in the soil that could affect the dielectric constant and therefore the backscattering coefficient. Indeed the Scatterometer acquisition over the Boissy-le-Chatel station is always around 22.00 UTC at night. For the other seasons the correlation is instead quite good.

The analysis for the incidence angles range [36°-40°] and HR products is shown in Fig. 6.17.

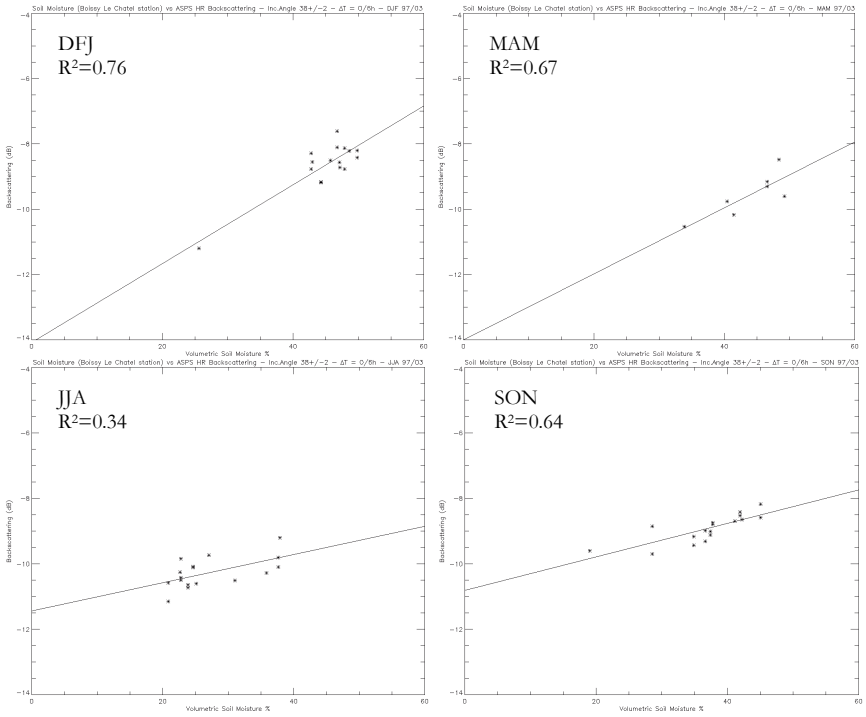

Figure 6.17 All beams Backscattering vs in-situ soil moisture: HR products analyzed as function of the season, incidence angles range [36°-40°].

For higher incidence angles the correlation for the winter season increases, while a degradation of the correlation is found for the summer season. This can be explained by the presence of vegetation during the summer months that, as mentioned above, mainly impact the sigma nought values at higher incidence angles.

This is confirmed by Fig. 6.18 where the analysis for the incidence angles range [46°-50°] is showed.

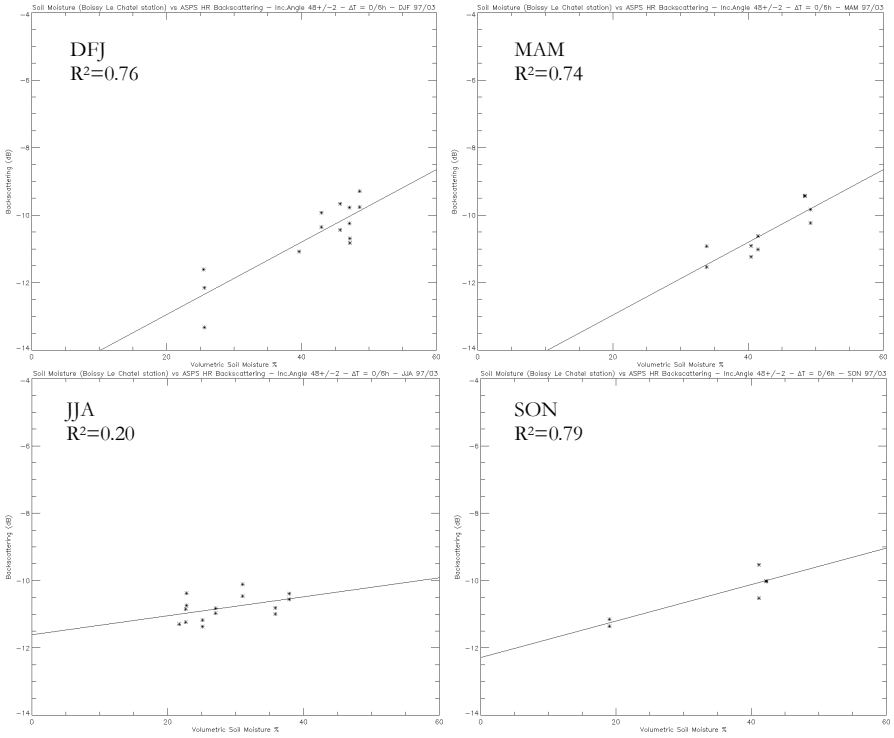

Figure 6.18 Backscattering as function of in-situ soil moisture measurements on seasonal base: HR products, incidence angles range [46°-50°].

Also on the seasonal analysis, the comparison of the results obtained for NR and HR products has been performed to verify the dynamic of sigma nought values in both cases. We focused our attention on the season with higher dynamic, the spring, taking into account that in this period influences of frozen water or high vegetation cover are very small. In Fig. 6.19 NR and HR data for the spring season and for incidence angles range [36°-40°] is shown.

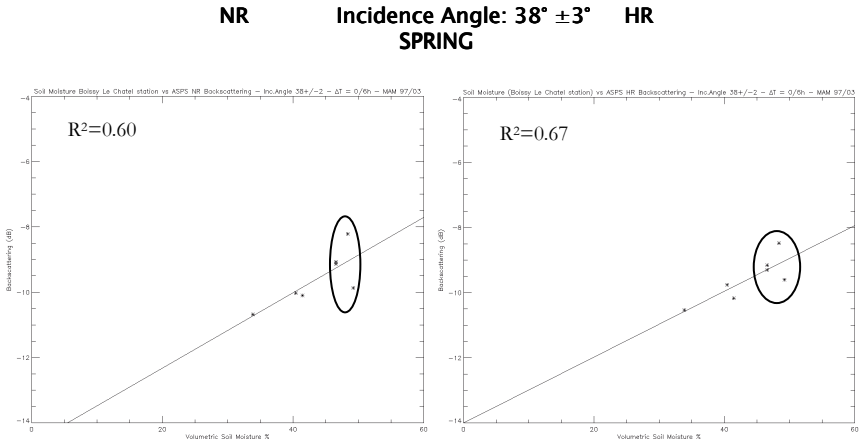

Figure 6.19 Backscattering as function of in-situ soil moisture measurements: spring season, incidence angles range [36°- 40°].

For HR data the variation of backscattering measurements for quite the same in-situ volumetric soil moisture values (points highlighted in the circle) is of about 1.2 dB against more than 1.5 dB for NR data. This shows that the HR Scatterometer measurements are more coherent with in-situ data.

In order to consider both the azimuthal and seasonal effects on the backscattering measurements, the seasonal analysis has been repeated by using Mid beam sigma nought values only. Due to the double filter applied, beam and season, only few measurements are available for this analysis and therefore in many cases the resulting statistics could be questionable. However we focused our attention on some cases to analyze the backscattering behavior in both NR and HR data.
In Fig. 6.20 NR and HR data is shown for Mid beam in spring season.

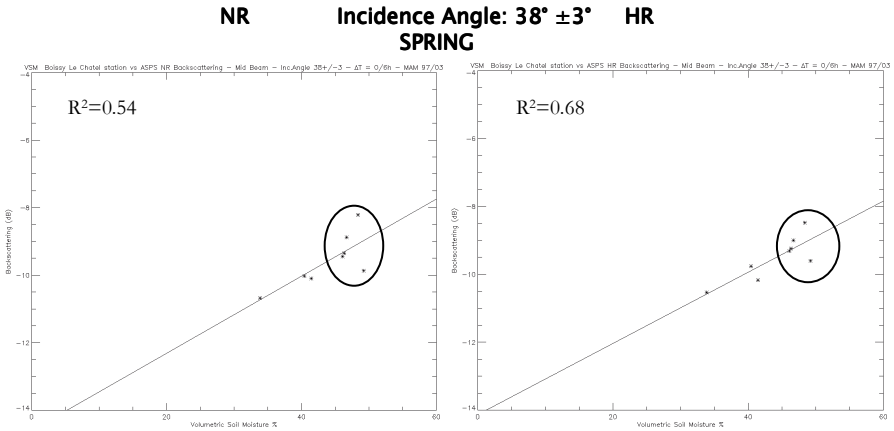

Figure 6.20 Mid beam backscattering vs in-situ soil moisture: spring season, incidence angles range [36°-40°].

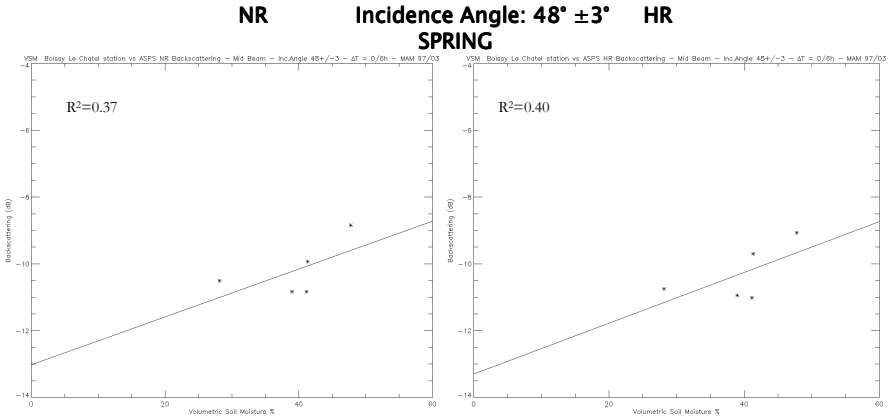

Figure 6.21 Mid beam Backscattering vs in-situ soil moisture: spring season, incidence angles range [46°-50°].

As shown in Fig. 6.21, Scatterometer measurements made at HR (highlighted in red) have less variability (~1.5dB) than the NR ones (delta sigma nought ~2dB).

b) Alabama Stations

The comparison of the backscattering measurements versus the volumetric soil moisture data has been repeated for the SCAN stations selected in Alabama. For this case study the analyzed time period covers only 3 years of data from January 2000 to January 2003 due to the limited in-situ soil moisture time series available. Furthermore, given that in-situ measurements are acquired each hour, the delta time between satellite acquisition and in-situ data has been set to 3 hours.

The resulting correlation between the backscattering signal and the in-situ volumetric soil moisture values is lower with respect to the results for Boissy-le-Chatel site case and strongly decreases for higher incidence angles.

For the station analyzed, at lower incidence angles [26°-30°], a correlation between the backscattering coefficient and in-situ volumetric soil moisture values exists. In particular, HR products show a higher correlation then NR ones (Fig. 6.22 and 6.23).

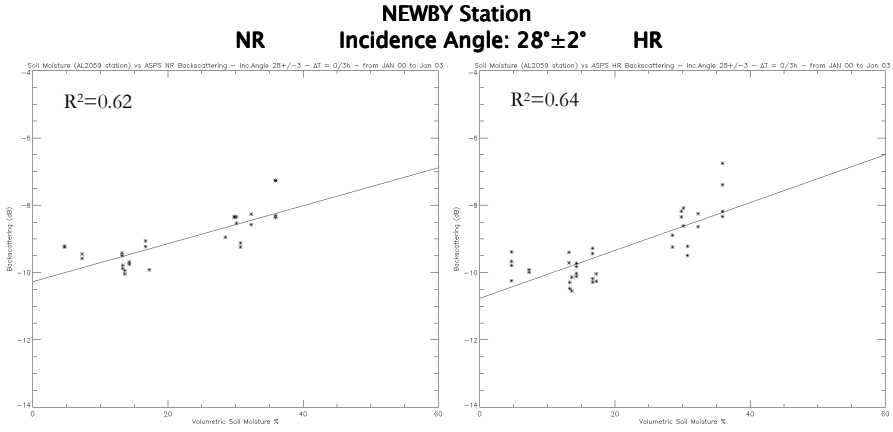

Figure 6.22 Backscattering coefficient against in-situ soil moisture: Newby station, incidence angle range [26°-30°].

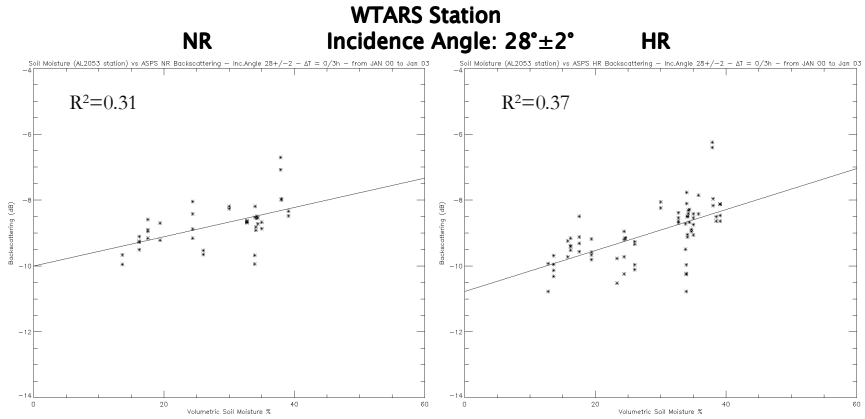

Figure 6.23 Backscattering vs in-situ soil moisture: WTARS station, incidence angle range [26°-30°].

At higher incidence angle ranges [36°-40°] or [46°-50], the dynamic of the backscattering coefficient cannot be distinguished anymore and the correlation coefficients strongly decrease. This behavior can be explained by the vegetation cover over the analyzed areas. In Fig. 6.5 it is evident (in particular for the WTARS and AAMU stations) that if we consider the area of the Scatterometer node (50x50km or 25x25km) centered on the in-situ stations, a consistent part of it is characterized by forest that strongly affects the backscattering coefficient.

For lower incidence angles, when the correlations coefficients is not poor, the azimuthal effects have been investigated. As illustrated in Fig. 6.24 and Fig. 6.25, even though the correlation values are lower than for the Boissy-le-Châtel case, Mid Beam HR products present a higher correlation between sigma noughts and volumetric soil moisture values.

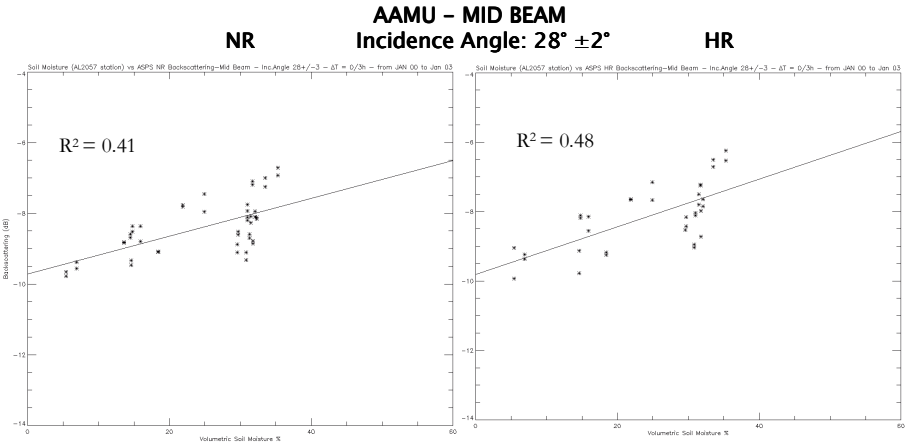

Figure 6.24 Mid Beam Backscattering vs in-situ soil moisture measurements: AAMU station, incidence angles range [26°-30°].

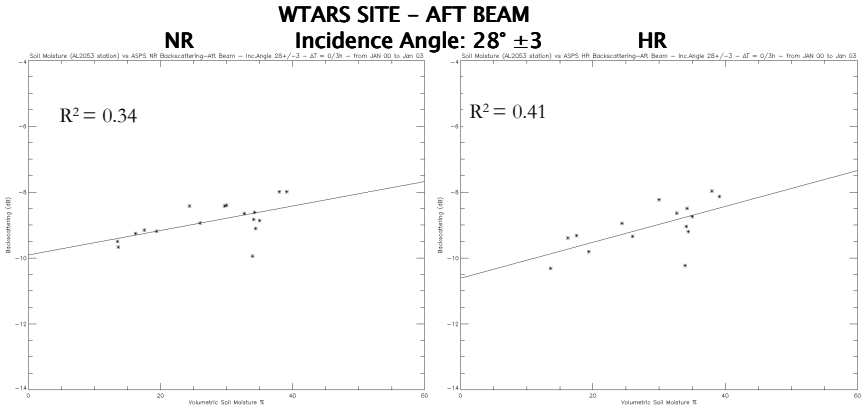

Figure 6.25 Mid Beam Backscattering vs in-situ soil moisture measurements: WTARS station, incidence angles range [26°-30°].

6.3 ANALYSIS RESULTS

The analysis performed shows that a relationship between the ASPS Scatterometer backscattering coefficient and the in-situ volumetric soil moisture exists and accounts for the incidence angle dependency.

For Boissy-le-Chatel in-situ station the analysis shows a quite good agreement between the Scatterometer backscattering coefficients derived

from the ASPS products and in-situ volumetric soil moisture measurements. As general behavior, the correlation decreases for higher incidence angles. For low incidence angles the correlation coefficient resulting is more than 0.6; analysis the increasing incidence angles shows a reduced correlation that is around 0.3.
The analysis performed to verify the Scatterometer measurements azimuthal dependency showed that the performances improve when case single beam data is used.
Yet, the effect of the vegetation cover has been investigated. Since the vegetation changes throughout the year, the investigation has been performed on seasonal base. The results show that the correlation coefficient decreases for higher incidence angles since, as explained, the vegetation mainly affects the signal at higher incidence angles. Lower correlation for the winter season at lower incidence angles was found and this could be justified by the frozen water in the soil that could exist due to the period of the year and the night acquisition. A low correlation has been also found for the summer period and this could be explained by the thicker vegetation cover. The outcomes from the seasonal analysis confirm that the type of coverage (e.g. vegetation influence, local azimuth properties on the ground) has to be considered in the retrieval of soil moisture from Scatterometer data.
As a final investigation, the evaluation of the backscattering behavior for both nominal and high resolution products has been carried out on the basis of spring season data, that is characterized by no effects of the frozen water in the soil and less vegetation cover. The results show that for HR products the backscattering values have less variability, resulting in a more clear dynamic, and therefore the correlation coefficient is higher with respect to the NR ones.

The study based on the Alabama stations presents lower performance results with respect to the French station analysis. This can be mainly explained by the different soil cover that for Alabama stations is characterized by the presence of forests that strongly affects the backscattering coefficient above all at high incidence angles. Comparison between HR and NR products shows an improvement if high resolution data is used. The azimuthal dependency has been also confirmed.

7 CONCLUDING REMARKS

This PhD Thesis work investigated the use of the satellite remote sensing observations to monitor the surface water content by using observed data acquired by different spaceborne sensors and in-situ measurements.
The Thesis started from an overview of the remote sensing principles and techniques with special regards to the satellite instruments used to carry out this project. The research activity is divided into two parts: in the first part the use of satellite images to map water bodies has been analyzed. The second part of the work deals with the soil moisture monitoring.
The integration of remote sensing in hydrological science has recently made important progresses thanks also to the extensive development over the last years. This technique is very helpful to acquire synoptic data at global scale, with a frequent temporal coverage allowing to observe also inaccessible areas. Despite the advancement technique achieved, one of the questionable points is the accuracy of remote sensing products, which is in general variable in space and times, and often not well known.
In the first part of this research was aimed to evaluate the use of satellite images for mapping inland water bodies. As first step, a case study has been selected: the artificial basin "Occhito Lake", located in the Southern Apennines, has been used thanks to the available daily measurements recorded by the dam owner and the knowledge of the basin dynamic. Then SAR and TM/ETM+ images over the study area have been then chosen in order to cover different levels and surface extension of the water basin. The selected method to retrieve the water surface extension consists in applying a filter to the backscattering values (for SAR images) or to the pixel values (for optical ones) in order to select a given object in the images. The achieved water surface extension values obtained with the threshold method have been then compared to in-situ lake extent measurements. Analysis based on SAR images shows a better agreement with the ground data than optical images one: the error in the SAR based analysis ranges from 0.7 to 4%; using Landsat images

the error ranges from 2.4 to 6.0 %. Generally, the main factors affecting SAR imaging of water surfaces are geometric problems connected to the incidence angle and the influence of wind on the water surface. This latter effect often requires a manual correction of the procedure from the operator returning in a less automatic method. Lower performances for the Landsat images may be connected to the characteristics of the water body. In fact deep water bodies have quite a distinct and clear representation in the imagery. However, very shallow water/turbid water can be mistaken for soil while saturated soil can be mistaken for water pixel. And very shallow water could have the same color and brightness as very turbid (high concentration of suspended sediment) water. For this data, thanks to the very different response of water and land, no manual corrections are needed.
The above described results confirm that the satellite images can be a useful instrument to monitor the extent of water body and suggest the use of a multi-sensor approach to reach more efficient analysis. For a more accurate analysis of the results obtained also proper hydrologic knowledge and considerations on the site analyzed are important.

The second part of this project was aimed first to generate new Scatterometer products and then to investigate the use of the C-band backscattering coefficient in the perspective of soil moisture applications. The use of Scatterometer measurements for soil moisture application is possible since the C-band backscattering coefficient depends on the dielectric properties of the soil that, in turn, are strongly affected by the moisture content.
Since the beginning of the ERS-1 Scatterometer mission in 1991 a long dataset of C-band backscattering signal from the Earth surface is available for studies and researches with a spatial resolution of 50km. Since 1991 many events impacted the Scatterometer mission that affected the quality of the data. The homogeneity of a time series is of great importance for climatic and modeling applications as well as the good data quality. This part of the research has been developed at Serco S.p.A. in the framework of the ASPS (Advanced Scatterometer Processing System) project initiated by ESA to reprocess the entire ERS Scatterometer mission and to provide a homogeneous dataset of the C-band Scatterometer measurements with enhanced spatial resolution (25km) and radiometric accuracy.

In the contest of the ASPS project, different activities has been performed with the main aim to generate the new ASPS products.
First of all a calibration analysis has been required with the aim to compute the best calibration constant and to evaluate the new antenna pattern computed in 2003 with TOSCA facility. Results of this activity showed that the new antenna pattern is flatter than the one used in the operational processing since the beginning of the ERS Scatterometer mission; moreover its gamma nought standard deviation is lower. These outcomes result into an improved radiometric quality of the data confirming the importance to use the new antenna pattern in the ASPS reprocessing activity. Moreover from the analysis of the gamma nought peak position is evident that the descending passes are more stable than the ascending ones as they show smaller differences between the beams (interbeam calibration) and the mid beam is biased for both ascending and descending passes. To compensate for this bias, and therefore to align the three beams response, a proper parameter of the ASPS configuration files has been tuned.
Once the calibration analysis was completed and the ASPS facility properly configured, the reprocessing phase has started. The new ASPS products have been generated, covering so far, only a part of the whole ERS Scatterometer mission. ASPS data represents a very important contribution to the C-band backscattering datasets available for the scientific community. These products are of a particular interest for scientists working with Scatterometer data that long required for homogeneous and enhanced products. A first geophysical validation of these new ASPS products has been performed by ECMWF with respect to the wind data retrieved from the Scatterometer products confirming the good quality of these new products.
The second aim of this part of the PhD project was to analyze the ASPS products in the perspective of soil moisture applications. In particular the relationship between the backscattering coefficient and the volumetric soil moisture has been investigated. This part of the research is innovative with respect to the existing studies as it benefited of the new enhanced ASPS products generated in the first part of this research. The analysis performed shows that a relationship between the ASPS Scatterometer backscattering coefficient and the in-situ volumetric soil moisture exists and accounts for the incidence angle dependency. For the case of Boissy-le-Chatel in-situ station the analysis shows a quite good agreement: as general behavior, the correlation decreases with

increasing incidence angle. Also the azimuthal dependency of the beams measurements has been analyzed and the results that the performances improve in case single beam data is considered. Furthermore the seasonal analysis performed to verify the effects of the vegetation cover on the backscattering measurements showed that the correlation coefficient decreases with increasing incidence angles since the vegetation mainly affects the signal at higher incidence angles. This confirms that Scatterometer data are more reliable for soil moisture application in case of 'moderate vegetation'. Lower correlation for the winter season at lower incidence angle has been found and could be justified by the frozen water in the soil that could exist due to the period of the year and the night acquisition. While the low correlation for the summer period detected can be explained by higher vegetation cover. Finally the analysis performed to evaluate the backscattering behavior for both nominal and high resolution products showed that for HR products the backscattering values have less variability and therefore the correlation coefficient is higher with respect to the NR ones.

The study based on the Alabama stations presents lower performance results with respect to the French station analysis. This can be mainly explained by the different soil cover that for the Alabama stations is characterized also by the presence of forests that strongly affect the backscattering coefficient above all at high incidence angles. Also for this cases the comparison between HR and NR products shows higher performances for the high resolution data and the azimuthal dependency has been confirmed.

This second analysis has proven that the ASPS products has strong potentiality for soil moisture applications indeed, though a comparison area against point measurements has been performed, a geophysical signal is evident. Despite high resolution products measurements are characterized by a higher noise level they seem to better represent the soil moisture dynamics. This confirm the efficacy to generate the new products. Finally, in case of further investigations to better define the relationship between backscattering coefficient and the volumetric soil moisture, the dependency from the incidence angles and azimuth angles need to be taken into account as well as the vegetation cover of the area to monitor.

REFERENCES

Ahtonen, P., Euro, M., Hallikainen, M., Solbø, S., Johansen, B., Solheim, I. (2003). *SAR and optical algorithms for discrimination of water body.* Floodman Project Report.

Barrett, A.H. (1990). *Satellite Remote Sensing for Hydrology and Water Management: The Mediterranean Coasts and Islands (Current Topics in Remote Sensing).* Gordon and Breach Science Publisher. CRC Press.1990.

Bartalis, Z., Scipal, K., Wagner, W. (2006). *Azimuthal anisotropy of scatterometer measurements over land.* IEEE Transactions on Geoscience and Remote Sensing, Volume 44, Issue 8, August 2006.

Benger, S. N. (2003). *Remotely sensed Determination of flood Surface Gradients for Hydrological Modelling of semi-Arid Floodplains.* Proceedings of IGARSS 2003, Vol. 4, pp. 2950 – 2952, 2003.

Brivio, P.A., Colombo, R., Maggi, M., Tomasoni, R. (2002). *Integration of remote sensing data and GIS for accurate mapping of flooded areas.* Int. J. Remote Sensing, vol. 23, no 3, pp 429-441, 2002.

Buiten, H.J., Clevers, J.G.P.W. (1993). *Land observation by remote sensing: theory and applications.* Gordon and Breach Science Publishers.

Campbell, J.B. (2006). *Introduction to remote sensing.* Third Edition. Taylor & Francis, London.

Crapolicchio, R., Sunda, M., Lecomte, P. (2004). *Impact of Satellite degraded attitude on ERS-2 Scatterometer data.* Atti della Fondazione Giorgio Ronchi Anno LIX, 2004, N. 5.

Crapolicchio R., Lecomte P. (2003). *On the Stability of Amazon rain forest backscattering during the ERS-2 Scatterometer mission lifetime.* Proceeding of ASAR Workshop 2003, Canada.

Crapolicchio R., Lecomte P. & Neyt X. (2004). *The advanced Scatterometer Processing System for ERS data: design, products and performances.* Proceedings of 2004 Envisat & ERS Symposium, 6-10 September 2004, Salzburg, Austria.

Le Vine, D., Abraham, S. (2002). *The effect of the Ionosphere on Remote Sensing of Sea Surface Salinity From Space: Absorption and Emission at L Band.* IEEE transaction of Geoscience and remote sensing vol 40, No 4 April 2002.

Elachi, C. (1988). *Spaceborne Radar Remote Sensing: Applications and Techniques*, IEEE Press, 1988.

Figa-Saldana, J., Wilson, J.J.W., Attema, E., Gelsthorpe, R., Drinkwater, M.R., Stoffelen, A. (2002). *The Advanced Scatterometer (ASCAT) on the meteorological operational (MetOp) platform: a follow on for European wind Scatterometer.* Can. J. Remote Sensing, Vol. 28, No.3, pp.404-412, 2002.

French R.H., J.J. Miller, C. Dettling, J.R. Carr (2006). *Use of remotely sensed data to estimate the flow of water to a playa lake.* Journal of Hydrology vol.325 , pp. 67–81, 2006.

Gianinetto, M., Villa, P., Lechi, G. (2006). *Postfllod Damage Evaluation Using Landsat TM and ETM+ Data Integrated with DEM.* IEEE Transaction on Geoscience and Remote Sensing, vol. 44. No 1, January 2006.

Hersbach, H. (2008). *CMOD5.N: A C-band geophysical model function for equivalent neutral wind.* ECMWF Technical Memorandum N. 554.

Jackson, T.J., Schmugge, J. (1996). *Remote sensing applications to hydrology: soil moisture.* Hydrological Sciences-Journal des Scinces Hydrologiques, 41 (4), August 1996.

Joseph, G. (2003). *Fundamentals of Remote Sensing.* Universities Press (India). Pvt Ltd, 3-5-819 Hyderguda, Hyderabad. 500 029. 2003.

Lecomte, P. (1998). *ERS Wind Product Specification*. Proceedings of Emerging Scatterometer Applications-from Research to Operation. ESA-ESTEC, The Netherlands , October 1998, ESA-SP-424.

Lecomte, P. (1998). *The ERS Scatterometer instrument and the On-Ground processing of its Data*. Proceedings of Emerging Scatterometer Applications-from Research to Operation", ESA-ESTEC, The Netherlands, October 1998, ESA-SP-424

Lecomte, P. (2002). *ERS-ASCAT The European Initiative on C-band Scatterometry*. Proceedings PORSEC 2002.

Liu, W.T. (2002). *Progress in Scatterometer Application*. Journal of Oceanography, Vol. 58, pp.121-136, 2002.

Lo Curzio S., Magliulo P., Russo F. (2004). *Analisi multitemporale delle modificazioni geomorfologiche del lago artificiale di Occhito (Italia meridionale) mediante tecniche di telerilevamento e GIS*. Atti 8° Conferenza Nazionale ASITA, vol. II.

Manise, N., Neyt, X., Acheroy, M. (2004). *Calibration of the ERS-2 Scatterometer in Gyro-less Mode*. Proceeding of the Envisat & ERS Symposium Salzburg (A) 6 – 10 September 2004.

Neyt. X., Pettiaux P. & Acheroy M. (2002). *Scatterometer Ground Processing Review for Gyro-Less Operations*. Proceeding of 9th International Symposium on Remote Sensing, Crete, Greece 22 - 27 September 2002.

Neyt. X., Pettiaux P., Manise, N., Acheroy M. (2004). *Neural Network based stateless Ice Detection in ERS Scatterometer Data*. Proceeding of the Enivsat & ERS Symposium, Salzburg, September 2004.

Parajka, J., Naemi, V., Bloschl, G., Komma, J. (2009). *Matching ERS scatterometer based soil moisture patterns with simulations of a conceptual dual layer hydrologic model over Austria*. Hydrol. Earth Syst. Sci., 13, 259-271, 2009.

Paris Anguela, T., Zribi, M., Hasenauer, S., Habets, F., Loumagne, C. (2008). *Analysis of surface and root-zone soil moisture dynamics with ERS scatterometer and the hydrometeorological model SAFRAN-ISBA-MODCOU at Gran Morin watershed (France).* Hydrol. Earth System Science Discussions, pp. 1903-1926.

Pellarin, T., Calvet, J.C., Wagner, W. (2006). *Evaluation of ERS scatterometer soil moisture products over a half-degree region in southwestern France.* Geophysical Research Letters, Vol. 33, 2006.

Pettiaux P. & Neyt X. (2002). *Validation of the ERS-2 Scatterometer Ground Processor Upgrade.* Proceeding of 9th International Symposium on Remote Sensing, Crete, Greece 22 - 27 September 2002.

Robock, A., Vinnikov, K.Y., Srinivasan, G., Entin, J.K., Hollinger, S.E., Speranskaya, N.A., Liu, S. & Namkhai, A. (2000). *The Global Soil Moisture Data Bank.* Bull. Amer. Meteorol. Soc., 81, 1281-1299.

Schyberg, H., Breivik, L. (1997). *Optimal Scatterometer Ambiguity Removal Using a Successive Correction Method.* Proceedings 3rd ERS Symposium on Space at the service of our environment, Florence March 1997.

Solbo, S., Malnes, E., Guneriussen, T., Solheim, I., Eltoft, T. (2003). *Mapping surface-water with Radarsat at arbitrary incidence angles.* Proceedings of IGARSS 2003, Vol. 4, pp. 2517 – 2519, 2003.

Stoffelen, A., and Anderson, D. (1997). *Scatterometer data interpretation: derivation of the transfer function CMOD4.* Journal of Geophysical Research C: Oceans, Vol. 102, No. 3, pp. 5767–5780.

Stoffelen, A. (1998). *Scatterometry.* Ph.D. Thesis, KNMI, De Bilt, The Netherlands, 1998.

Ulaby, F.T., Moore, R. K. , Fung, A. K. (1981, 1982, 1986). *Microwave Remote Sensing: Active and Passive.* Addison Wesley, (3 vols).

Verhoef, A., Portabella, M., Stoffelen, A., Hersbach, H. (2008). *CMOD5.n – the CMOD5 GMF for neutral winds.* Ocean and OSI SAF Technical Note (SAF/OSI/CDOP/KNMI/TEC/TN/165), 2008.

Wagner, W., Bloschi, G., Pampaloni, P., Calvet, J.C., Bizzarri, B., Wigneron, J.P., Kerr, Y. (2006). *Operational Readness of microwave remote sensing of soil moisture for hydrologic applications*. Nordic Hydrology, Vol 38 No 1, pp1-20, IWA Publishing 2007.

Wagner, W. (1998). *Soil Moisture Retrieval from ERS Scatterometer Data.* Ph.D. Thesis, Vienna University of Technology. 1998

Wismann, W. (1998). *Land Surface Monitoring with Spaceborne Scatterometer.* Proceedings of Emerging Scatterometer Applications-from Research to Operation", ESA-ESTEC, The Netherlands, October 1998, , ESA-SP-424.

Zhang, Z., Prinet, V., MA, S. (2003). *Water Body Extraction from Muti-Source Satellite Images.* Proceedings of IGARSS 2003, Vol. 6, pp. 3970 – 3972, 2003.